Volume 8, No. 4

June, 1961

THE SOVIET JOURNAL OF

ATOMIC ENERGY

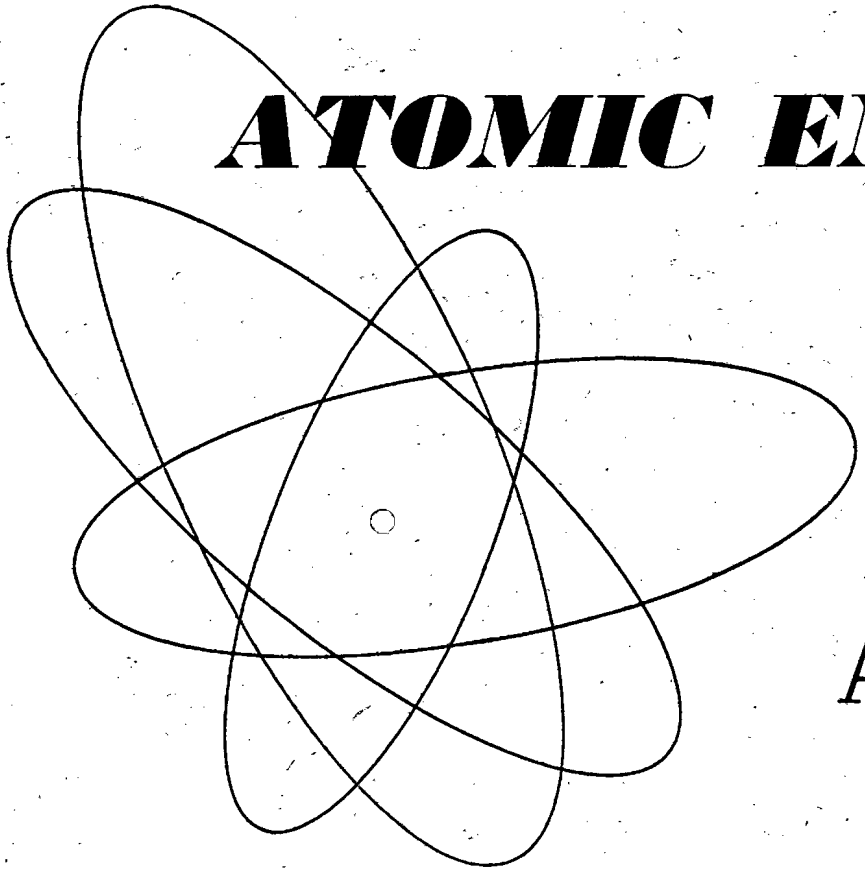

Атомная энергия

TRANSLATED FROM RUSSIAN

CONSULTANTS BUREAU

2 outstanding new Soviet journals

KINETICS AND CATALYSIS

The first authoritative journal specifically designed for those interested (directly or indirectly) in kinetics and catalysis. This journal will carry original theoretical and experimental papers on the kinetics of chemical transformations in gases, solutions and solid phases; the study of intermediate active particles (radicals, ions); combustion; the mechanism of homogeneous and heterogeneous catalysis; the scientific grounds of catalyst selection; important practical catalytic processes; the effect of substance – and heat-transfer processes on the kinetics of chemical transformations; methods of calculating and modelling contact apparatus.

Reviews summarizing recent achievements in the highly important fields of catalysis and kinetics of chemical transformations will be printed, as well as reports on the proceedings of congresses, conferences and conventions. In addition to papers originating in the Soviet Union, KINETICS AND CATALYSIS will contain research of leading scientists from abroad.

Contents of the first issue include:

Molecular Structure and Reactivity in Catalysis. A. A. Balandin

The Role of the Electron Factor in Catalysis. S. Z. Roginskii

The Principles of the Electron Theory of Catalysis on Semiconductors. F. F. Vol'kenshtein

The Use of Electron Paramagnetic Resonance in Chemistry. V. V. Voevodskii

The Study of Chain and Molecular Reactions of Intermediate Substances in Oxidation of *n*-Decane. Z. K. Maizus, I. P. Skibida, N. M. Emanuél' and V. N. Yakovleva

The Mechanism of Oxidative Catalysis by Metal Oxides. V. A. Roiter

The Mechanism of Hydrogen-Isotope Exchange on Platinum Films. G. K. Boreskov and A. A. Vasilevich

Nature of the Change of Heat and Activation Energy of Adsorption with Increasing Filling Up of the Surface. N. P. Keier

Catalytic Function of Metal Ions in a Homogeneous Medium. L. A. Nikolaev

Determination of Adsorption Coefficient by Kinetic Method. I. Adsorption Coefficient of Water, Ether and Ethylene on Alumina. K. V. Topchieva and B. V. Romanovskii

The Chemical Activity of Intermediate Products in Form of Hydrocarbon Surface Radicals in Heterogeneous Catalysis with Carbon Monoxide and Olefins. Ya. T. Eidus

Contact Catalytic Oxidation of Organic Compounds in the Liquid Phase on Noble Metals. I. Oxidation of the Monophenyl Ether of Ethyleneglycol to Phenoxyacetic Acid. I. I. Ioffe, Yu. T. Nikolaev and M. S. Brodskii

Annual Subscription: $150.00

Six issues per year – approx. 1050 pages per volume

JOURNAL OF STRUCTURAL CHEMISTRY

This significant journal contains papers on all of the most important aspects of theoretical and practical structural chemistry, with an emphasis given to new physical methods and techniques. Review articles on special subjects in the field will cover published work not readily available in English.

The development of new techniques for investigating the structure of matter and the nature of the chemical bond has been no less rapid and spectacular in the USSR than in the West; the Soviet approach to the many problems of structural chemistry cannot fail to stimulate and enrich Western work in this field. Of special value to all chemists, physicists, geochemists, and biologists whose work is intimately linked with problems of the molecular structure of matter.

Contents of the first issue include:

Electron-Diffraction Investigation of the Structure of Nitric Acid and Anhydride Molecules in Vapors. P. A. Akishin, L. V. Vilkov and V. Ya. Rosolovskii

Effects of Ions on the Structure of Water. I. G. Mikhailov and Yu P. Syrnikov

Proton Relaxation in Aqueous Solutions of Diamagnetic Salts. I. Solutions of Nitrates of Group II Elements. V. M. Vdovenko and V. A. Shcherbakov

Oscillation Frequencies of Water Molecules in the First Coordination Layer of Ion in Aqueous Solutions. O. Ya. Samilov

Second Chapter of Silicate Crystallochemistry. N. V. Belov

Structure of Epididymite $NaBeSi_3O_7OH$. A New Form of Infinite Silicon–Oxygen Chain (band) $[Si_6O_{15}]$. E. A. Podedimskaya and N. V. Belov

Phases Formed in the System Chromium–Boron in the Boron-Rich Region. V. A. Epel'baum, N. G. Sevast'yanov, M. A. Gurevich and G. S. Zhdanov

Crystal Structure of the Ternary Phase in the Systems Mo(W)–Fe(CO,Ni)–Si. E. I. Gladyshevskii and Yu. B. Kyz'ma

Complex Compounds with Multiple Bonds in the Inner Sphere. G. B. Bokii

Quantitive Evaluation of the Maxima of Three-Dimensional Paterson Functions. V. V. Ilyukhin and S. V. Borisov

Application of Infrared Spectroscopy to Study of Structure of Silicates. I. Reflection Spectra of Crystalline Sodium Silicates in Region of 7.5-15μ. V. A. Florinskaya and R. S. Pechenkina

Use of Electron Paramagnetic Resonance for Investigating the Molecular Structure of Coals. N. N. Tikhomirova, I. V. Nikolaeva and V. V. Voevodskii

New Magnetic Properties of Macromolecular Compounds with Conjugated Double Bonds. L. A. Blyumenfel'd, A. A. Slinkin and A. E. Kalmanson

Annual Subscription: $80.00

Six issues per year – approx. 750 pages per volume

Publication in the USSR began with the May-June 1960 issues. Therefore, the 1960 volume will contain four issues. The first of these will be available in translation in April 1961.

(c/b) CONSULTANTS BUREAU 227 W. 17 ST., NEW YORK 11, N. Y.

Declassified and Approved For Release 2013/02/19 : CIA-RDP10-02196R000100050004-5

THE SOVIET JOURNAL OF

ATOMIC ENERGY

A translation of ATOMNAYA ÉNERGIYA, a publication of the Academy of Sciences of the USSR

(Russian original dated April, 1960)

Vol. 8, No. 4 June, 1961

CONTENTS

Annual subscription $75.00
Single issue 20.00
Single article 12.50

CONTENTS (continued)

NOTE

The Tables of Contents lists all material that appears in Atomnaya Énergiya. Those items that originated in the English language are not included in the translation and are shown enclosed in brackets. Whenever possible, the English-language source containing the omitted reports will be given.

Consultants Bureau Enterprises, Inc.

LENIN ON SCIENCE AND INDUSTRY

I. I. Kul'kov

Translated from Atomnaya Energiya, Vol. 8, No. 4, pp. 301-304, April, 1960

The shaping, the undeviating forward advance, and the successes of Soviet science are indissolubly associated with the name of the founder of the Communist Party and of the Soviet Government, leader and teacher of toilers of the entire world, superlative thinker, and coryphaeus of science, Vladimir Il'ich Lenin.

In Lenin were combined in brilliant fashion the wisdom of the political organizer and leader of the popular masses with the theoretical power of the scientist. Lenin's great merit before the international workers and Communist movement resides in the fact that in the struggle with every different type of opportunist, he held high the purity of Marxist theory, and enriched it with new discoveries and deductions corresponding to new historical conditions. Lenin's contributions to Marxist philosophy, political economy, and the theory of scientific communism number among the most glorious conquests of scientific thought.

Lenin's theoretical heritage constitutes an enormous contribution to the further development of the social sciences and to all of natural science.

The juncture of the Ninteenth and Twentieth Centuries is marked, as we know, by great discoveries in the field of natural science: x-rays were discovered in 1895 (Röntgen), the phenomenon of radioactivity was discovered in 1896 (Becquerel), the electron was discovered in 1897 (Thomson), polonium and radium were discovered in 1898 (Pierre and Marie Curie), the foundations of quantium theory were laid in 1900 (Planck), the theory of relativity was founded in 1905 (Einstein), etc. These achievements of science produced a radical change in the views of scientists about nature.

Probing further and more profoundly into their concepts of the structure of matter, its forms of motion and so forth, scientists saw demonstratively in the new discoveries the narrowness and limited range of the philosophical basis of the old physics, i.e., metaphysical and mechanistic materialism. Many physicists-scientists, while lacking any grasp of materialist theory and being unacquainted with Marxist dialectics, proved to be at a loss in the face of these new discoveries; being unable to make generalizations philosophically and to interpret the discoveries, they fell victim to idealists who drew reactionary conclusions, viz., disappearance of matter, existence of motion without matter, concepts and laws of science which were not a reflection of objective reality but rather were "conventionalisms," "symbols," the results of conventions arrived at between scientists, etc. The upshot of all this was a crisis in physics. "The essence of the crisis in modern physics," wrote Lenin, "resides in the breakdown of the old laws and fundamental principles, in the rejection of objective reality as independent of consciousness, i.e., in the replacement of materialism by idealism and agnosticism" (V. I. Lenin, Collected works [in Russian], Vol. 14, p. 245). Analyzing the substance of the crisis, uncovering its social and gnosiological causes, Lenin indicated the way out of the dilemma, the road to the correct solution of the philosophical problems raised in connection with the development of natural science. Lenin's work of genius, "Material and Empirio-Criticism," marked a new epoch in the development of science and has now become part of the standard bookshelf of every materialist-scientists. There remains no doubt but that the influence of this book will far transcend the bounds of the Twentieth Century. Lenin demonstrated that previous concepts held on the structure of matter vary to the degree that our knowledge is enriched and deepened. But, however much our knowledge of the structure and properties of matter undergo change, the fact remains unaltered that matter constitutes an objective reality, existing independently of our consciousness. Pointing to the limitless structural complexity of matter, Lenin at the same time took note of the fact that the capabilities of human reason to reveal the secrets of the world surrounding us is also limitless. Worthy of particular note is Lenin's ingenious prediction of the cleavability of the atom, on the inexhaustibility of the atom and electron, confirmed by the entire subsequent development of nuclear physics.

Lenin taught that philosophy plays an exceptional role in natural science. In his article "On the Value of Militant Materialism," he wrote that it would be impossible for natural science to progress without a philosophical outlook, and that, to successfully cope with bourgeois influence, every natural scientist would have to become a dialectical materialist. This tenet is of decisive importance in the problem of the shaping and development of Soviet science, and has aided the most advanced scientists in struggle against the reactionary idealogy which acts as a brake on the development of scientific thought.

Being himself an outstanding scientist, Lenin grasped the decisive significance of science, terming it the "pride of humanity." From the very first days of the Soviet power, Vladimir Il'ich devoted an enormous amount of attention to science, despite the tremendous burdens weighing upon the leadership of the young Soviet government, then beating off the murderous onslaught of the foreign interventionists and the internal counterrevolution. He felt that science must be of service to the working class, as one of the most important tools for building the new socialist society: "No sinister or ignorant force of any nature will be able to stand up before the union of the representatives of science, of the proletariat, and of technology" (V. I. Lenin, Collected Works [in Russian] Vol. 30, p. 376).

Lenin saw clearly the gigantic possibilities for the development of science presented by socialism – the new social system, since only this system "liberates science from its bourgeois fetters, from its enslavement to capital, from its groveling before the interests of the sordid capitalist greed for profits. Only socialism provides the opportunity for the broad expansion and genuine disciplining of social production and of the distribution of commodities in line with scientific considerations aimed at rendering the life of all the toiling masses comfortable, at providing them with ample opportunity for welfare. Only socialism is capable of achieving this" (V. I. Lenin, Collected Works [in Russian] Vol. 27, p. 375).

A multiplicity of documents: government decrees, letters and notes, speeches and reports, rough copies, and outlines of articles, these attest convincingly to the paramount place which Lenin accorded to science in the development of the productive forces of the country, in carrying out a cultural revolution.

This is most strikingly illustrated by the "Rough draft of a plan of scientific and technological work," embodying a proposal to the Supreme Soviet of the National Economy to immediately authorize the Academy of Sciences to proceed to drawing up a plan for the reorganization of industry and for promoting the economic prosperity of Soviet Russia. The overall problem was tackled concurrently with the concrete content of the plan intended to include a "rational apportionment of industry in Russia" and a "rational ... concentration of productive facilities" (V. I. Lenin, Collected Works [in Russian] Vol. 27, p. 288). Particular attention was given to the electrification of industry and transportation facilitiies, to the use of electricity in agriculture, etc. Thus, having outlined a concrete program of action for the Academy of Sciences under conditions of socialist construction, Lenin defined the fundamental trends of development of Soviet science and technology.

All of the measures envisaged by Lenin could have been realized only on the basis of the latest achievements in advanced science and technology. With the aim of bringing science into closer harmony with the practice of socialist construction, a Science and Technology division was set up under the aegis of the Supreme Soviet of the National Economy. The Academy of Sciences and the Commission for the Study of the Productive Forces of the Nation received the necessary financial means to carry into realization a plan of scientific work conceived on a broad front. Lenin always saw to it that no obstacles of any kind were put in the way of scientific research fraught with great significance for the development of the national economy. The achievements of science and technology awakened a lively interest in Lenin's mind, and attracted his most concentrated attention. Academician G. M. Krzhizhanovskii recalls on this theme: "During his infrequent minutes of leisure which Vladimir Il'ich had available for a simple friendly chat with me, I knew that there existed no better way of drawing Vladimir Il'ich away from his heavy affairs and concerns than a conversation on the latest in science, and particularly a conversation on the general run of conquests registered by technology. And among those conquests, what interested him most, of course, were those achievements which might have some immediate application here among us, in Russia" [The Scientific Worker, Book 1, p. 41 (1925)]. Lenin was intrigued by electrical engineering, radio and electronic engineering, underground gasification of coalbeds, the assimilation of chemistry in production, locomotive construction, aeronautical engineering, and many other branches of technology and engineering.

It is a matter of common knowledge what colossal significance Lenin attributed to the electrification of the entire country. It was on his initiative and with his direct participation that the now famous GOÉLRO plan, the state plan for the electrification of Russia, was drawn up. By electrification of the country, Lenin understood the creating of the material and productive basis of communism, the development of large-scale and above all heavy, industry resting on the most advanced technology and high labor productivity. "Communism," Lenin pointed out, "is the Soviet power plus electrification of the entire country." This remarkable statement is fundamental to the activity of the Communist Party and of the whole Soviet people. It is being successfully carried out in life. Not only powerful steam plants and gigantic hydroelectric stations are being built in our country to generate electric power, but also large nuclear-fueled power stations as well.

In the very heat of the civil war, in the midst of an atmosphere of famine and ruin, Lenin, exhibiting an exceptional farsightedness, correctly evaluated the significance of the Kursk magnetic anomaly (KMA). He wrote: "I am paying attention to the exceptional importance of research work on investigation of the

Kursk magnetic anomaly...we have here what is certainly a source of wealth never before seen in the world, capable of completely transforming metallurgy" (The XXXVI Lenin Symposium [in Russian], p. 466). Lenin's instructions have now been successfully fulfilled, and Kursk ore is being worked into product metal in ever increasing quantities.

At the very dawn of the development of radio, Lenin made an evaluation of its importance, from the vantage points of political value and service to the national economy, and called it an area of work of "gigantic importance." In a letter addressed to the foremost scientist and radio engineer of the time, M. A. Bonch-Bruevich, Vladimir Il'ich stated: "I take the opportunity to express to you my profound gratitude and sympathetic interest for the great work in radio inventions which you are engaged in. A newsparer without paper, and "without limitations as to distances," such as you are creating, will be a great thing. I promise you whatever assistance, and to whatever extent, which can be rendered you in this and similar endeavors" (V. I. Lenin, Collected Works [in Russian] Vol. 35, p. 372). As a result of Lenin's constant personal support, Soviet radio engineering rapidly developed into a great branch of science and technology, and even during the time when Vladimir Il'ich was still alive occupied a leading position in its field in the world.

Lenin always took a deep interest in those achievements of science and technology which held promise of easing Man's labor and raising his living standards. For example, in the article entitled "One of the Greatest Victories of Technology," which dates back to 1913 and deals with the problem of underground gasification of coal, Lenin wrote that this discovery will bring about an enormous revolution in industry since, as a result of underground gasification, it would become possible to save a huge quantity of human labor spent in mining and conveying the coal. While this discovery will inevitably lead to increased unemployment and misery under capitalism, under socialism it will make it possible to immediately cut down the working day for all workers from 8 hours, for example, to 7, or even shorter hours. The 'electrification' of all the factories and railroads will render working conditions safer, will free millions of workers from the fumes, dust, and grime, will accelerate the transformation of the filthy and repulsive sweatshops into clean, bright laboratories worthy of Man" (V. I. Lenin, Collected Works [in Russian] Vol. 19, p. 42). It was only in this way that Lenin conceived of the significance of the latest achievements in science and technology – to serve the interests of Mankind, and not the reverse.

Lenin pointed out the necessity to keep up continually with the scientific and engineering achievements in foreign countries, and to make use of these achievements in the cause of building the new society. It was precisely for that reason that he gave his support to the initiative for setting up a Bureau of Foreign Science and Technology under the auspices of the Science and Technology division of the Supreme Soviet of the National Economy. Lenin likewise suggested sending scientists and engineers abroad to study experience accumulated in other countries and to assemble the literature on the latest scientific and engineering achievements, for the purpose of putting these to immediate use for the successful creation of the new socialist economy.

Lenin placed high significance on the development of international collaboration in science and technology. This is attested to the notes Lenin added to the letter of G. V. Chicherin, People's Commissar of Foreign Affairs, on the Soviet proposals for the Genoa conference (cf. Lenin symposium XXXVI [in Russian], p. 452).

In fulfilling Lenin's legancy, the Soviet Union strives for international technological collaboration on a broad scale, including in the field of peaceful uses of the atom: "We are ready to collaborate with all peoples in the cause of the peaceful uses of atomic energy, and it would please us if this appeal were taken up by all other governments" (from the reply by N. S. Khrushchev to the letters and telegrams received in connection with his trip to the USA, in "Pravda" dated September 15, 1959). The most shining example of international scientific and technological cooperation in the peaceful uses of atomic energy is the activity of the Joint Institute for Nuclear Research, at Dubna near Moscow. At this Institute, scientists of 12 nations are joining their efforts in common work on the investigation of the atomic nucleus. The Soviet Union has provided the Institute with equipment unique in its kind, including elementary-particle accelerators of 680 million and 10 billion electron-volts.

Striving to reach the stage where the blessings of the peaceful atom might become the property of the many, the Soviet Union is voluntarily assisting many nations to set up their own scientific-research nuclear centers, turning over to them equipment, instruments, research reactors, accelerators, isotopes.

In consonance with Lenin's legacy, Soviet science has scored tremendous successes. N. S. Khrushchev, at the Twenty-first Congress of our Party, stated the following: "Soviet scientists, designers, engineers have brought great merits to our Homeland, and are making a worthy contribution to the cause, common to all our people, of the building of communism" (N. S. Khrushchev, On the Control Figures for the Development of the National Economy of the USSR for 1959-1965 [in Russian] (Gospolitizdat, Moscow, 1959) p. 12.

Soviet scientists and engineers have scored outstanding successes in the area of research, transformation, and peaceful uses of atomic energy. The achieve-

ments of nuclear physics are notable. Much progress has been recorded toward the solution of the grandiose and exceedingly difficult problem of bringing about a controllable thermonuclear reaction. The world's first nuclear-fueled electric power station went on line in the USSR, and other, bigger power stations are on line or being built. The world's first nuclear-powered icebreaker, the "Lenin," is on the seas. Radioactive and stable isotopes are commonly used throughout the national economy.

The outstanding victory of Soviet science and technology is constituted by the artificial earth satellites, the orbiting of the first artificial planet of the solar system, the launching of the space rocket which planted the Soviet pennant on the moon, the photographing of the far side of the moon, and many other great achievements bearing witness to the astounding successes of Soviet science, whose pathways and perspectives were traced out in advance by Vladimir Il'ich Lenin.

DESIGN OF THE VVR-S RESEARCH REACTOR

V. F. Kozlov and M. G. Zemlyanskii

Translated from Atomnaya Energiya, Vol. 8, No. 4, pp. 305-315
April, 1960
Original article submitted, December 26, 1959

A water-cooled, water-moderated reactor for facilitating scientific research endeavors on applications of nuclear energy in peaceful pursuits has been built in the Soviet Union.

Such reactors are currently completed and in operation in the Soviet Union and in other Socialist countries. Six such reactors were put into operation during 1957-1959; five reactors (four of which are built to handle power surges) are in the stage of preparation, assembly, and start-up tests.

This article describes the design of the VVR-S reactor and its experimental facilities. The physical characteristics of the reactor have been described in an earlier paper [1].

Experimental Possibilities Inherent in the VVR-S Reactor

This nuclear reactor was designed to produce neutron flux levels of $\sim 2 \cdot 10^{13}$ neutrons/cm^2 · sec. It has high enough excess reactivity to facilitate research work [2] as well as the production of radioactive isotopes. Eight channels 40 mm in diameter plus one dry channel 60 mm in diameter in the core are provided for those purposes, in addition to twenty channels 60 mm in diameter in the displacement rods positioned in the core at the start of the reactor run.

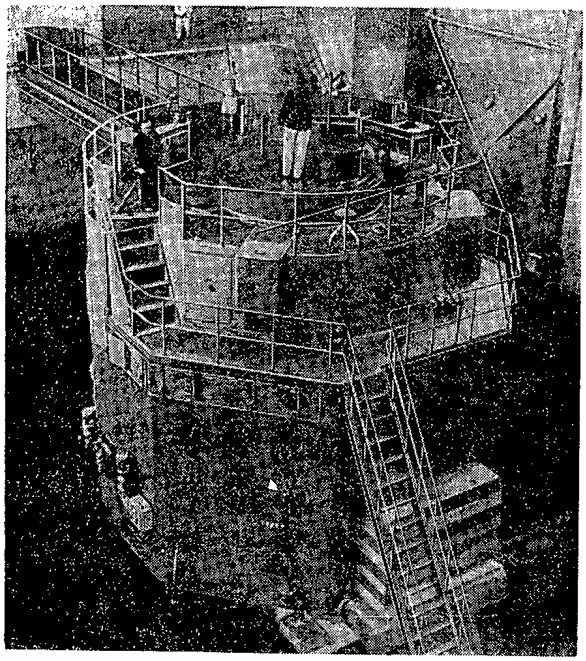

Fig. 1. General view of the VVR-S, seen from the direction of the thermal column.

Nine horizontal channels (opened or shut off by gate valves) lead toward the periphery of the core, and of these nine, six channels are 100 mm in diameter and the remaining three are 60 mm in diameter. In addition, a trolley-track thermal column with four vertical channels 80 mm in diameter, connected up to a horizontal channel 100 mm in diameter, is led to the core periphery. The horizontal channel of the thermal column is opened or shut by a manually operated gate valve. The gate valve is housed in a cast-iron shielding.

All of the vertical and horizontal channels are serviced by special-design manipulator devices. Three biological channels 350 mm in diameter and four monitoring channels 80 mm in diamter are placed in the concrete shielding zone of the reactor.

The possibility of installing two experimental loops in the reactor core was provided for in the design of the reactor vessel.

Basic Reactor Data

The VVR-S reactor (see Fig. 1) has the following basic characteristics:

Thermal power, kw	2000
Peak thermal flux, kcal/m^2 · hr	$0.44 \cdot 10^6$
Number of fuel assemblies:	
at start of run	31
at end of run	51
Flowrate of primary-loop distillate, for cooling core, m^3/hr	650
Flowrate of secondary-loop technical-grade water, for cooling distillate, m^3/hr	250-300
Fuel loading, kg U^{235}	
at start of run	4
at end of run	5.6

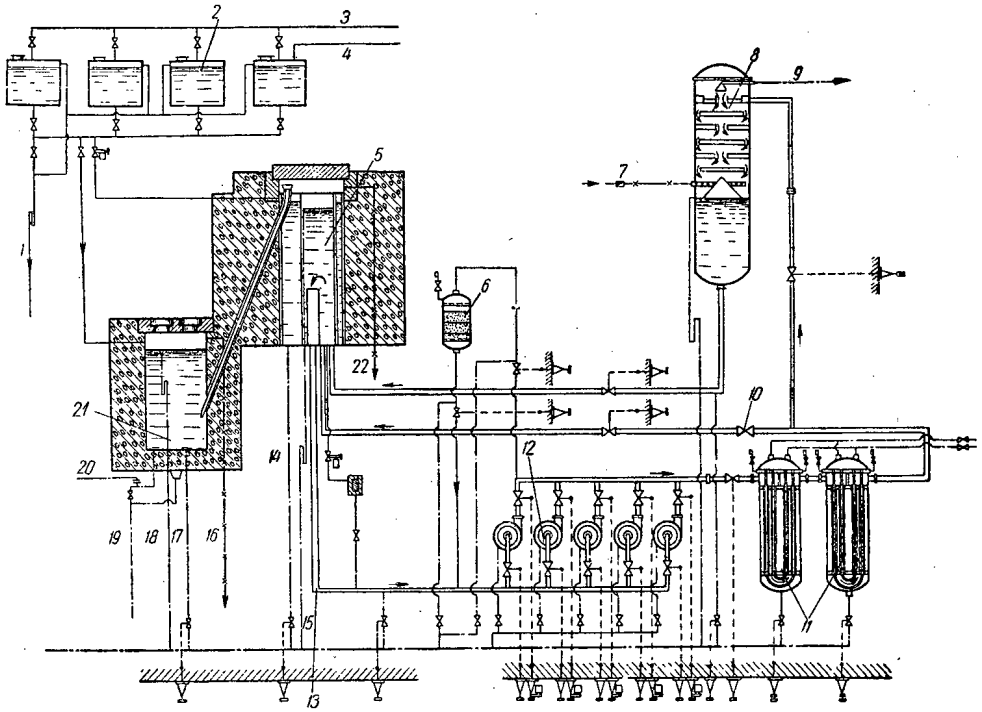

Fig. 2. Overall flowchart of the reactor system. 1) Downflow to drainage system; 2) distillate tanks; 3) distillate line; 4) process water; 5) reactor; 6) filter; 7) air from main room; 8) deaerator; 9, 16, 22) venting ducts; 10) throttle valve; 11) heat exchange units; 12) pumps; 13) headers; 14, 17) downcomers; 15, 18) overflow ducts; 19) to drainage system; 20) to tank-level indicator; 21) graveyard for used fuel assemblies.

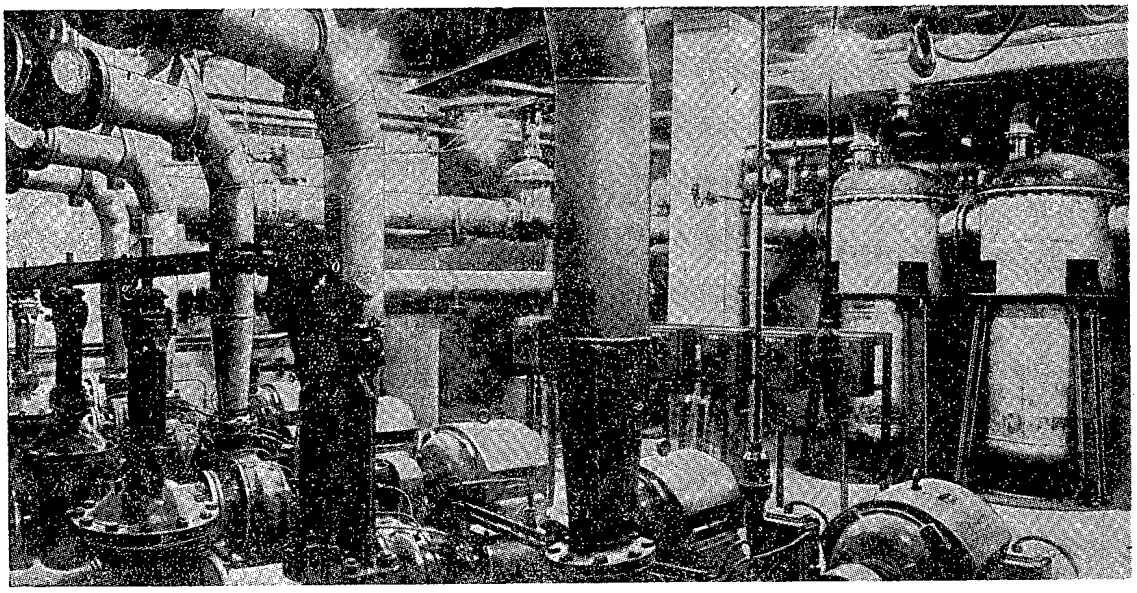

Fig. 3. View of the reactor pump house.

Water, cast iron and concrete (ordinary and heavy) were used for radition shielding. For reactor shielding in the radial direction, water (800 mm), cast iron (200 mm), and concrete of 3.2 g/cm^3 density (1600 mm) were employed. At points where piping, ducting, and ventilation facilities were passed through the shielding, lead and cast-iron reinforcements were installed. The protective layer of water was 3.5 m deep over the core and 1.15 m under the core. 800-mm-thick cast-iron disks were also used for top shielding.

To avert the spreading of radioactive air and vapors, the space above the reactor, the space below the reactor, and the space above the fuel-element storage tank are ventilated by means of a constant rarefaction established in those volumes.

The reactor loading made for an excess reactivity $\Delta k = 0.05$. Compensation of reactivity and reactor control are carried out by control rods, some of which function as scram rods.

Flow Scheme of the Primary Reactor Loop

A flowchart of the entire installation is shown in Fig. 2.

Distillate is heated from 34° to 36°C in the reactor core. Centrifugal pumps take care of circulation of the distillate. Heat transfer from the distillate to the water flowing through the secondary loop takes place in two heat exchanger units (each with a surface area ~95m^2). Filters are employed to clean up the distillate and remove fission fragments. Cation and anion exchangers and activated charcoal are used in the filter system. These sorbents undergo special processing prior to incorporation into the filter. The filter is placed in the loop only periodically, when activity due to fragments appears in the distillate.

To remove explosive gas mixtures forming during the operation of the reactor, a deaerator is provided, with up to 10% of the total flow of distillate being pumped continuously through the facility.

Figures 3 and 4 give some idea of the arrangement of ancillary equipment serving the primary loop. Most of this equipment is placed underground in the basement section protected by thick shielding walls.

The reactor room is built for easy accessibility and safe maintenance of the equipment, as well as automatic compensation of the ducts and piping.

The pumping units are placed well below the level of the reactor, to provide head in the suction tube, and to eliminate cavitation during pump performance, which leads to reactor power surges.

Dump valves and slide valves are manually operated, to avoid random errors on the part of the service personnel, so that an accidental opening of the draining facilities, possible where electrically actuated valves are used, may be averted. An error of this type would lead to loss of water from the reactor, and in turn to severe damage due to residual heat release.

The heat exchangers are set up vertically, so that they may serve a concurrent function as traps for mechanical impurities in the loop. The distillate in the b bottom of the exchanger flows at low speed and changes direction abruptly, a circumstance which favors the settling out of such mechanical impurities. The impurities are removed by periodic drainage and routed to a waste tank.

In order to control distillate flow through the deaerator within the loop (downstream of the heat exchangers), a special throttling device, remote-controlled from a local control post and from the operator console (Fig. 2), was installed. The design of the throttling device excludes the possiblity of the piping becoming overloaded, since a rapid total overloading such as occurs when electric-relay controls are relied upon may result in waterhammer.

To avoid any overflow when the reactor tank is being filled with distillate or when makeup is being added, overflow ducts are built in above the present level (an overflow might result in the distillate gaining access to the ionization-chamber channels and gate valves, with the ionization chambers being rendered inoperative and gate-valve parts becoming subject to corrosion). When the deaerator is on, the distillate level in the reactor tank is lowered, for which reason distillate makeup is added to the reactor tank to reach the present level only when the pumps are shut off, i.e., when circulation in the loop is cut off. The pipe cross sections in the auxiliary loop and overflow ducts are calculated such that the overflow ducts are cut out of the system when circulation stops. To avert formation of condensate on the cast-iron shielding roof, and to keep condensate out of the ionization chambers, a certain degree of rarefaction is maintained above the reactor tank.

Reactor Design

The reactor subassemblies and mechanisms are assembled on a baseplate and support structure (Fig. 5). The use of such intermediary elements (i.e., baseplates and support structure) has made it possible to completely assemble the reactor, to run-in individual parts and assemblies, to make final adjustments of mechanisms and devices, and to freeze the relative positions of the various subassemblies, all under factory conditions prior to installation. This resulted in appreciable simplification of the work in installing the reactor in situ, eliminated the need for concrete shielding as a structural element during the assembling operation, and enhanced the quality and efficiency of the assembling operation while cutting down on assembly time. This solution in design made it possible to standardize the reactor type, to carry out the assembling operation successfully, and to put a series of reactor facilities into operation. Figure 6 shows the assembling of the

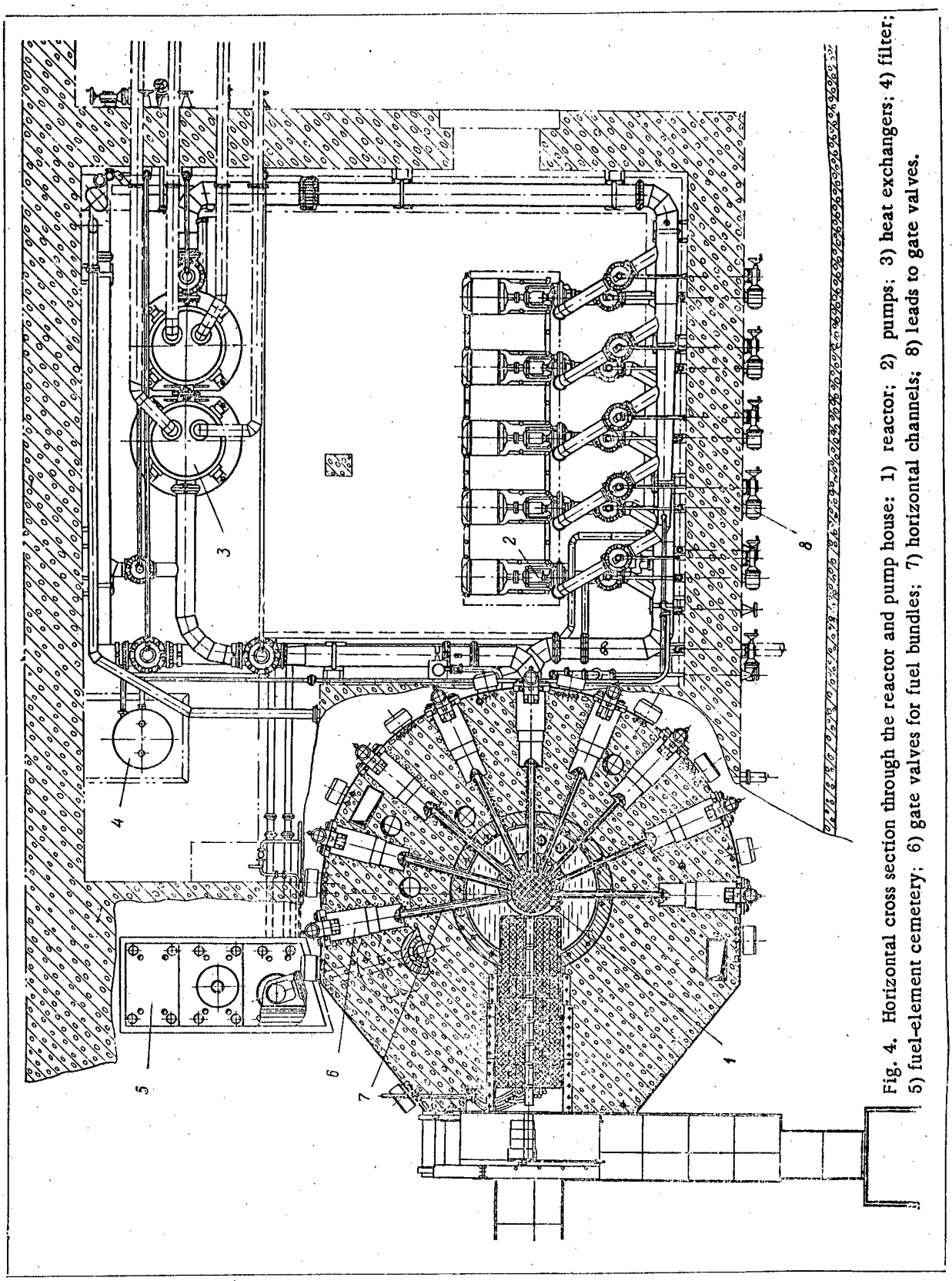

Fig. 4. Horizontal cross section through the reactor and pump house: 1) reactor; 2) pumps; 3) heat exchangers; 4) filter; 5) fuel-element cemetery; 6) gate valves for fuel bundles; 7) horizontal channels; 8) leads to gate valves.

reactor, on baseplate and support structure, under shop conditions.

The reactor core is housed in a tank measuring 2.3 m in diameter and 5.9 m high, made of aluminum alloy. The tank also accomodates experimental channels and transporting chutes (Fig. 7), plus the control rods.

The tank consists of three cylindrical shells welded to a spherical bottom, and two removable tops. Use of a middle shell allowed the further possibility of reducing coolant volume in the loop, while at the same time reducing the capacity of the discard tanks into which fouled coolant is drained off in the event that the hermetic sealing of the fuel-element jackets is damaged. Into the tank are welded: nine horizontal channels (see Fig. 4), a recess accomodating the forward disks of the thermal column, and seven vertical straight-through channels designed for experimental purposes, for transporting irradiated samples into the hot cells, and for housing experimental loops. The inclined tube of the transporting chute (see Fig. 7), with an I.D. of 200 mm, is welded into the tank, to carry fuel-element assemblies into the spent-fuel graveyard. Welded into the tank bottom are the overflow, drainage, and circulation ducts, as well as tubes for control and measuring instruments. Housed at the top of the tank are: an X-shaped bracket supporting the nine vertical channels for the control rods, irradiated-sample channels, two channels for preliminary charging of fuel-element assemblies, and seven channels to accomodate ionization chambers.

On the baseplate rests: the support structure, consisting of some cast-iron rings at the bottom, an outer shell, and cast-iron rings at the top, gate valves for the horizontal experimental channels, with supporting struts, beams supporting the pipework, and a trolley track servicing the thermal column. The cast-iron rings of the foundation unit were included primarily to reduce radiative heat release inside the concrete. A large rotating lid is built into the top of the support framework (cf. Fig. 5), fulfilling the function of supplementary top shielding for protecting personnel from radiation. The lid is rotated both manually and by electrical power. A smaller hand-operated lid is placed within the larger one, eccentrically. Manipulating devices and optical equipment are mounted on the smaller

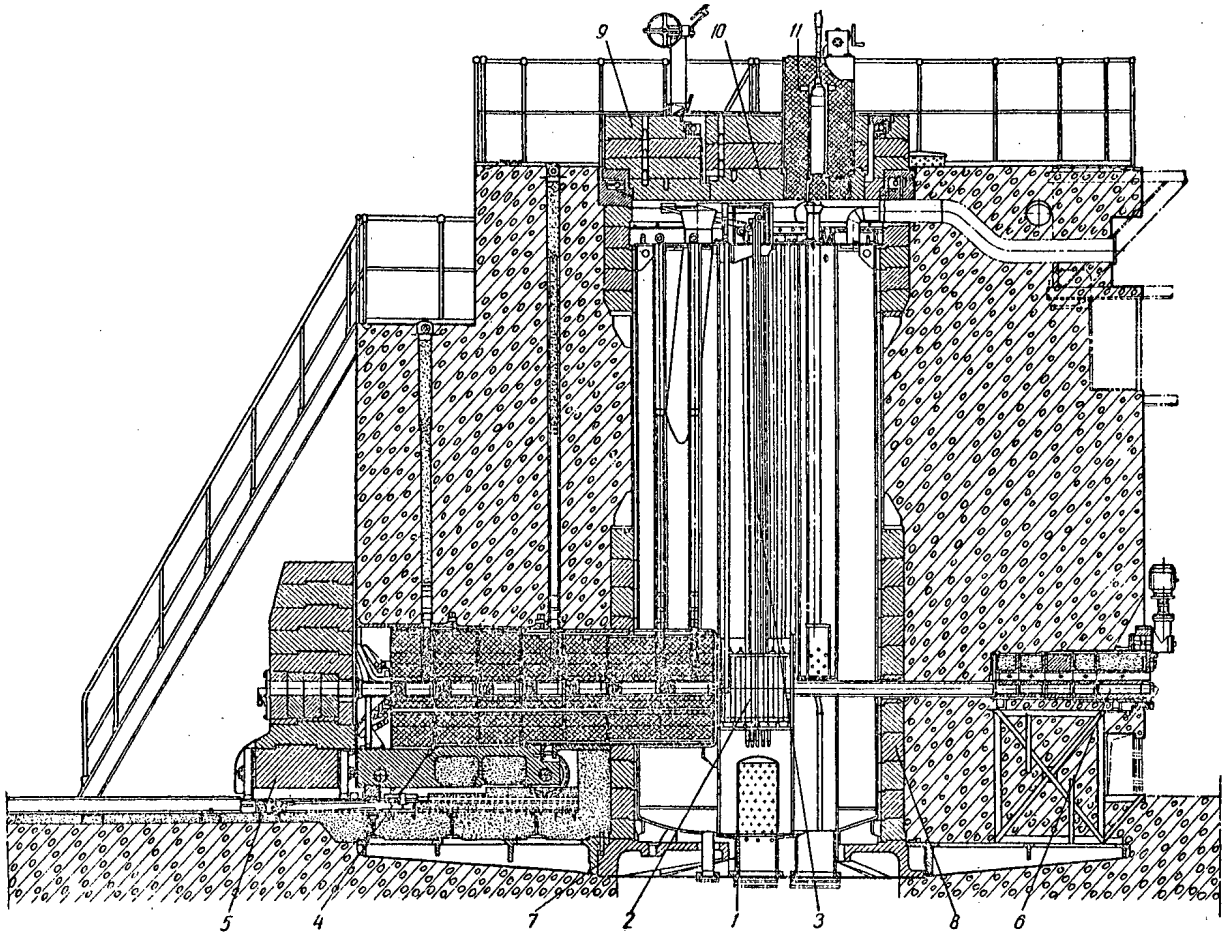

Fig. 5. Crosss section through the reactor at thermal-column depth: 1) reactor vessel; 2) reactor core; 3) control-rod channels; 4) thermal column; 5) shielding for thermal column; 6) gate valve; 7) baseplates; 8) support structure; 9) rotating upper lid; 10) smaller rotating upper lid; 11) fuel-element coffin.

lid while the reactor is in operation(cf. Fig. 7), as well as the fuel-element coffin (cf. Fig. 5), which is used to transport fuel assemblies when the core is unloaded manually.

The supporting structure of the reactor is encompassed by concrete shielding, in which rest the inclined transporting chute (dump chute) with cast-rion shielding, an experimental channel for the thermal column, channels for storing probes and optical equipment, ducts, air vents, electric switchbox, laboratory-type box for electric cabling, drainage and telemetering tubes serving the control and measuring instruments, and health-physics instrumentation. The thermal column, covered on its side by movable cast-iron shielding (cf. Fig. 5), passes through a space not used for tubing or pipework.

The upper portion of the reactor concrete shielding is lined with stainless steel. Brackets on which mechanisms for positioning removable and fixed ionization chambers and control rods are mounted (Fig. 8) fit into the upper openings through this shielding.

Control System and Shielding Mechanisms

Five manually controlled rods serve to compensate excess reactivity, three rods act as scram rods, and one is used to automatically sustain the present power level.

The automatic-control rod is made of boron steel, while the remaining rods are made of boron carbide. The rods are arranged crosswise in the core. Each rod is placed with its guide tube between the fuel-element assemblies. Cabling leading from the control rods to the servo actuators runs in bundles having a cross configuration. This arrangement groups the control-rod servoes in three distinct spots for assembly. By this means, mechanized loading and unloading of the reactor core is made possible, and optimum conditions are created for maintenance of the servomechanisms and protection of the cable transmission from harmful external effects. The rod positions are controlled by position sensors.

Seven ionization chambers, KNT-52 type, are installed in the reactor tank to monitor reactor power levels during startup and steady-state operation.

Three ionization chambers (triggered) are connected by cabling to three servomechanisms and may be arranged vertically. The position of the ionization chambers is controlled by position transducers and indicators. Four ionization chambers (continuously operating) are positioned at specified heights relative to the core.

For accurate determination of the change in reactivity when different materials are introduced into the core, a precision servo-actuated control rod was designed (Fig. 8). The linear velocity of displacement of this precision rod is 2 mm/sec. At its extreme upper and lower position, the electric motor of the servo drive unit is shut off by limit microswitches mounted inside the position transducer.

The emergency scram rod falls into its lowest position, impelled by a compressed spring and by its

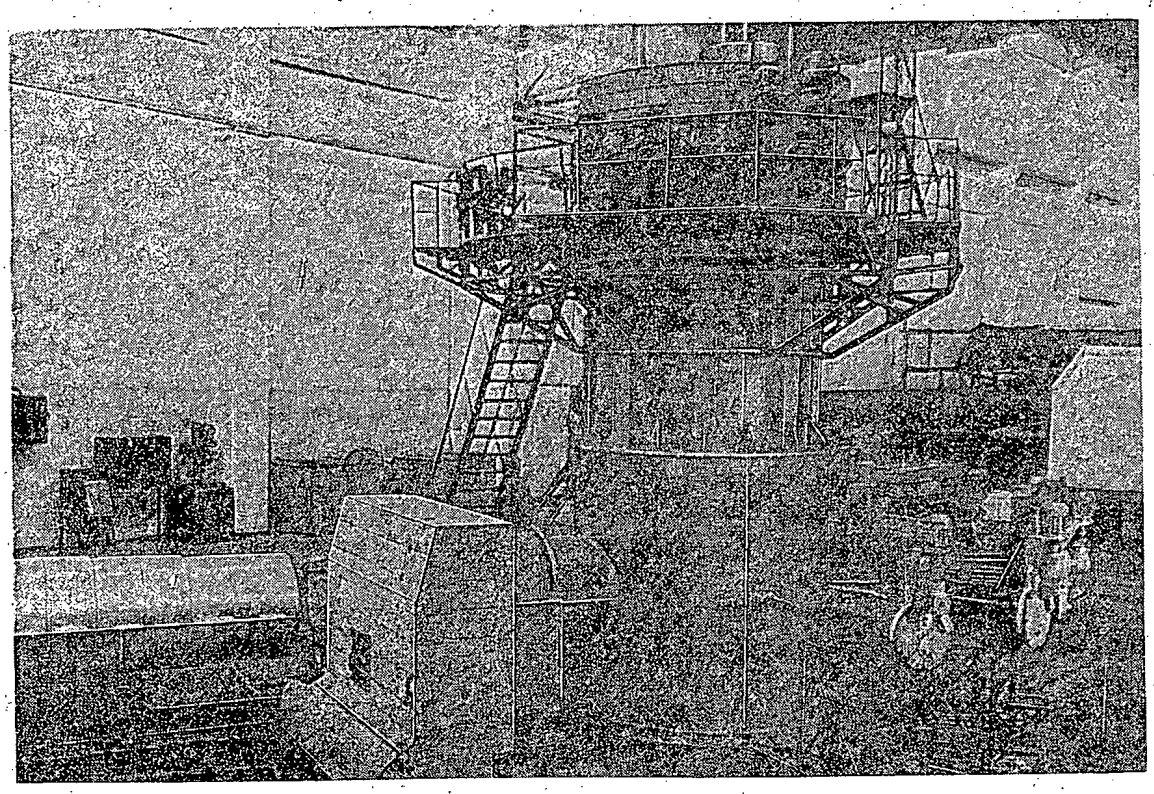

Fig. 6. Assembly of reactor under shop conditions.

own weight, within 0.2-0.3 sec after the appropriate signal is transmitted. At the low end of its travel, the rod is braked by a friction coupling housed in the servomechanism, which softens the impact of the rod against the cabling system and the drum portion of the servomechanism.

The servomechanism serving the emergency scram rod is coupled to its electric motor by a friction clutch which protects the cable transmission against sharp blows and overloading in case the upper limit switch should fail to function. A manually operated servo drive provides a choice of two linear velocities for the rod: a normal operating speed (6 mm/sec) and an emergency scram speed (37 mm/sec); the servo automatic-control drive moves the rod at a speed of 6 mm /sec when operated manually, and can step up the speed to 35 mm when operated by automatic control.

Unloading and Reloading of Reactor Core

A system of mechanisms consisting of two rotating lids (one larger, one smaller nested in the former), servocontrolled manipulator outfit, transportation chutes for the fuel assemblies and specimens, optical viewing equipment, and illumination is employed, to facilitate removal and recharging of fuel assemblies and specimens from and into the reactor. The manipulator equipment may be set up above any coordinate point to be serviced, by proper use of the rotating lids. All of the points to be serviced have their angular coordinates, recorded in tabular form, indicated on the rotation mechanisms of the lids. The manipulator system may be used to remove the fuel assemblies from the core to shift them to the spent-fuel graveyard, and to remove irradiated specimens to forward them to the hot cells. Changing of fuel is carried out inside the reactor vessel without removing the protective lids. This procedure eliminates the hazard of radioactive contamination of the reactor top or irradiation of per-

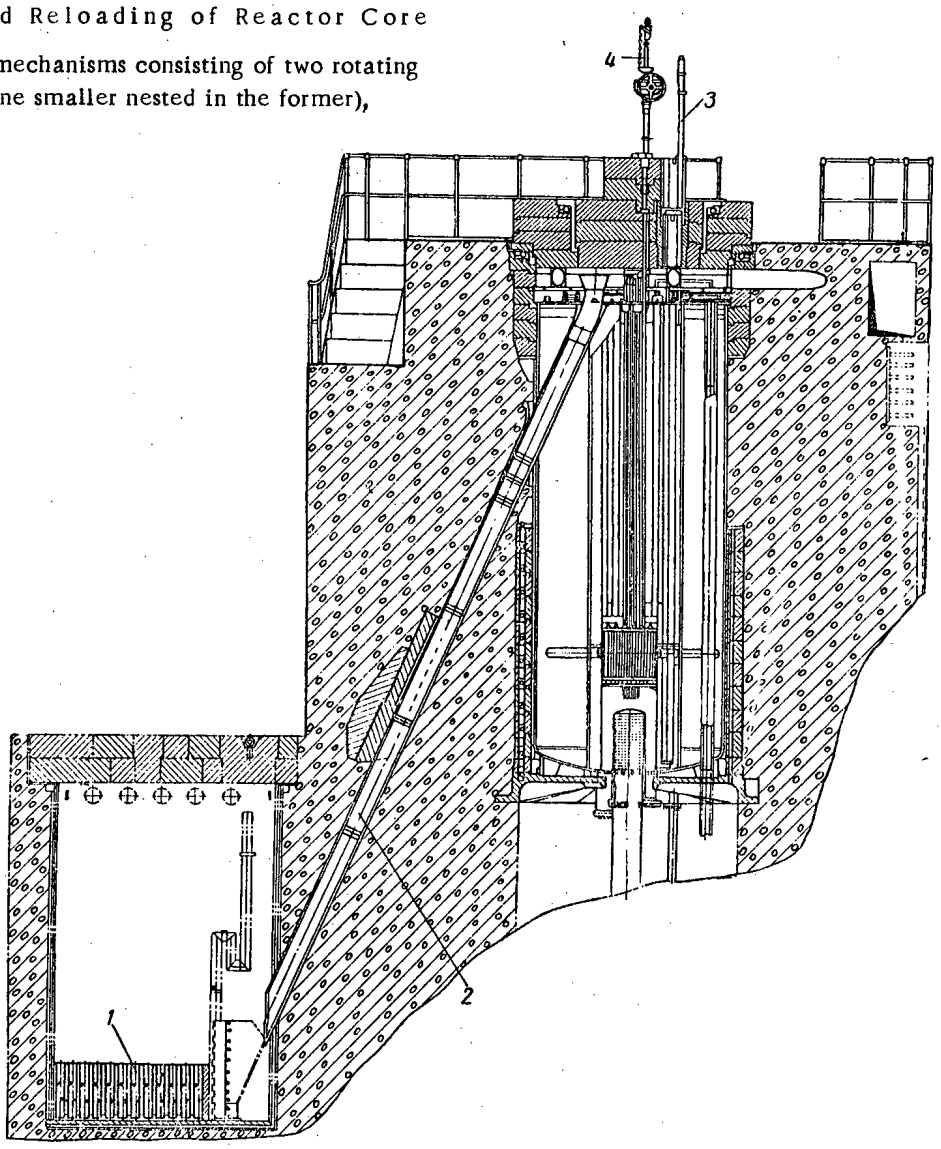

Fig. 7. Cross section through the reactor at the depth of the fuel-element dump chute: 1) fuel-element graveyard (storage tank); 2) dump chute for spent-fuel assemblies; 3) optical viewing equipment; 4) manipulating devices.

sonnel. Charging of fresh fuel-element assemblies and specimens is carried out by the same mechanisms, with the use of supplementary channels for preliminary charging.

The manipulator unit incorporates a long rod with grips, a servo control for the grips, and a servo for elevating and lowering the rod. The unit is mounted in a special packet forming part of the smaller lid, but is in position only during recharging or unloading.

Optical equipment is available for viewing the central portion of the reactor. This equipment consists of shielding plugs and an optical viewing device. To secure better observation during charging and unloading of fuel assemblies, the central portion of the reactor is illuminated by a movable automobile headlight.

Gate Valves

The shielding gate valves (cf. Figs. 4, 5) are designed for opening and closing nine horizontal experimental channels, which are fully closed by the valves only after a successive rotation of five shielding disks through a certain angle. To avert a direct beam of radiation emerging through the valve opening, the valve jacket, valve pocket, and valve axis are designed to vary stepwise, while the valve disks are of different diameters.

The disks are rotated by an electric motor, through the intermediary of a planetary reducing-gear transmission. When the gear transmission and the electric motor are shut off, rotation may be carried out manually. The gear transmission is coupled to the disks via the toothed rim of the forward disk. At the terminal positions of the forward disk, the electric motor is automatically shut off by microswitches and the corresponding annunciator lamps are switched on. An appropriate opening is provided in the valve bonnet, for mounting a collimater in the forward disk.

The gate-valve design as described here has also found application in other reactors, viz. the IRT-1000 and the VVR-2.

Thermal Column

The thermal column (Figs. 4, 5) consists of a trolleyway with a trolley, five removable graphite disks, and a cooling facility consisting of eight Field tubes and a system for delivering and removing coolant water. The trolley rides on rails. Graphite disks integral with aluminum cylindrical drums have one central (axial) and four vertical openings, which constitute experimental channels for physical experiments. The channels are covered with graphite plugs. The outside of the thermal column is fitted with cast-iron biological

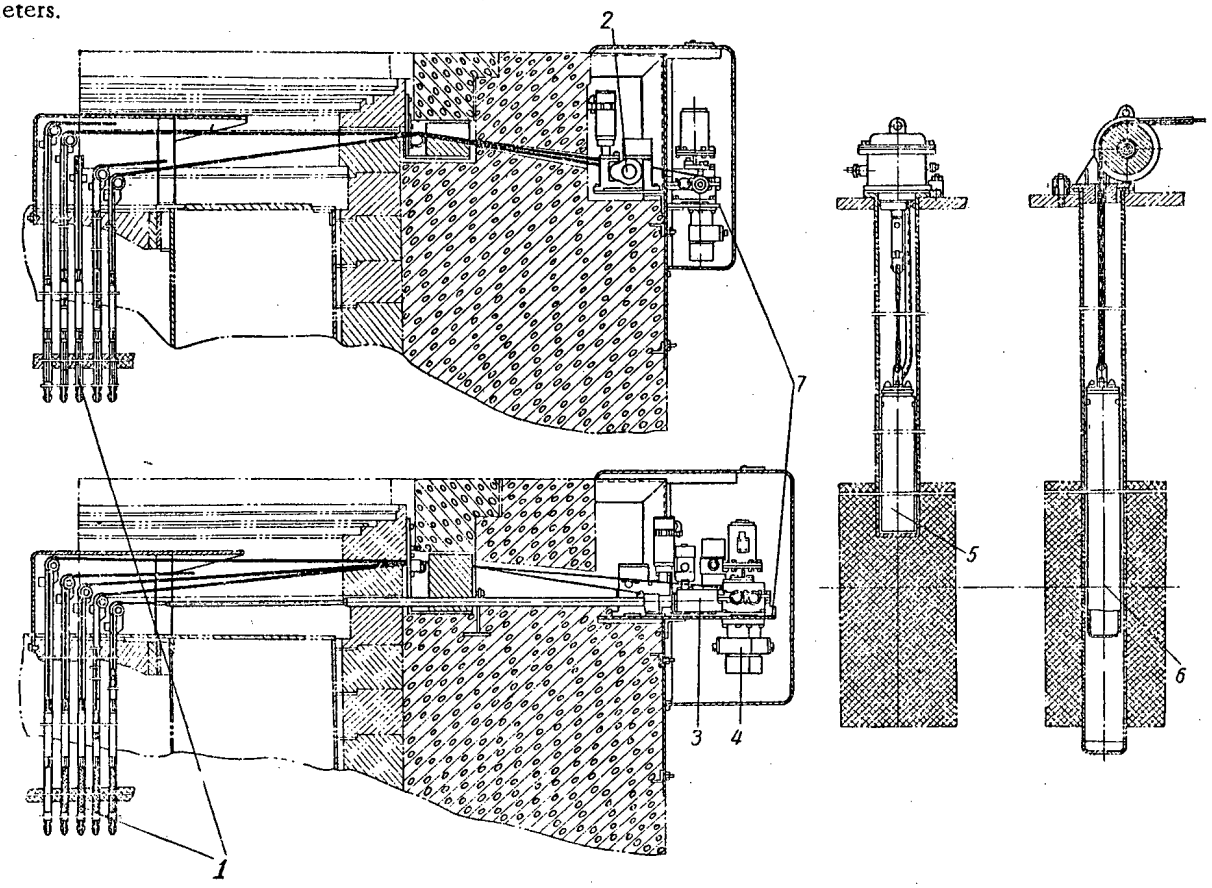

Fig. 8. Lengthwise cross sections showing control and shielding systems: 1) control rods; 2) scram-rod servo; 3) precision servo; 4) automatic-control servo; 5) ionization chamber fixed in place (continuously operating); 6) ionization chamber movable up and down (functioning when triggered); 7) support bracket.

shielding. The gate valve serving the central channel is mounted within this shielding, along the axis of the thermal column. This valve is operated by hand. The thermal-column shielding is placed on rails and may be run down the rails by means of a winch and wire rope. On reaching the extreme positions of their travel, the thermal column and shielding are brought to a halt by limit switches with annunciator lamps connected to them, and the limit switches switch the electric motor to a reduced number of revolutions and switch on timers to disconnect the electric motors from the power supplies.

After the thermal column is rolled out, the recess into which it fits is covered over with the cast-iron shielding. Control of the motion to and fro of the thermal column and cast-iron shielding may be carried out by remote control from two points inside the reactor room. When the thermal column is being rolled back into place and the cast-iron shielding is replaced, these units are driven in till they meet limit stops, and come to rest in their thermal positions within a tolerance of 0.1 mm. This assures that the vertical channels of the thermal column will be aligned with the vertical channels of the reactor, and that the horizontal reactor channel will be aligned with the channel in the cast-iron shielding.

The Fuel-Element Graveyard

The graveyard (cf. Figs. 4 and 7) for the spent fuel elements or failed fuel elements is designed especially for that purpose. The bottom of the tank contains a bay with 60 equally spaced cells for accomodating the assemblies. When fuel assemblies are being put into place, the graveyard is illuminated by an underwater floodlamp. The inclined transporting chute down which the fuel-element assemblies are transferred from the reactor to the graveyard dips into a receptacle in the graveyard tank bottom. To avert deformation of the fuel-assembly casing as the assemblies are being discharged down the chute, the walls and bottom of the receptacle are rubber-coated.

Welded into the graveyard tank are tubes for delivering distillate, a dump pipe, and tubes for the control and measuring instruments. Cast-iron plates covering the graveyard on top are fitted with two openings through which fuel assemblies may be extracted or shifted in position. These openings are plugged. The upper cavity of the tank is ventilated.

Test-stand Performance of the Equipment

In view of the fact that the design project worked out here had to serve as basis for the simultaneous construction of a series of VVR-S type reactors, and that most of them are to be built outside the USSR, a good deal of attention was given to the performance of separate subassemblies and reactor parts on the test stand.

The following tests were performed on test stands, and the following phenomena were noted:

1. The hydrodynamic characteristics of the core were tested; the flowspeed and flowrate of the distillate was determined in three throttled-flow regions (corresponding to predicted radial patterns of heat release). Severe vibration of the hydraulic test stand was observed, simulating the response of the reactor vessel. However, after the point where the distillate gains access to the reactor vessel was fitted with a conical cap, this vibration came to a halt.

2. Owing to an insufficient number of radial openings in the walls of the channels carrying the distillate used to cool the rods, air is drawn into the primary loop through the control-rod channels. The presence of air in the loop may lead to power surges and improper functioning of the pumps. This suction of air into the loop was eliminated by increasing the number of such openings in the walls of the reactor control channels.

3. The pressure seals were adjusted and the pump characteristics were recorded.

4. It was noted that, when the distillate flowrates through the core surpassed 1500 m^3/hr, the walls of some of the fuel-element assemblies were being deformed on the inside, because of a loss of static pressure inside the assemblies.

5. The fuel-assembly transport chute and the receptacle for the fuel-element graveyard were performance-tested. It was found that protruding areas on the contact surfaces and rough spots due to dents in the inner surface of the fuel-element dump chute resulted in deformations and scoring of the outer surface of the fuel-element assemblies. Removal of these protrusions and rough spots eliminated fuel-assembly damage as the assemblies were dumped into the graveyard.

6. The operation of the manipulator equipment and the loading and unloading operations of the fuel-element assemblies and specimens for irradiation into and out of the core were checked out. These operations call for proper training of operating personnel.

7. Neutron-physics core parameters were determined [1].

8. The scram system servomechanisms were checked out by repeated operation of the scram rods. The scram-rod servo, for example, held up well under testing with 2000 drops of the rod. The friction-braking unit performed normally. The spread of terminal positions of the rod was found to remain within a range of 5-12 mm.

9. The gate valve was performance-tested for accuracy of alignment of channel disks upon opening of the valve. Channel alignments to within 0.05 mm were obtained as a result. Sharp impacts were recorded as the gate valve was opened or closed. These impacts caused deformation and malfunction of the main disk coupling designed to take the thrust. This phenomenon

might be eliminated by balancing the disks, but this would incur a penalty of excess metal in the valve (with attendant deterioration of the protective properties of the gate valve and a sharp increase in the gamma background in the neighborhood of the valves). Only the two middle disks of the valve were balanced for opening and closing of the valve, to set up a constant torque. The gate valve was run through 2000 cycles of alternate opening and closing.

Reactor Power Excursions

The VVR-S reactor facility design takes into account the possiblity of power excursions. To cope with power excursions, the reactor is provided with reinforced biological shielding to combat neutron and gamma radiations (940 g/cm^2), and stand-by and back-up equipment is liberally provided for.

In order to reduce the amount of heat released inside the concrete shield, cast-iron rings with 14 vertical openings for cooling of the shielding were included in the design of the support structure. All of these precautions allow for handling a power surge up to 10-20 thousand kw, provided the heat-release surface and heat-transfer coefficient α are increased.

Two such reactors with power-excursion provisions are in the stage of start-up and performance testing.

LITERATURE CITED

1. N. A. Lazykov, I. E. Chelnokov, and V. P. Ivanov, Atomnaya Énergiya 5, 1, 44 (1958).*
2. Yu. G. Nikolaev, Geneva 1955, International Conference on the Peaceful Uses of Atomic Energy [in Russian] (Izd. AN SSSR, 1957) Vol. 2, p. 469.

* Original Russian pagination. See C. B. translation.

ION CYCLOTRON RESONANCE IN DENSE PLASMAS

L. V. Dubovoi, O. M. Shvets, and S. S. Ovchinnikov

Translated from Atomnaya Énergiya, Vol. 8, No. 4, pp. 316-323,
April, 1960
Original article submitted May 4, 1959

The possibility of heating a plasma by means of the ion cyclotron resonance is investigated. It is shown that in plasmas with charged-particle densities of $10^7 - 10^{11}$ cm^{-3}, the use of short (compared with the length of the pinch) heating sections mades it possible to weaken the effect of transverse ionic polarization fields by virtue of the motion of electrons along the lines of force of the external magnetic field. In a low-ionization plasma the efficiency of transfer of energy from the rf field to the ions is reduced as the ion velocity increases; this reduction is due to cooling of the ions by neutral atoms.

Introduction

In this paper we present the results of experiments undertaken to investigate the possibility of heating a plasma by rapidly varying electromagnetic fields. Heating based on ion-cyclotron resonance has been studied; this mechanism is of special interest because of the possiblity of direct transfer of energy from the rf field to the ion. In spite of its apparent simplicity, this method actually involves a number of difficulties; to a considerable extent the practicable utilization of this method depends upon the degree to which these difficulties can be overcome. Thus, an investigation of the properties of a hydrogen plasma in the region of the ion-cyclotron resonance [1] has verified the possiblity of heating the ionic component of the discharge to temperatures of the order of several kilovolts at charged-particle densities smaller than $10^8 - 10^9$ cm^3. A further increase in density causes a sharp reduction in heating efficiency because of the appearance of internal plasma fields due to ion currents. The results of these experiments are in agreement with the calculations carried out in [2], according to which the criterion for the appearance of polarization effects in the region of the cyclotron resonance is that the inequality $\omega_0^2/\omega^2 < 1$ is not satisfied, (ω_0 is the ion Langmuir frequency and ω is the heating generator frequency).

In accordance with the basic assumptions of the analysis [2], in the experimental work reported in [1] the discharge tube defining the plasma geometry was placed in a spatially uniform radio-frequency electric field (the analysis is based on the model of an infinite plasma cylinder in an oscillating field which is uniform in the axial direction). In configurations of this type, with magnetic field strengths of $10^3 - 10^4$ gauss, it is difficult to heat plasmas with densities greater than 10^9 cm^{-3} because of the strong skin effect; because of the skin effect the external rf field can intereact only with ions close to the surface of the plasma column.

Only one of the possible means of reducing the effect of plasma self fields is indicated in [3]. This method consists of choosing a spatial distribution for the rf heating field such that the space charge produced by the transverse ionic currents is compensated by the motion of the electrons along the lines of force of the external magnetic field. The simplest system of this kind is an infinitely long cylindrical plasma in a longitudinal magnetic field with heating sections in the form of a short solenoid or a condenser. [4]. The ionic polarization fields arising within the heating section are neutralized by the longitudinal displacement of the electrons.

According to the analysis of [3] the inequality $\omega^2_0/\omega^2 < 1$, which governs the appearance of polarization effects in a plasma in a uniform rf heating field, becomes $\omega^2_0/k^2c^2 < 1$, for a nonuniform field; here, k is the wave number which corresponds to the wavelength equal to twice the dimension of the heating section in the longitudinal direction and c is the velocity of light

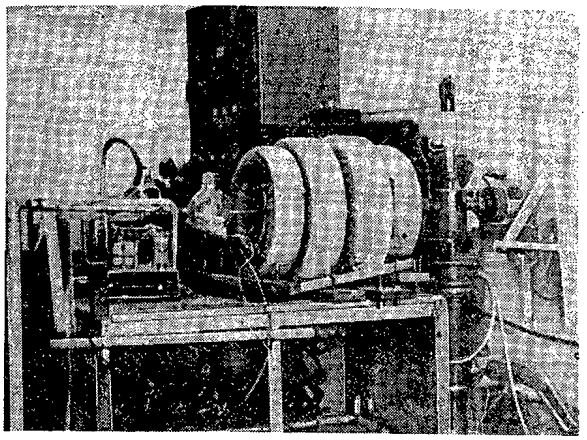

Fig. 1. External view of the apparatus.

in vacuum. Calculations show that for a section 10 cm in length the skin effect is important only at densities greater than 10^{14} cm^{-3}. This result indicates the advantage of this type of system.

In this paper we report the results of an investigation of various methods of introducing rf energy into the plasma in which this method is used.

The rf power source in this work was a generator with a power output of several hundred milliwatts. The rf absorption in the region of the ion-cyclotron resonance in atomic hydrogen has been studied as a function of the plasma parameters and the rf electrode configuration. The results are compared with the analysis given in [3, 5].

Description of the Apparatus

The plasma is produced in an oscillating-electron electric discharge. The advantages of a system of this kind are the relatively high degree of ionization, the simplicity of the auxiliary apparatus, and the wide range of operating pressures which can be used.

In contrast with conventional designs [6], the present system has two anode rings which are displaced in the axial direction [7]. Under these conditions the space between the anodes is free from the electric fields which maintain the discharge and the fields due to stationary currents which flow in the plasma. Plasma parameters such as the shape of the discharge column, the intensity of the optical radiation, and the discharge current (for magnetic fields between 700 and 1900 gauss) were found to be essentially unchanged during the experiments; this results serves as a definite indication that the plasma density remains constant when the magnetic field is changed.

In the work carried out with aluminum electrodes the discharge density could be varied from 10^7 to 10^{12} cm^{-3} by varying the anode voltage from 0.5 to 3.5 kv. In all experiments the discharge current was less than 100-150 ma.

The discharge chamber, made from molybdenum or quartz, is located in a longitudinal magnetic field (an external view of the apparatus is shown in Fig. 1) which is uniform to within 1% in the region of the rf electrodes. The rf power is introduced by a set of coils or condensers. Each element is connected in opposite phase with the neighboring element. The number of sections can be varied from one to four. A typical discharge chamber with a sectionalized coil is shown in Fig. 2.

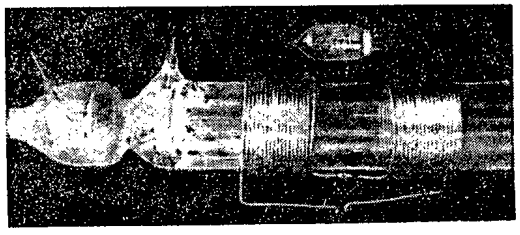

Fig. 2. Discharge tube with a sectionalized solenoid.

The limiting vacuum in the apparatus is $1 \cdot 10^{-5}$ mm Hg when liquid air is used. No provision is made for degassing the chamber. The hydrogen pressure in the system is controlled by means of a heated palladium thimble.

A diagram of the measurement system is shown in Fig. 3. The signal generator (GSS-6 or GS-27) is connected to the resonance circuit, whose capacity or self-inductance, serves as the means of introdicing rf-power into the plasma. The measurements are carried out with a series resonance circuit. The detected signal, which is proportional to the voltage in the circuit, is applied to the input of the dc amplifier used for vertical deflection in the ENO-1 oscilloscope. A signal proportional to the magnetic field is applied to the horizontal plates. With this scheme it is possible to obtain a continuous record of the shape of the resonance absorption of the rf plasma in the frequency range between 1.1 and 2.7 Mcs.

The magnetic field is calibrated by a nuclear-resonance technique which provides an accuracy of 0.5%.

The power absorbed by the plasma is determined by means of calibration curves which are obtained by connecting the generator to a dummy load [4].

In Fig. 4 we show oscillograms of the resonance curves of the circuit with no load, and with a dummy load which is equivalent to power transfer from the generator with an efficiency of 30%; these curves are obtained with a sweep generator. A typical value for the Q of the unloaded circuits is 150-200. The symmetry of the resonance curves and the absence of parasitic resonances in the measurement system makes it possible to eliminate errors due to reactance introduced by the plasma in the region of the gyromagnetic resonance.

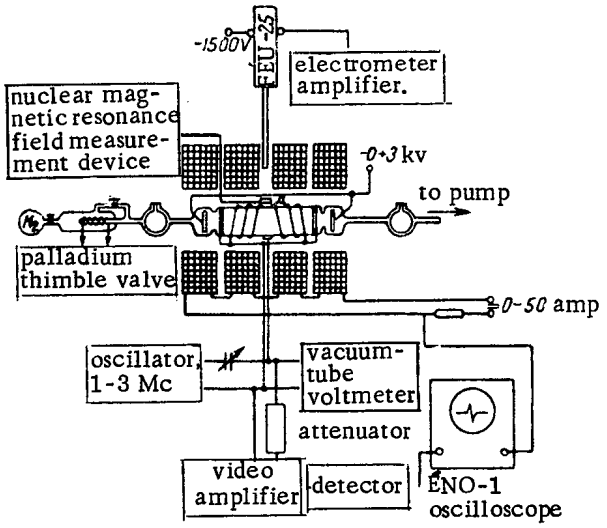

Fig. 3. Measurement system.

The concentration of charged particles in the discharge at densities $n < 10^{11}$ cm^{-3} is determined by the double rf-probe method [8]; at $n \simeq 10^{12}$ cm^{-3} the concentration is determined by measuring the transmission of a 3-cm microwave signal [7]. The dependence of plasma density on discharge current is found to be approximately linear. Extrapolation based on the discharge current gives a value of $3 \cdot 10^{12}$ cm^{-3} for the maximum density in the present system.

The radial distribution of the density in the discharge is estimated by the halfwidth of the electron Langmuir resonance curves obtained by the rf-probe technique while the density is varied. The radial density inhomogeneity determined by this method is found to be less than 15-20%, in accordance with qualitative results obtained by photometry of the visible light radiated by the discharge in the wavelength region 4,000-6,000 A. The optical measurements also indicate the existence of a sharp plasma-vacuum boundary.

Even when the electric component of the probing signal is parallel to the field and the electron temperature is taken into account, the method used here for determing density is suitable only for negligibly small magnetic fields. Hence, the measurements must always be carried out in fields for which the inequality $\omega^2_{ce}/\omega^2_1 \ll 1$, is satisfied, where ω_{ce} is the electron cyclotron frequency and ω_1 is the frequency of the measurement oscillator. At frequencies below 3000 Mcs, corresponding to densities $n \lesssim 10^{11}$ cm^{-3}, the minimum magnetic field for the discharge does not allow this inequality to be satisfied. In order to make control measurements at these frequencies, a method was developed for determining the density of the electrons as a function (taken by the rf-probe method) of the dielectric constant of the plasma in the magnetic field in the region of the electron cyclotron resonance. The values of the density are found by comparing the measured dependence with the computed in [7]. The data obtained by this method are found to be in good agreement with the results of the other density measurements.

Experimental Results

Figure 5 shows a typical oscillogram of the voltage in the plasma circuit as a function of magnetic field strength. The vertical deflection of the beam is proportional to the Q of the circuit while the horizontal deflection is proportional to magnetic field. At field values such that the oscillator frequency approaches the ion gyromagnetic frequency there is a reduction in the voltage, because of absorption of rf power by the plasma. A clearly defined absorption resonance peak is visible.

The data of the oscillogram measurements are converted into absolute values of oscillator loading by the plasma. The use of simple techniques, which follow direction from the calculations [5], makes it possible to obtain power transfer from the oscillator to the plasma with efficiencies of 30-40%. One of the important factors in ion heating by the cyclotron resonance method is the width of the resonance curve, which is an indication of the time of interaction between the accelerated particles and the rf field; for this reason no attempt was made to improve the matching between the oscillator on the plasma.

Below we consider the variation of the resonance absorption region as a function of various plasma parameters. In Fig. 6 are shown curves for the normalized rf power P absorbed at resonance as a function of magnetic field for various oscillator frequencies. In the range of plasma densities 10^7-10^{10} cm^{-3} the measurements show exact agreement between the oscillator frequency and the gyromagnetic frequency of the ions ω_{ci} (atomic hydrogen) at the point corresponding to maximum absorption. The dependence of resonance a absorption strength on oscillator frequency is approximately linear.

In Fig. 7 the variable parameter is the gas pressure. The half-width $\Delta\omega_{ci}$ at pressures greater than $3 \cdot 10^{-3}$ mm Hg varies in approximately linear fashion and is to

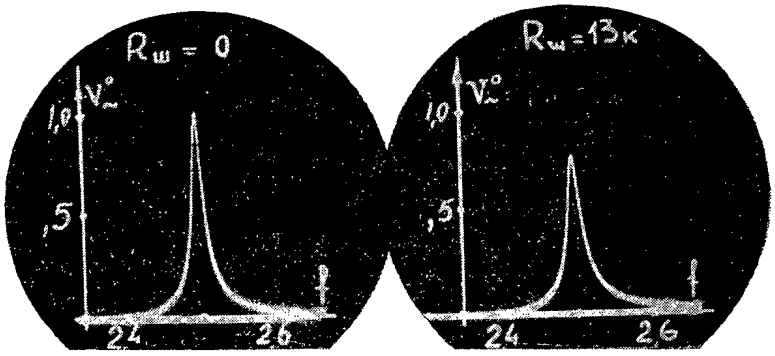

Fig. 4. Callibration curves for the resonance circuit.

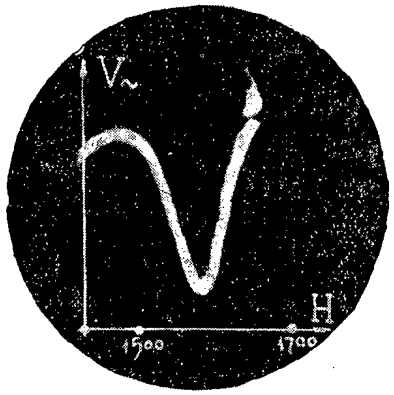

Fig. 5. Oscillogram showing the voltage in the plasma circuit as a function of magnetic field.

be compared with the frequency of collisions between atomic ions and neutral atoms [9] by the relation $\nu_c = \frac{1}{\tau_c} = 1.3 \cdot 10^8 p$, where p is the pressure (mm Hg) and τ_c is the time between collisions.

The effect of density on absorption of rf power P is shown in Fig. 8. The absorption measured in the density range 10^7-10^{11} cm^{-3} (as a function of n) is approximately linear. A saturation effect is observed at $n \simeq 3 \cdot 10^{11}$ cm^{-3}; this saturation is follows by a drop (Fig. 9) when $n > 6 \cdot 10^{11}$ cm^{-3}. When the dependence of maximum absorption on density becomes nonlinear the main resonance peak is split into two absorption peaks; as n increases these two peaks are then monotomically displaced in opposite directions from the value of the magnetic field which corresponds to resonance for a given oscillator frequency.

Reducing the spatial period of the rf system by a factor of two (for the same density values) reduces the displacement of the absorption maxima by a factor of two or three.

Discussion of the Results

The absence of constant electric fields, and fields due to stationary currents, in the region of the heating section, and the relatively uniform radial distribution of plasma density in the discharge configuration used here mean that we have a fairly good approximation to the basic model used in the theoretical analysis [3, 5].

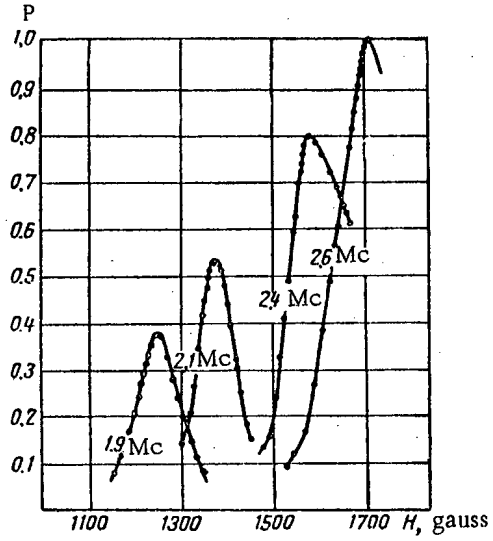

Fig. 6. Resonance curves for the absorption of ion power at various oscillator frequencies ($p = 6 \cdot 10^{-3}$ mm Hg; $n \simeq 10^{10}$ cm^{-3}).

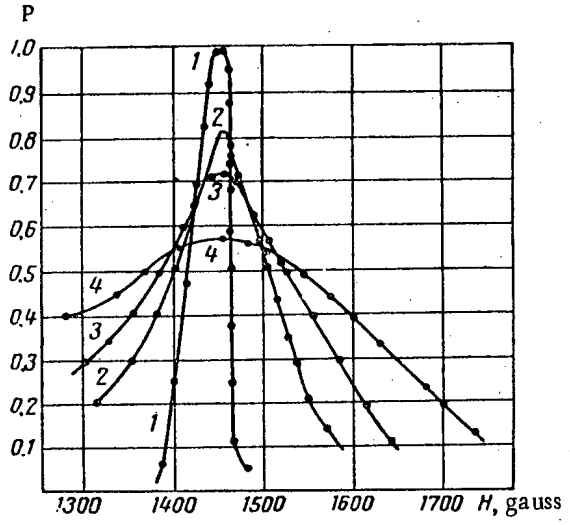

Fig. 7. Resonance absorption curves for various pressures (f = 2.2 Mcs), mm Hg; 1) $p = 9 \cdot 10^{-4}$; 2) $p = 5 \cdot 10^{-3}$; 3) $p = 9 \cdot 10^{-3}$; 4) $p = 1.5 \cdot 10^{-2}$.

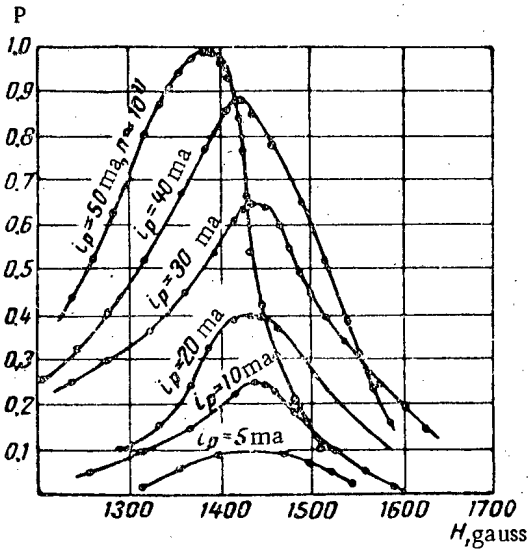

Fig. 8. Resonance curves for various plasma densities (f = 2.2 Mcs; $p = 6 \cdot 10^{-3}$ mm Hg).

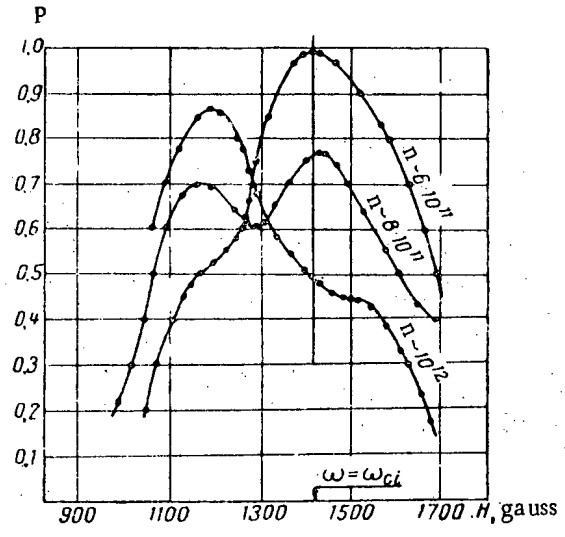

Fig. 9. Absorption curves at high densities (f = = 2.12 Mcs; $p = 10^{-2}$ mm Hg).

According to this analysis, if the inequality $\omega^2_0/k^2c^2 < 1$ is satisfied there are no polarization effects. The absorption in the region of the cyclotron resonance is th then proportional to the product of the plasma density and the oscillator frequency. Maximum absorption takes place when ω is exactly equal to ω_{ci}.

At higher densities (more precisely, when $\omega^2_0/k^2c^2 \lesssim 1$, self-fields arise in the plasma; a consequence of the appearance of these fields is the displacement of the region of effective penetration of the rf field from values of the magnetic field such that ω is equal to ω_{ci} to values such that $\omega > \omega_{ci}$ [2, 10] or $\omega < \omega_{ci}$ [3, 5]. If the displacement, which is given by $\omega\omega^2_0/k^2c^2$ is large enough to exceed the half width of the cyclotron resonance ΔH the ions are no longer heated and the absorbed power is dissipated in weakly-damped hydromagnetic oscillations in the plasma [2, 3, 5].

For the system ($k = \frac{1}{16}$ cm^{-2}) used in obtaining the curves shown in Figs. 8 and 9 the critical density above which the efficiency of resonance heating is reduced is $\sim 5 \cdot 10^{11}$ cm^{-3} and the linear increase in the absorption of rf power observed in the experiments as the density n increases from 10^7 to 10^{11} cm^{-3} is to be expected. The measured value of the optimum density ($3 \cdot 10^{11}$ cm^{-3}) also corresponds to the calculated value.

As far as polarization effects are concerned, a change in density is equivalent to a change in the square of the length of an element of the heating section; this fact one can easily explain as the qualitative agreement with theory of the displacement of the absorption maximum as a function of k.

Unfortunately, it is difficult to make a quantitative comparison of the results of the measurements for various values of k at charged-particle densitities greater than 10^{11}-10^{12} cm^{-3}, because of the Coulomb interaction; this effect can be avoided only if the plasma is heated to temperatures such that the ion energies are greater than several electron volts. In experiments with small values of k it is necessary to have large volumes with strong magnetic fields.

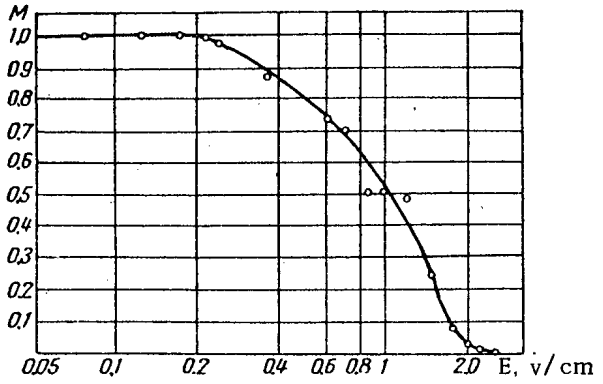

Fig. 10. Effect of electric field strength on the time of interaction between the ion and the rf field.

Data for different values of k can be obtained from a comparison of the results of these experiments with the results obtained in [1], which was a study of the case equivalent to $k = 0$; further information can be obtained from effects which accompany the polarization of the plasma (the nonlinear increase in the absorption of rf power with increasing density and the dependence of the half width and the position of the absorption maximum on density) when the inequality $\omega^2_0/\omega^2 < 1$. is no longer satisfied. It should be noted that in looking for effects associated with the skin effect for $\omega^2_0/\omega^2 \simeq 1$ ($\omega^2_0/k^2c^2 \simeq 10^{-8}$) we have not observed any noticeable departure from the results to be expected from [3] whereas the described polarization effects appear when the inequality $\omega^2_0/k^2c^2 < 1$ is not satisfied (for $\omega^2_0/\omega^2 \simeq 10^4$). Hence, in spite of the absence of direct proof of the penetration of the rf fields into the plasma in the systems which have been investigated,* the satisfactory agreement between the measured and calculated values of the density at which plasma polarization effects appear, and the fact that there is a shift of the absorption maximum with increasing n, rather than smearing, which would be the case if only the boundary layer (continuous density variation) were heated, all seem to indicate it is possible to set up systems in which the skin effect is small.

If we assume complete compensation, the fact that the fields inside and outside the plasma are equal allows us to estimate the ion heating. According to [11], when a charged particle moves in a constant magnetic field H which is perpendicular to a variable electric field [$E = E_0 \sin(\omega t)$], at exact resonance the ion will rotate in an orbit of radius $R(t) = E_0/2H,t$ seconds after acceleration starts. The quantity t, which is equal to τ_c (the time of interaction between the ion and the rf field between two successive collisions), can be found from the experimental data from the relation $\Delta\omega\tau_c = 1$ [9]. The product HR(t), measured in this way, then serves as a measure of the energy acquired by the ion in the heating process. For an electric field strength of 0.2 v/cm, which is typical of the majority of the experiments which have been carried out, the growth in ion energy as a result of interaction with the probing signal ($\sim 10^{-2}$ev) is small compared with the thermal energies of particles in the discharge so that the perturbation introduced by the measuring process is inconsequential.

In order to explore the possiblitiy of increasing the ion energy, curves were taken to determine the dependence of ion lifetime M (referred to the lifetime corresponding to a resonance width of 5%) on the electric field E produced by a plane condenser (Fig. 10). An

*It is impossible to measure the radial field distribution of the rf field by means of probes because of the distortion of the field caused by the probe; impurities from the probe also affect the properties of the plasma.

estimate of the velocity increment $v_\perp$ acquired by the ion in the heating process, with respect to the thermal velocity v_0 corresponding to a temperature of approximately 300°K (characteristic of the majority of the discharges) shows that at the break in the M(E) curve, at the field strength $E \simeq 0.3$ v/cm, $v_\perp \simeq v_0$. In accordance with [12], when $v_\perp > v_0$ the quantity τ_c is inversely proportional to $\sqrt{E}$. However, the curvature of the M(E) curve in the region $E \simeq 1$ v/cm cannot be explanined in this way. The stronger dependence of M(E) when $v_\perp > v_0$ may be explained by a process similar to that proposed in [13]; in this process the plasma tries to equalize any anisotropy such as $v_\perp > v_0$ which arises in the heating process. The increase in the magnitude of the longitudinal velocity component $v_\parallel \simeq v_\perp > v_0$ to values $\tau_c(E)$ means that it is necessary to take account of the additional reduction of $\tau_\parallel$ due to the reduction in the time spent by the ion in the region of the heating section: $\tau_\parallel \simeq 1\ kv_\parallel$.

Taking account of the relation $\tau_c \sim 1/\sqrt{E}$ for $v_\perp > v_0$ under the assumption that $v_\parallel \simeq v_\perp$ leads to the possibility of a quantitative description of the observed function M(E). At the same time, the variation the time between collision $\tau_c \simeq 1/\sqrt{E}$ for strong energy exchange between ions and neutral atoms has been rather well studied in the theory of atom motion [12]. It is found that at high ionization, the neutral atoms, which are not restrained by the magnetic field, transfer a large amount of energy to the chamber walls.

Conclusions

The results of experiments in which we have used a spatially periodic system for introducing rf power in the region of the ion cyclotron resonance for cold plasmas characterized by densities of $10^7 - 10^{11}$ cm^{-3} are found to be in satifactory agreement with the theoretical analysis which predicts a reduction in the effect of the self polarization fields on the penetration of the oscillating fields for totally ionized hot plasmas at densities up to $10^{13} - 10^{14}$ cm^{-3}.

The experiments show that in order to achieve successful plasma heating by the cyclotron resonance technique it is necessary to keep the percentage of neutral atoms to a minimum.

The dependence of plasma behavior in the region of the ion gyromagnetic resonance on particle density and on temperature can be used to develop methods of studying the properties of gaseous discharges.

The authors are indebted to K. D. Sinel'nikov for his interest in this work and for valuable discussions.

LITERATURE CITED

1. L. V. Dubovoi, et al., Report No. 2211, International Conference on the Peaceful Uses of Atomic Energy (Geneva, 1958).
2. K. Kerper, Z. Naturforsch. 12a, 815 (1957).
3. T. Stix, Phys. Rev. 106, 1146 (1957).
4. Stix and Palladino, Proceedings of the Second International Conference on the Peaceful Uses of Atomic Energy (Geneva, 1958). Selected Reports of Foreign Scientists. Plasma, Physics and Thermonuclear Reactions [Russian translation] (Atomizdat, Moscow, 1959) Vol. I, p. 242.
5. Stix, Proceedings of the Second International Conference of the Peaceful Uses of Atomic Energy (Geneva, 1958). Selected Reports of Foreign Scientists, Plasma, Physics and Thermonuclear Reactions [Russian translation] (Atomizdat, Moscow, 1959) Vol. I, p. 254.
6. E. M. Reikhrudel', G. V. Smirnitskaya, Izvest. Vyssh. Ucheb. Zavedenii, Radiofizika 2, 36 (1958).
7. Horton, Howard and Heinz, Procedings of the Second International Conference on the Peaceful Uses of Atomic Energy (Geneva, 1958). Selected Reports of Foreign Scientists. Plasma, Physics and Thermonuclear Reactions [Russian translation] (Atomizdat, Moscow, 1959) Vol. I, p. 675.
8. T. Yeung and T. Seyers, Proc. Phys. Soc. 451 B, 663 (1957).
9. C. Kelley, H. Margenau, and S. Brown, Phys. Rev. 108, 13 7 (1957).
10. P. Doyle and J. Neufeld, Phys. Fluids 2, 390 (1959).
11. J. Amoignon and G. Rommel, Vide 12, 377 (1957).
12. L. Loeb, Basic Processes of Gaseous Electronics (Berkeley and Los Angeles, University of California Press., 1955) Chapt. 1.
13. A. A. Vevdenov and R. Z. Sagdeev, Plasma Physics and the Problem of Controlled Thermonuclear Reactions [in Russian] (Izd. AN SSSR, Moscow, 1958) Vol. III, p. 273.

ELECTROLYTIC ISOLATION OF SMALL AMOUNTS OF URANIUM, NEPTUNIUM, PLUTONIUM, AND AMERICIUM

A. G. Samartseva

Translated from Atomnaya Énergiya, Vol. 9, No. 4, pp. 324-329, April, 1960
Original article submitted September 4, 1958

In the study of the nuclear properties of elements and the investigation of isotopic composition, it is necessary to prepare thin, homogeneous layers; in the analytical chemistry of transuranium elements, the quantitative isolation of these elements, including those in tracer amounts, is important. An original electrolytic method for the quantitative isolation of traces of uranium, neptunium, plutonium, and americium from acid solutions is described in the present work. It was shown that the yield of the elements in the electrolysis is independent of the electrolyte anion and is primarily determined by the solution pH. Conditions were found for the quantitative electrolytic isolation of plutonium in the presence of various foreign metals; the effect of iron was eliminated by the introduction of oxalic acid into the electrolyte.

The electrolytic isolation of transuranium elements from aqueous solutions is an excellent method of depositing thin, homogeneous layers in the study of nuclear properties or the isotopic composition of these radioelements. In addition, this method may be used successfully in the analytical chemistry of transuranium elements as it makes it possible to isolate these elements quantitatively and without carrier, even when they are present in solution in tracer amounts.

We previously developed a method for the quantitative isolation of uranium [1] and also transuranium elements [2] from mineral acid solutions. The present work is a continuation of these investigations.

Uranium, neptunium, plutonium, and americium were isolated in a normal electrolytic cell, consisting of a small platinum dish (anode) and an elongated platinum plate with a working area of 1 cm^2 (cathode). In this cell it was possible to work with an electrolyte at any pH value without appreciable losses of radioelement due to adsorption on the walls, which is observed when a glass or plexiglass electrolyzer is used. The solution was stirred with the cathode which rotated at 60-80 rpm. Electrolytic separation of the radioelement occurred simultaneously on both sides of the platinum plate cathode; the α-activity on this electrode was measured in a special chamber [3].

In the work we used the isotopes U^{233}, Np^{237}, Pu^{239}, and Am^{241}. With an ionization chamber and a multichannel amplitude analyzer it was shown that the Pu^{239} contained 0.7 - 0.9 % of a mixture of Am^{241} and Pu^{238}, and the Np^{237} contained ~2.0% of Pu^{239}. No impurities were detected in the isotope Am^{241}; the U^{233} was not analyzed. Weighable amounts of the hydroxides of the elements were dissolved in the acids which were used as electrolytes. A study of the valence states of the elements in the starting solutions showed that the U^{233} was in the hexavalent state; the Np^{237} consisted of 10.2% of Np (VI), ~90% of Np(V), and < 1% of Np(IV); the Pu^{239} consisted of 14.3% Pu(VI), 56.1% of Pu(IV), and 28.9% of Pu(III); the Am^{241} was in the trivalent state.

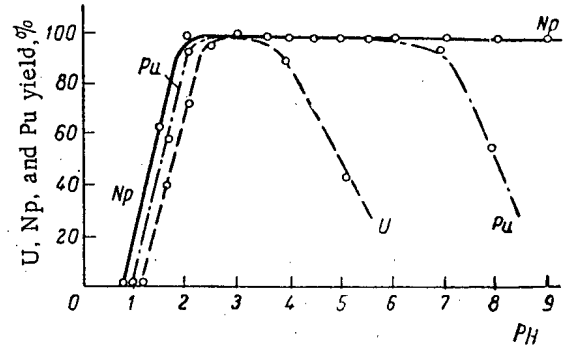

Fig. 1. Relation of element yield to solution pH. The current density on the cathode was 100 ma/cm^2 and the electrolysis time, 2 hr.

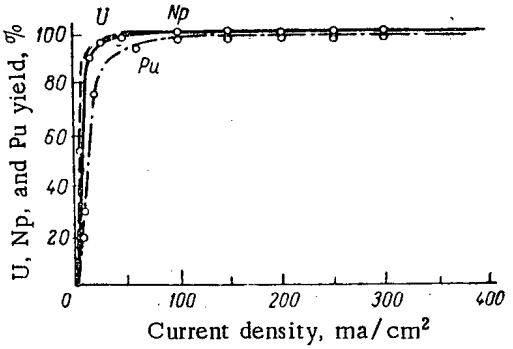

Fig. 2. Relation of element yield to current density. pH = 3 and electrolysis time 2 hr.

TABLE 1. Optimal Conditions for Electrolytic Isolation of Thorium, Uranium, Neptunium, Plutonium, and Americium from Nitric Acid Solution

Element	Solution volume, ml	pH	Current density, ma/cm²	Electrolysis time, min	Yield, %
Th (Io)	20	2.5	100	120	99 8
U	20	2.5	100	120	100.1
Np	80	3	250	10	100.4
Pu	20	3	100	120	100.0
Am	20	3	100	5	99.7

The electrolytes were nitric, hydrochloric, perchloric, sulfuric, and oxalic acids with hydrogen ion concentrations of 10^{-1}-10^{-4} M and buffered solutions with hydrogen ion concentrations of 10^{-5}-10^{-9} M. The investigation was carried out with the following molar concentrations of the radioisotopes in the electrolyte: $U^{233} - 1.3 \cdot 10^{-8}$; $Np^{237} - (0.2 - 1.2)\ 10^{-6}$; $Pu^{239} - 4.1 \cdot 10^{-9}$; $Am^{241} - 1.4 \cdot 10^{-10}$.

In all cases in the present work, the experimental data, which are given in tables and curves, are the mean results of three to five experiments.

Electrolytic Isolation of Uranium, Neptunium, Plutonium, and Americium from Weakly Acid Solutions

Experimental data on the relation of the element yields to the pH of nitrate solutions, current density, and experiment duration are given in Figs. 1-3, respectively.

Figure 1 shows that the maximum yield of uranium was observed at pH = 2.5 and of neptunium and plutonium, at pH = 2.0. The sharp fall in uranium yield at pH > 4 apparently indicates that uranium is hydrolyzed to a greater extent than neptunium and plutonium. The two latter elements are probably in the pentavalent state under these conditions and therefore are not hydrolyzed up to a pH of 7-8 [4].

Figure 3 shows the very great difference in the rates of electrolytic isolation of uranium, neptunium, and plutonium. This is explained apparently not only by a difference in the mechanism of electrolytic reduction of each element, but the different stabilities of their pentavalent ions as intermediate products in the first stage of reduction in the region adjacent to the cathode. According to literature data [5], at pH = 2.5 on a mercury dropping cathode, uranium is first reduced to the pentavalent state:

$$UO_2^{++} + e^- \rightarrow UO_2^+,$$

and then disproportionates:

$$2U\,(V) \rightarrow U\,(IV) + U\,(VI).$$

Due to the repeated oxidation-reduction reactions, the rate of uranium separation on the cathode becomes less. Neptunium, which is in the original solution in the stable pentavalent state, is immediately reduced to the tetravalent state on the cathode itself. The rate of its electrolytic separation is determined mainly by the mobility of the ions; this is 20 times the rate of separation of uranium (see Fig. 3).

Due to the fact that in the starting solution plutonium is mainly in the tri- or tetravalent state, it is first oxidized to the pentavalent state and then, at the moment when it separates on the cathode, it is reduced again to the tetravalent state. As Fig. 1 shows, during the electrolytis plutonium is oxidized to Pu(V) as it is not hydrolyzed in solutions with pH = 7, i.e., under these conditions it behaves as Np(V).

The results obtained made it possible to select separately the optimal conditions for the quantitative

TABLE 2. Electrolytic Isolation of Uranium Neptunium, Plutonium, and Americium from Solutions of Various Acids (pH 2-3, current density 100 ma/cm²)

Number of experiment	Acid	Element yield, %			
		U	Np	Pu	Am
5	H_2SO_4	100.1	99.8	97.8	99.2
13	HCl	100.0	100.0	98.9	98.9
7	$HClO_4$	100.6	100.2	100.1	99.7
50	HNO_3	100.0	100.2	100.6	100.2
28	$H_2C_2O_4$	100.2	98.9	99.7	98.7

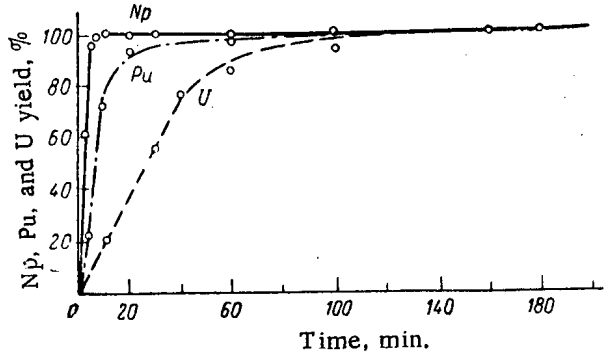

Fig. 3. Relation of element yield to electrolysis time. pH = 3 and current density 100 ma/cm².

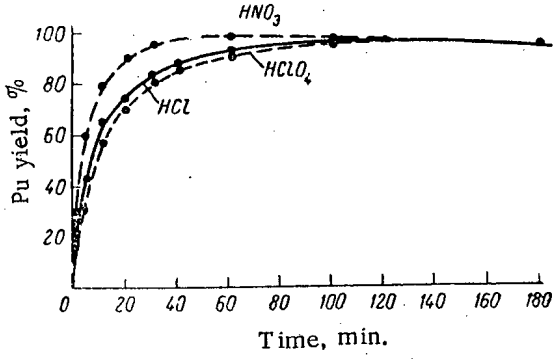

Fig. 4. Relation of plutonium yield to experiment duration. pH = 3, current density 100 ma/cm².

electrolytic isolation of thorium, uranium, neptunium, plutonium, and americium (Table 1).

Tracer amounts of thorium, uranium, neptunium, plutonium, and americium are quantitatively deposited on a platinum cathode under approximately the same electrolysis conditions.

Experimental data on the electrolytic isolation of transuranium elements from solutions of various mineral acids are given in Table 2.

As the table shows, transuranium elements separate quantitatively from the solutions studied and, consequently, the yield of the elements is independent of the nature of the electrolyte anion, but depends strongly on the concentration of hydrogen ions.

Figure 4 gives data on the kinetics of electrolytic isolation of plutonium from hydrochloric and perchloric acids. As the electrolyte it is better to use nitric acid rather than hydrochloric or perchloric acids.

Electrolytic Isolation of Uranium, Neptunium, and Plutonium from 0.1 M Nitric Acid Solution

Since it is not always convenient to work with low (0.01-0.001 M) acid concentrations, we attempted to find conditions for the electrolytic isolation of transuranium elements from more acid solutions. It was previously noted that with an increase in the hydrogen ion concentration, it was necessary to increase the current density. However, the first experiments in this direction were unsuccessful as over a wide range of current densities (400-3000 ma/ cm^2) there was very slight electrolytic separation of neptunium and plutonium; under these conditions, uranium separated quantitatively at current densities of 700-1000 ma/ cm^2.

It was found that if the starting solution of plutonium was evaporated to dryness with a small amount of concentrated nitric acid three or four times (i.e., the plutonium was converted to the tetravalent state) and then the residue dissolved in 20 ml of 0.1 M nitric acid solution and electrolyzed, the plutonium was deposited quantitatively from 0.1 M nitric acid solution. Experimental data on the relation of the uranium, plutonium, and neptunium yields to current density and experiment duration for 0.1 M nitric acid solutions are given in Figs. 5 and 6, respectively.

The difference in the rates of electrolytic separation of uranium, neptunium, and plutonium is probably explained by the different valence of the elements in the starting solution and, consequently, the different mechanism of their electrolytic reduction.

On the basis of the data obtained we selected the following optimal conditions for the electrolytic separation of uranium, neptunium, and plutonium from 0.1 M solutions of nitric acid: 1) cathode current density 750-1000 ma/ cm^2; 2) experiment duration 2-3 hr; 3) solution volume 20-40 ml.

We subsequently used these conditions for the electrolytic isolation of transuranium elements in the presence of foreign ions.

Electrolytic Isolation of Plutonium in the Presence of Foreign Ions

All existing methods of electrolytic isolation of transuranium elements from alkaline, weakly acid, and especially from alcohol–acetone–water solutions are only suitable for very pure solutions. In practice it is very often necessary to deal with solutions containing a large amount of foreign elements. The electrolysis of plutonium from such solutions is either nonquantitative or is not observed at all. In electrolysis from alkaline solutions, iron and aluminum hydroxides precipitate and entrain the radioactive element. Hydrolysis of foreign elements occurs during electrolysis of weakly acid solutions and precipitates form, while in alcohol–acetone–water solutions, plutonium itself is hydrolyzed and precipitates.

We attempted to find conditions for the quantitative electrolytic isolation of plutonium directly from a starting solution containing up to 10 mg (total) of iron, aluminum, lanthanum, barium, chromium, manganese, calcium, magnesium, potassium, and sodium. Of all the the elements listed, iron interferes most in the electrolysis of plutonium. Oxalic acid, a solution of which is

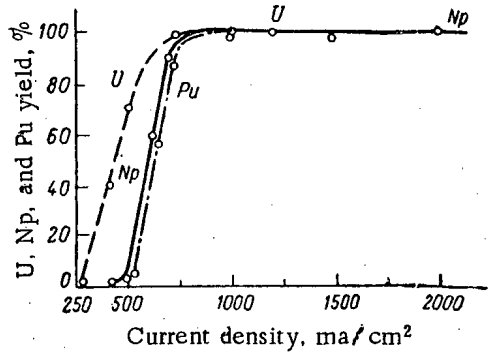

Fig. 5. Relation of element yield to current density. 0.1 M nitric acid solution, electrolysis time 2 hr.

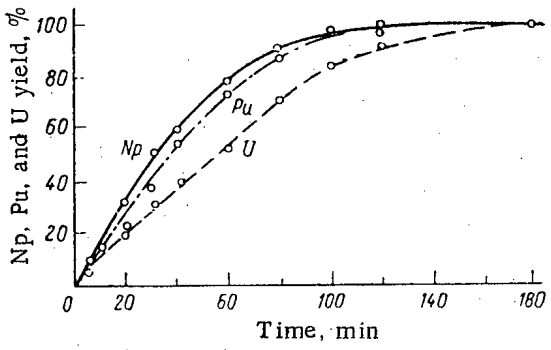

Fig. 6. Relation of element yield to electrolysis time. 0.1 M nitric acid solution, current density 1000 ma/ cm^2.

also a good electrolyte for plutonium, was used to complex the iron. The experiments were carried out in 0.1 N nitric acid solution to increase the hydrogen ion concentration.

In order to find the optimal conditions for electrolytic isolation of plutonium from a mixture of oxalic and nitric acids in the presence of foreign ions, it was first important to find how a change in the oxalic acid concentration affects the plutonium yield. The results obtained are given in Fig. 7.

It is interesting to note that quantitative yield of plutonium was obtained from a mixture of the two acids at the same oxalic acid concentration as in the absence of nitric acid. Therefore, it may be assumed that nitric acid does not participate directly in the mechanism of electrolytic separation of plutonium on the cathode. The data in [6] also confirm that under these experimental conditions, plutonium must be in the form of the positively-charged complex ion $PuC_2O_4^{++}$.

We then investigated the relation of the plutonium yield to the nitric acid concentration in this system. The results are given in Fig. 8. They show that the electrolytic separation of plutonium from a mixture of the two acids occurs over a very wide range of pH values. The best results were observed at a pH value of 1.2-1.4. The sharp jump in the plutonium yield at pH = 0.8 in Fig. 8 indicates that it is not advisable to use a nitric acid concentration of more than 0.25 M for the quantitative electrolysis of plutonium under the given conditions.

We also studied the relation of the plutonium yield to the cathode current density. The results are given in Fig. 9, which shows that under these conditions a quantitative yield of plutonium was observed at a current density of 1000-2000 ma/ cm^2.

Data on the effect of electrolysis time on plutonium yield are given in Fig. 10, which shows that the electrolytic separation of plutonium under the conditions adopted is complete after 1.5-2 hr.

The investigation of the electrolytic separation of plutonium from a mixture of oxalic and nitric acids made it possible to select the following optimal conditions for the given method: 1) oxalic acid concentration 0.002 M; 2) nitric acid concentration 0.125 M; 3) solution pH 1.3; 4) cathode current density 1000 ma/ cm^2; 5) solution volume 20-40 ml; 6) electrolysis time 1.5-2 hr.

The experiment was carried out in the following way. An aliquot portion (0.15-5 ml) of the starting solution was placed in a platinum dish and the solution

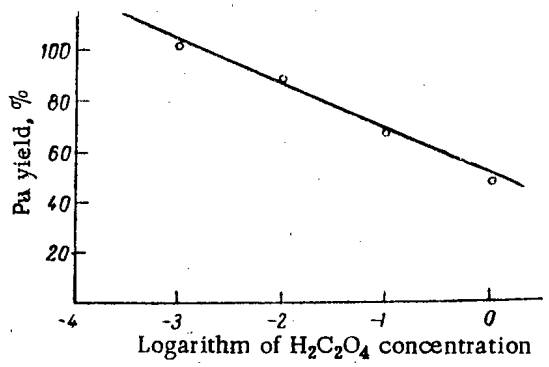

Fig. 7. Relation of plutonium yield to oxalic acid concentration. 0.1 M nitric acid solution, current density 1000 ma/ cm^2, electrolysis time 2 hr.

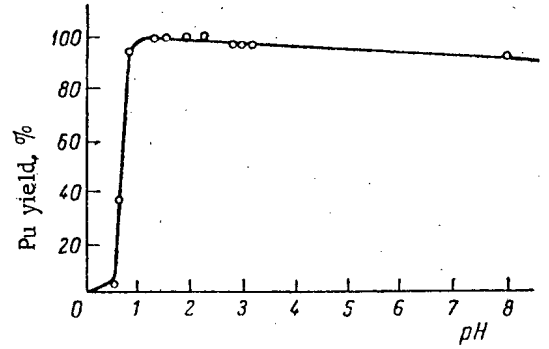

Fig.8.Relation of plutonium yield to nitric acid concentration. 0.002 M oxalic acid solution, current density 1000 ma/ cm^2, electrolysis time 2 hr.

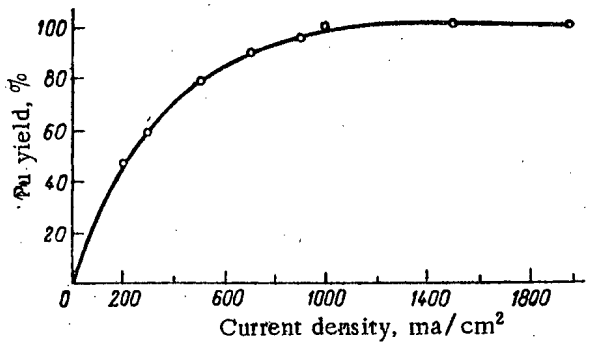

Fig. 9. Relation of plutonium yield to current density. Solution 0.1 M with respect to nitric acid and 0.002 M with respect to oxalic acid; pH = 1.3, electrolysis time 2 hr.

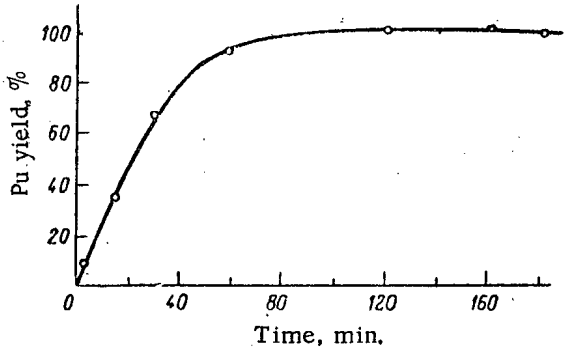

Fig. 10. Relation of plutonium yield to electrolysis time. Solution 0.1 M with respect to nitric acid and 0.002 M with respect to oxalic acid; pH = 1.3, current density 1000 ma/ cm^2.

TABLE 3. Electrolytic Isolation of Plutonium from a Mixture of Oxalic and Nitric Acids in the Presence of Foreign Ions.

$H_2C_2O_4$, M	pH	Pu	
		taken, counts/min	yield, %
0.002	1.3	2020	98.9
0.002	1.3	2020	99.2
0.002	1.3	2020	99.0
0.002	1.3	2020	100.0
0.002	1.3	2020	99.4
0.002	1.3	2020	100.6
0.002	1.3	2020	100.2
		Mean	99.9±0,7%

evaporated to dryness on a water bath. The residue was treated with concentrated nitric acid two or three times. Then 0.1 ml of 1 M oxalic acid and 10 ml of 0.5 M nitric acid were added and the mixture left on a water bath under a clock glass for 10-15 min (for complete solution of the dry residue). The 30 ml of distilled water was poured into the dish and the electrolysis carried out under the conditions described.

When all these conditions were observed there was quantitative electrolytic isolation of plutonium as is shown by Table 3. The results obtained show that there is quite satisfactory reproducibility of electrolytic isolation of plutonium in the presence of foreign ions. Therefore, this method may be used in the analytical chemistry of plutonium as it makes it possible to determine plutonium in solution more accurately and much more rapidly than a chemical method. Uranium and neptunium also undergo quantitative electrolytic deposition under these conditions. All foreign ions remain in solution.

From what has been stated, the following conclusions may be drawn:

1. A quantitative method has been developed for the electrolytic isolation of uranium, neptunium, plutonium, and americium from solutions of nitric, sulfuric, hydrochloric, perchloric, and oxalic acids at hydrogen ion concentrations in the electrolyte of 10^{-3} M.

2. It was shown that the determining factor in the quantitative electrolytic isolation of uranium, neptunium, plutonium, and americium is not the nature of the electrolyte anion, but the hydrogen ion concentration.

3. The kinetics of electrolytic isolation of uranium, neptunium, and plutonium from nitric acid solution at hydrogen ion concentrations of 10^{-3} and 10^{-1} M were studied.

4. The kinetics of electrolytic isolation of plutonium from hydrochloric and perchloric acid solutions at a hydrogen ion concentration of 10^{-3} M were studied.

5. The relation of the yield of uranium, neptunium, and plutonium to the cathode current density and also electrolyte pH was investigated.

6. An analytical method is proposed for the electrolytic isolation of plutonium in the presence of foreign ions, which makes it possible to isolate tracer amounts of plutonium directly from the starting solution quantitatively and without carrier.

7. This method of electrolytic isolation of transuranium elements may be used both in the analytical chemistry of these elements and for the preparation of standards and targets.

LITERATURE CITED

1. A. G. Samartseva, Tr. Radievogo Inst. 7, 137 (1956).
2. A. G. Samartseva, Coll.: Isotopes and Radiation in Chemistry [in Russian] (Izd. AN SSSR, Moscow, 1958) p. 318.
3. S. S. Bugorkov, L. Z. Malkin, K. A. Petrazhak, V. A. Yakovlev, and M. I. Yakunin, Tr. Radievogo Inst. 9, 214 (1958).
4. L. Gevantman and C. Kraus, The Trans-Uranium Elements (New York, 1949) Sect. IV, Vol. 14 B, part I, p. 500.
5. C. Kraus, F. Nelson, and J. Johonson, J. Am. Chem. Soc. 71, 7, 2510 (1947).
6. W. Reas, The Trans-uranium Elements, (New York 1949) Sect. IV, Vol. 14B, part I, p. 423.

ROLE OF OXIDATION-REDUCTION PROCESSES IN THE SOLUTION OF URANIUM OXIDES IN ACID MEDIA

G. M. Nesmeyanova and G. M. Alkhazashvili

Translated from Atomnaya Énergiya, Vol. 9, No. 4, pp. 330-335, April, 1960
Original article submitted January 11, 1960

The degree of oxidation of the components of the ore material is of decisive importance in the extraction of uranium. Since the solution of uranium is composed of various chemical processes and complicated by the presence of impurities in the ores, it is necessary to study the rules of uranium oxidation and the effect of various compounds which dissolve during the leaching of uranium ores.

In the present work we present the results of an investigation of the oxidation and solution of uranouranic oxide in acid media and the effect of ferrous compounds on it. A comparison of the oxidizing power of various oxidants with respect to uranium is given for the first time. It was shown that the oxidation of tetravalent uranium is not determined unequivocally by the normal oxidation-reduction potential. The results obtained show that the reasons for incomplete extraction of uranium by a mixture of nitric and sulfuric acids at low concentrations when considerable amounts of iron ions are present in the solutions are associated with the formation of complexes between Fe^{2+}, SO_4^{2-}, and NO_3^- ions.

Unoxidized uranium mineals dissolve poorly in weak solutions of mineral acids and alkali carbonates. As a result of this it is necessary to use various oxidants for the maximum possible solution of uranium.

The solution of uranium is composed of various chemical processes and is complicated by the presence of many impurities contained in the ores. Therefore, it is necessary to study not only the rules of uranium oxidation, but also the effect on this process of various compounds dissolving during the acid leaching of uranium ores.

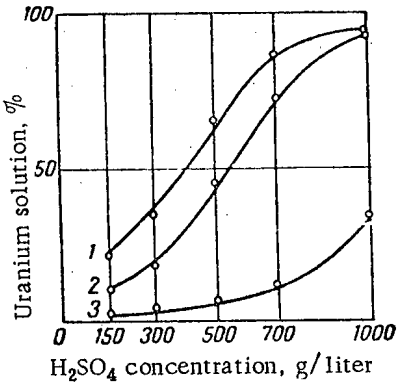

Fig. 1. Effect of sulfuric acid concentration on the solution of: 1) hexavalent uranium from uranouranic oxide; 2) tetravalent uranium from uranouranic oxide; 3) tetravalent uranium from dioxide.

A study of these problems not only provides a theoretical basis for the processes occurring during the extraction of uranium from ore, but also ways of accelerating them.

In recent years a large number of papers has appeared on the effect of various factors on the degree of solution of uranium. In [1], in addition to data on the extraction of uranium in relation to experiment time, temperature, acid concentration, and particle dimensions, data are presented which indicate that the use of oxidants in leaching in an acid medium improves the solution of uranium. It has been shown [2] that an increase in the total concentration of nitric (25%) and sulfuric (75%) acids from 13.5 to 107.6 g/liter increases the solution of uranium from 61 to 80 and from 82 to 97%, depending on the coarseness of the particles and the mixing time. With a sulfuric acid concentration of 16.5 g/liter, the introduction of potassium chlorate, potassium permanganate, sodium bichromate, and other oxidants into the reaction mixture increases the solution of uranium. At the same time, it was reported that the presence of ferric ions guarantees successful solution of uranium without the addition of an oxidizing agent. In this work and also in [3, 4], the results were given of a study of the effect of various factors on the extraction of uranium from ore material. Since the ores include a whole complex of different minerals, data on the solution of uranium reflect the effect of not only leaching factors (concentration, tem-

perature, etc.), but also of various impurities present in the ores.

In order to study the effect of reagent concentration, temperature, and process duration of uranium solution, we carried out a series of experiments with uranium oxides. The solvent was sulfuric acid and as an oxidant we used nitric acid, potassium chlorate, manganese dioxide, potassium permanganate, and stannic salts. The experiments were carried out with air thermostatting. The uranium oxide sample weighed 2 g and had a grain size of −0.15 mm and the reagent consumption corresponded to stoichiometry. Uranium oxides and sulfuric acid solutions of various concentrations with the oxidant were placed in glass tubes, fixed to a disk. The disk was rotated at 200 rev/min during solution. The contents of tetravalent and hexavalent uranium were determined by the methods described in [5, 6].

Figure 1 gives the results of experiments on the solution of uranium oxides in sulfuric acid in relation to the concentration of the latter. Uranium dioxide hardly dissolved in sulfuric acid with a concentration of 150 g/liter at a temperature t = 90°C with an experiment time τ = 3 hr. This may be explained by the fact that the heat of formation of uranium dioxide is extremely high (270 kcal/mole). The uranium for uranouranic oxide dissolved to a greater extent under the same conditions.

In [2] a ratio of nitric to sulfuric acid of 25 : 75 was considered optimal for the solution of uranouranic oxide. According to the reaction equations

$$3U_3O_8 + 2HNO_3 + 9H_2SO_4 = \\ = 9UO_2SO_4 + 2NO + 10H_2O$$

and

$$3UO_2 + 2HNO_3 + 3H_2SO_4 = \\ = 3UO_2SO_4 + 2NO + 4H_2O$$

for complete solution of uranouranic oxide the ratio of nitric and sulfuric acids should be as follows: 12.5% HNO_3 and 87.5% H_2SO_4, and for the dioxide, 30% HNO_3 and 70% H_2SO_4. By changing the ratio of nitric and sulfuric acids over a wide range (Fig. 2), we showed that the maximum oxidation of uranium in uranouranic oxide is observed at a ratio $HNO_3 : H_2SO_4$ = 12.5 : 87.5; a further increase in the nitric acid content of the sulfuric acid did not affect the uranium oxidation and at t = 90°C it was 100%. For uranium dioxide, complete oxidation and solution corresponded to the ratio $HNO_3 : H_2SO_4$ = = 30: 70, as is expected from stoichiometry. An analogous picture was observed at t = 20°C for uranouranic oxide, but uranium dioxide behaved differently. This is explained not only by the greater difficulty of the oxidation of uranium in the dioxide, but also by the weaker oxidizing properties of nitric acid at low temperatures. Under the same conditions (constant temperature and process time), the effect of the initial sulfuric acid concentration is different with different oxidizing agents (Fig. 3). At t = 20°C, an increase in sulfuric acid concentration from 5 to 100 g/liter had l little effect on the oxidation of uranium in uranouranic oxide by potassium permanganate and chlorate and nitric acid, but at t = 90°C, the sulfuric acid concentration played a decisive part in the oxidation of uranium by nitric acid. Complete solution of uranouranic oxide was observed at a sufluric acid concentration of 100 g/liter in the presence of the oxidants nitric acid and ferric salts. In the presence of manganese dioxide, a change in the sulfuric acid concentration over the range 50-150 g/liter had an insignificant effect on uranium oxidation.

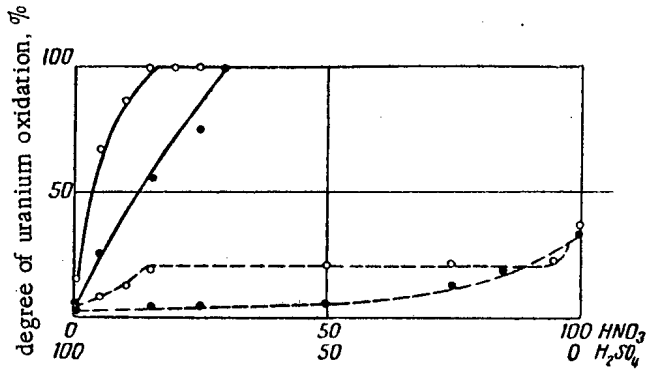

Fig. 2. Relation of uranium oxidation to amount of nitric acid in the mixture of nitric and sulfuric acids with a total acid concentration of 100 g/liter and τ = 3 hr; ○) uranouranic oxide; ●) uranium dioxide; ——) t = 90°C; – – – –) t = 20°C.

Since complete oxidation and solution of uranium at a sulfuric acid concentration of 100 g/liter was observed only when ferric compounds and nitric acid were used as oxidants, we studied the effect of process time on the solution of uranouranic oxide (Fig. 4). At t = = 20°C, none of the oxidants used gave complete oxidation and solution of uranium even after 38 hr. At t = = 90°C, the worst results were obtained with manganese dioxide. The complete solution of uranouranic oxide required a longer time when potassium chlorate was used than in the case of nitric acid and iron salts.

Figure 5 gives some of the most typical curves for the effect of temperature on the degree of oxidation and solution of uranium. Particularly rapid oxidation of uranium was observed with nitric acid over the range t = 20-40°C. In the case of sulfuric acid with nitric acid or potassium chlorate added, the temperature dependence of the degree of uranium solution was almost linear. For mixtures of sulfuric acid with ferric sulfate, manganese dioxide, and potassium permanganate, there was a more rapid increase in the degree of uranouranic oxide solution at t = 20-60°C than at t = 60-90°C. A comparison of the curves in Fig. 5 clearly shows that the the effect of temperature on uranium solution was comparatively small only when potassium permanganate was used. This is explained by the fact that in this

case the process occurred in the diffusion region. The results obtained show that the solution of uranouranic oxide in the presence of oxidants is determined to a large extent by purely kinetic factors and the process mechanism.

If we compare the degrees of oxidation of uranium by different oxidants at a sulfuric acid concentration of 25 g/liter, it can be seen that the most effective oxidant of uranium is potassium permanganate. The worst results are given by a mixture of nitric and sulfuric acids acids and potassium chlorate. The picture changes sharply in the presence of divalent iron. If the oxidation and solution of uranouranic oxide proceeds according to one of the following equations:

$$3U_3O_8 + 3FeSO_4 + 24HNO_3 = 9UO_2(NO_3)_2 + Fe(NO_3)_3 + Fe_2(SO_4)_3 + 3NO + 12H_2O;$$

$$2U_3O_8 + KClO_3 + 2FeSO_4 + 7H_2SO_4 = 6UO_2SO_4 + Fe_2(SO_4)_3 + KCl + 3H_2O;$$

$$2U_3O_8 + 3MnO_2 + 2FeSO_4 + 10H_2SO_4 = 6UO_2SO_4 + Fe_2(SO_4)_3 + 3MnSO_4 + 10H_2O;$$

$$2U_3O_8 + 2HNO_3 + 2FeSO_4 + 7H_2SO_4 = 6UO_2SO_4 + Fe_2(SO_4)_3 + 2NO + 8H_2O,$$

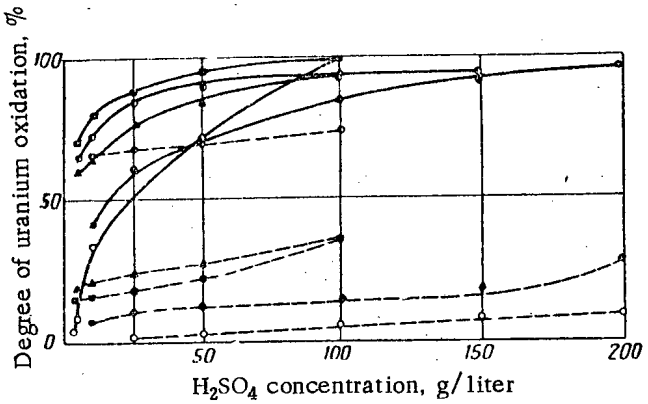

Fig. 3. Effect of initial sulfuric acid concentration on the degree of uranium oxidation with the oxidants: ○) nitric acid; ●) potassium chlorate; ◐) potassium permanganate; ▲) manganese dioxide; ■) ferric sulfate; ——) t = 90°C; – – ——) t = 20°C; τ = 3 hr.

then for such oxidants as potassium chlorate, manganese dioxide, and nitric acid in the absence of sulfuric acid, an increase in the degree of uranium oxidation is observed (Fig. 6). On the other hand, there is a sharp fall for a mixture of nitric and sulfuric acids. In the first case, the iron acts as a catalyst, accelerating the process, and in the second case it retards it.

An analogous picture was described in [2]. In the treatment of ore with a mixture of nitric and sulfuric acids at a total concentration of 108.5 g/liter, the best solution of uranium was obtained with ores as coarse particles. The longer the ore was ground in a ball mill, the less was the solution of uranium (95-72%) as a considerable amount of iron passed into the solution during the treatment of the finely ground ore. However, it was considered in [2] that the presence of iron could hardly explain the fall in uranium extraction as nitric acid was taken in excess in comparison with the amounts of iron present.

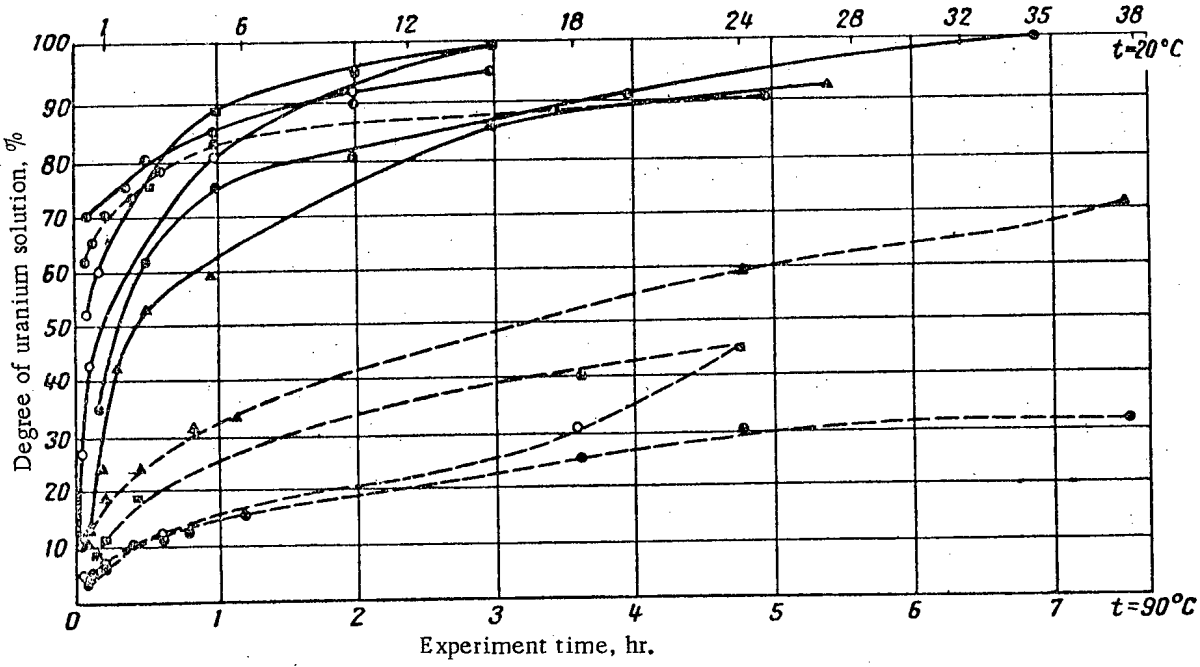

Fig. 4. Effect of process time on the solution of uranium during treatment of uranouranic oxide with sulfuric acid and the oxidants: ○) nitric acid; ●) potassium chlorate; ◐) potassium permanganate; ▲) manganese dioxide; ■) ferric sulfate; ——) t = 90°C; – – ——) t = 20°C.

Figure 7 shows the effect of ferrous compounds on the oxidation of uranium by a mixture of nitric and sulfuric acids in relation to their total initial concentration. At concentrations of 25-150 g/liter a sharp fall in uranium solution was observed and this was connected with complex-formation processes in the system Fe^{2+}, SO_4^{2-}, NO_3^-.

The oxidation processes occurring in the presence of nitric acid are autocatalytic and nitrogen oxides play the part of the catalyst in them. Therefore, the binding of the nitric acid decomposition products in a complex of the type $[Fe(NO)]SO_4$, $NO^+[Fe(NO_3)_3]^-$ or $Fe_2(SO_4)_3NO$, which give the solution a dark brown color, reduces the oxidizing power of the nitric acid.

According to data in [7], the solution acidity has a large effect on the absorption of nitrogen oxides. In [8] it was reported that the solubility of nitric oxide in solutions of ferrous salts in relation to temperature is expressed by the Clausius–Clapeyron equation, but deviates from Henry's Law. With an increase in nitric acid concentration, the absorption of nitrogen oxides by iron salts decreases [9]. As follows from Fig. 8, when the total concentration of the mixture of nitric and sulfuric acids was increased to 200 g/liter, the negative effect effect of ferrous iron disappeared and the uranouranic oxide dissolved completely.

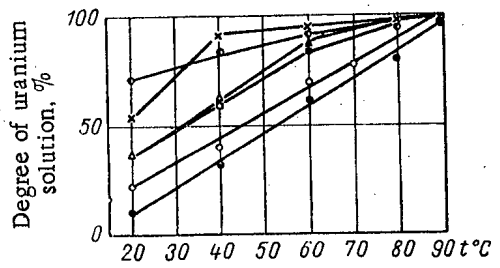

Fig. 5. Effect of temperature on the solution of uranium during the treatment of uranouranic oxide with nitric acid (×) and sulfuric acid with oxidants: ○) nitric acid; ●) potassium chlorate; ◐) potassium permanganate; ▲) manganese dioxide; ■) ferric sulfate. Concentration of acids 100 g/liter; τ = 3 hr.

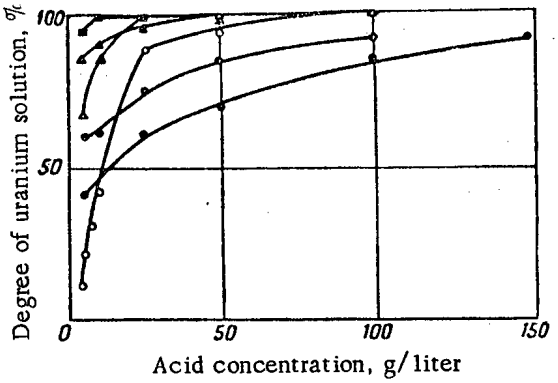

Fig. 6. Effect of ferrous compounds on the solution of uranium by nitric acid (○, △) and sulfuric acid with oxidants – potassium chlorate (●, ▲) and manganese dioxide (◐, ■) – at t = 90°C in relation to initial acid concentration: ○, ●, ◐ – without Fe^{2+}, τ = 3 hr; △, ▲, ■ – with Fe^{2+}, τ = 1 hr.

Although the normal oxidation-reduction potential of the system Fe^{2+}/Fe^{3+} = 0.77 v is the lowest among the oxidants studied, at t = 90°C, ferric compounds are better oxidants than potassium chlorate or manganese dioxide (Fig. 8). Hence it follows that in a sulfuric acid medium containing two oxidizing agnets, nitric acid and a ferric salt, the ferric compound is the uranium oxidant. Over the range of total concentration of nitric and sulfuric acid mixture of 25-150 g/liter, the nitric acid complexes the ferrous ions liberated and does not participate in the uranium oxidation. The retardation of uranium oxidation when ferric ions are added begins to appear when the ratio of nitric acid to ferric sulfate is equimolar. A gradual increase in the amount of added ferric salt increases the degree of uranouranic oxide solution. Thereupon the content of ferrous ions corresponds to the amount of uranium oxidized according to the reaction:

$$U_3O_8 + Fe_2(SO_4)_3 + 2H_2SO_4 = 3UO_2SO_4 + 2FeSO_4 + 2H_2O,$$

i.e., the oxidation of uranium proceeds as if the nitric acid were not in the reaction mixture.

What has been presented may be summarized as follows:

1. A study was made of the effect of reagent concentration, process time, and temperature on the degree of oxidation and solution of uranium oxides in an acid medium.

2. The reagent concentration and temperature had least effect on uranium oxidation when potassium permanganate was used. Despite the relatively low oxidation-reduction potential of Fe^{2+}/Fe^{3+} relative to U^{4+}/UO_2^{2+}, iron salts are the most effective oxidants of uranium in an acid medium at t = 90°C.

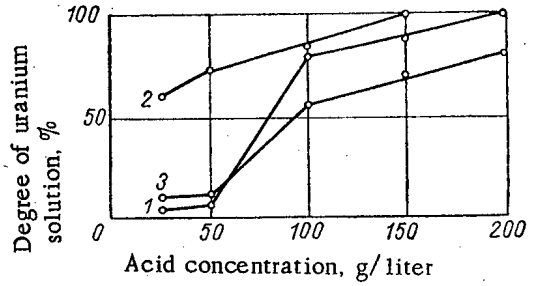

Fig. 7. Effect of ferrous compounds on the solution of uranium by a mixture of nitric and sulfuric acids in relation to the total acid concentration: 1) in the presence of Fe^{2+}; 2) in the absence of Fe^{2+}, t = 90°C, τ = 3 hr; 3) oxidation of Fe^{2+}.

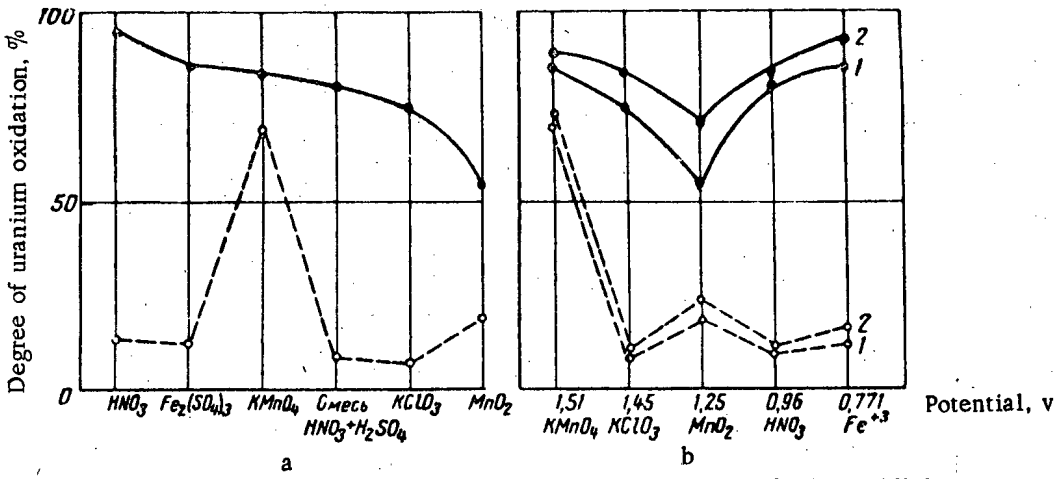

Fig. 8. Comparative characteristics of oxidants: a) with respect to falling oxidizing power relative to uranium; b) with respect to falling oxidation-reduction potential. Experiment time: 1) 1 hr; 2) 2 hrs; ————) t = 90°C; – – – –) t = 20°C.

3. It was established that when iron compounds are absent from solution, potassium chlorate and manganese dioxide are the least efficient oxidants with respect to uranium. When ferrous ions are introduced into the reaction mixture, these oxidants completely oxidize uranium even in comparatively dilute acid solutions. High concentrations of a mixture of nitric and sulfuric acid are required for the oxidation of uranium and iron in the presence of iron ions.

4. It was established that in the presence of considerable amounts of iron ions the oxidation of uranium by a mixture of nitric and sulfuric acids is retarded due to complex-formation processes.

LITERATURE CITED

1. G. Mervin, T. Apchurch, et al., Chemistry of Nuclear Fuel [Russian translation] (Goskhimizdat, Moscow, 1956) p. 91.
2. Gunn By Brad, S. Cavers, and A. Van Cleave, Canad. J. Technol. 34, 6, 379 (1956).
3. T. Arden, Ind. Chemist. 32, 37 , 202 (1956).
4. A. Gandin and R. Schuhmann, J. Metals, 8, 8, 1065 (1956).
5. C. J. Rodden, Analytical Chemistry of Uranium and Thorium [Russian translation] (IL, Moscow, 1956) p. 66.
6. I. P. Alimarin, Zavodskaya Lab., 5-6, 545 (1940).
7. C. Addison and J. Lewis, Uspekhi Khim. 25, 9, 1121 (1955).
8. S. N. Ganz and L. I. Mamon, Zhur. Priklad. Khim. 26, 10, 1005 (1953).*
9. G. D. Sirotkin and V. V. Starostin, Zhur. Priklad. Khim. 27, 11, 1141 (1954).*

*Original Russian pagination. See C. B. translation.

COMPOSITE RADIOMETRIC WORK IN MINING

I. M. Tenenbaum

Translated from Atomnaya Energiya, Vol. 8, pp. 336-339,
April, 1960
Original article submitted May 30, 1959

Problems of the composite use of mine radiometry methods and the association of these methods with specific mining-geological conditions are described. The optimum conditions for ensuring the maximum efficiency of qualitative and quantitative measurements in a mine are given.

Since uranium deposits are diverse in character, their classification is given here according to the particular kinds of radiometric measurements indicated, together with the most effective combinations of radiometric methods for the respective classes. The principles enumerated in the article can be used for planning radiometric work simultaneously with the planning of new mining undertakings. The article is of practical and scientific interest to mining engineers, geologists and geophysicists, engaged in surveying and working uranium deposits and the planning of ore mining undertakings.

In the past ten years, various types of radiometric measurements have been developed and adopted in the practice of prospecting and exploitation of uranium deposits; these measurement techniques are used to detect, map and sample ore bodies in the solid, take account of the losses of metal and working out of the ore and employ measures to overcome these factors, and grade and assess the quality of the ore-bearing rock body and the commercial ores.

These problems are solved most satisfactorily if the geological-morphological characteristics of the deposits, the radiological properties of the ores and the particular features of the mining operations carried out during the prospecting and working of a deposit are taken into account when the radiometric procedure and the equipment to be used are selected.

The methodology of mine radiometry includes qualitative and quantitative measurements in mine workings and on the surface. The qualitative measurements include geophysical documentation of mine workings, faces, benches of quarries, sorting the ore won in a face, sorting the ore-bearing rock body in mine cars, radiometric sorting of the ore mass in ore-picking units; quantitative measurements included radiometric sampling of workings, faces, benches and waste, rapid γ-analyses of the ore in mine cars, trucks and boxes, and on conveyers. The γ-logging of boreholes and the logging of prospect holes and shot holes can be used for both the qualitative and quantitative characteristics of a mineralization.

By a "complex" or "scheme" we mean a combination of a number of these types of radiometric work. The character of different schemes is determined by the relative volume and purpose of each type of work, the procedure of the latter, the volume of the necessary experimental observations and the equipment employed.

The necessity of measuring a particular one of the above-listed objects (sections of the solid mass and the volumes of the ore-bearing rock mass) depends on the methods of prospecting and testing the deposit, the system of working and other characters of the technological complex of the mine, which are determined, in turn by the geological-morphological characteristics of the deposits, the modes of occurrence of the ore bodies, the physical properties of the ores, the topography and certain other (in particular, economic) factors.

Qualitative radiometric measurements carried out on the surface are least dependent on the geological characteristics of the deposit and mining operations. The radiometric sorting of the ore-bearing rock body forms an exception. The importance of this type of work in the general complex is very great. The sorting efficiency is determined by the radiometric contrast of the ores, which depends mainly on the distribution of uranium in the ore body.

The purpose of qualitative measurements in the solid is determined by the method of ore extraction, which depends primarily on the thickness of the ore bodies and the distribution of uranium in them.

The following conditions are necessary for obtaining maximum accuracy and efficiency of quantitative radiometric measurements:

1) the presence of a thick layer, saturated for γ-rays;

2) continuous and uniform distribution of the emitter in the investigated object;

3) absence of thorium in the uranium ore;

Classification of Uranium Deposits in Accordance with the Characteristics of Radiometric Work

Class	Geological-morphological characteristics of the uranium deposit	Group	Subgroup	Radiological characteristics	Examples of deposits
I	Uranium-bearing seams of thickness greater than 0.5 m, occurring over extensive areas, with uniform, persistent, poor mineralization.	1	Without thorium With thorium	With equilibrium ores.	Sedimentary deposits of the Blind River and Witwatersrand type.
		2	Without thorium With thorium	With non-equilibrium ores.	
II	Stratiform, columnar and vein-like seams and single veins of thickness greater than 0.5 m with nonuniform, discontinuous mineralization. Metal content usually low.	1	With thorium Without thorium	With equilibrium ores.	Certain sedimentary (in lagoon-marine sandstones), sedimentary-metamorphic deposits, certain hydrothermal (metasomatic, single veins and deposits forming broad fault zones), infiltration deposits; migmatization zones and pegmatites.
		2	With thorium Without thorium	With non-equilibrium ores.	
III	Systems of thin veins of thickness less than 0.5 m, with very nonuniform, extremely discontinuous and generally rich mineralization.	1	With thorium Without thorium	With equilibrium ores.	Hydrothermal deposits (systems of thin veins) and certain pegmatites.
		2	With thorium Without thorium	With non-equilibrium ores.	

4) the presence of radioactive equilibrium between radium (B + C) and uranium (or constant displacement of equilibrium).

In deposits where such conditions do not obtain, quantitative radiometric measurements are complicated and must be accompanied by a considerable volume of experimental work.

When an ore-bearing rock body transported in standard volumes is measured, highly accurate results can be obtained relatively simply. Allowance for the heterogeneity of the mineralization, the absence of a saturated layer, and in many cases, the heterogeneity of the ores and the presence of thorium in them can be made by selecting appropriate ore standards.

The effect of the absence of favorable conditions is greatest with regard to the reliability of quantitative measurements in the solid. If radiometry is to be fully utilized in all stages of prospecting and development of a deposit, this fact must be taken into account when the scheme of radiometric work is selected.

In all cases, the choice of equipment must be made in accordance with the range of variation of the metal content in the ores. The thickness of the ore bodies, the distribution of uranium in them, and the maximum and mean concentrations of uranium and thorium in the ore vary widely, due to the genetic diversity of workable uranium deposits. As a result of supergene alteration of depsoits, the state of radioactive equilibrium in ores is often disturbed: local, local-zonal and zonal displacements of this equilibrium are observed. The distribution of uranium in ore bodies of different deposits (from uniform to extremely heteregeneous) determines the radioactive contrast of the ore (from very contrasted to nonconstrasted).

The essential differences in the geological characteristics of deposits, including the intensity and spectral composition of the recorded γ-radiation, exclude the possibility of employing a standard scheme of radiometric work.

To select the most appropriate scheme for given geological conditions, all deposits are best devided into three classes. In deposits of the same class, the thickness of the ore bodies, the character of the distribution of the mineralization and its intensity must be very similar to each other. Deposits with thick and thin ore bodies must be classified according to these features;

similarly, distinctions must be drawn between deposits with uniform, nonuniform and extremely nonuniform distribution of uranium in the ore bodies, and, again, between deposits with a low, average and high concentration of metal in the ore.

To establish an unequivocal relationship between the recorded γ-radiation and the uranium content in the ore, deposits of each class are best divided into groups, in accordance with the radiological characteristics of the ores (radium-uranium equilibrium and the complexity of the uranium-thorium mineralization). This type of classification of deposits is shown in Table 1.

Thus, taking into account their geological-morphological characteristics, all uranium deposits are incorporated in three major classes; within each class, groups of deposits are distinguished, taking into account the radiological characteristics of the ores. A single scheme of radiometric work is recommended for each class. For individual groups of deposits, the main scheme of radiometric work is distinguished with respect to the relative complexity of the procedure employed, the depth of the metering network, the degree of reliability of the results, the extent, character and proportion of experimental work, and certain secondary features of the measurement work. But ore bodies or zones with differing geological-morphological or radiological characteristics can be found within a deposit. Such zones must be investigated separately in accordance with the same classification.

A description of three schemes of radiometric work is given below. The first scheme is best used for deposits of class I, the second for deposits of class II, and the third for deposits of class III.

The basis of the first scheme is formed by quantitative measurements in the solid, radiometric sampling of mine workings, faces and benches, and quantitative γ-logging of boreholes and shotholes. Rapid gamma analyses of the ore-bearing rock body, in mine cars and trucks and on conveyers also play an important part. Ordinary γ-logging of boreholes, the data of which can be successfully employed for calculating the reserves of a deposit, occupy the most important place in the scheme of work. In all these stages of the work, qualitative measurements play only a secondary role. Determination of the radioactivity of the ore-bearing rock body is unprofitable and can be carried out in individual cases only with the most sensitive scintillation equipment during loading of lumps onto the conveyer.

The second scheme of work is distinguished from the first by the fact that quantitative γ-logging of boreholes, carried out to a considerable extent during prospecting, is largely replaced by radiometric sampling of the mine workings. In this case, underground qualitative measurements are no longer secondary but, to a considerable degree, perform independent functions: they are used for carrying out separate extraction of ore during selective extraction, sorting of ores at the face, preventing losses of metal as a result of incomplete extraction of ore, etc. As in the previous case, rapid gamma analyses of the ore won are carried out without first separating the ore and rock. The role of radiometric concentration of the rock-ore mass increases appreciably; it can be carried out with limited-sensitivity equipment during lump or batch charging of the ore-sorting units.

Qualitative measurements in the solid form the basis of the third complex: geophysical documentation of the mine workings and faces, qualitative γ-logging of shotholes, prospect holes and boreholes, and sorting into ore and rock at the face. The object of the measurements is to control the direction of the mine workings, ensure selective extraction of ore and prevent losses of metal and depletion of the ore. Underground quantitative measurements are limited to radiometric sampling of the waste. Individual rapid γ-analyses of rich and poor ore and rock are carried out on the surface. The object of the express analyses is to obtain a face-by-face calculation of the metal in the sorted rock-ore mass; this is necessary for calculating the reserves (by the overall method) and determining the lossesof metal and depletion of the ores. In this complex the role of measurement of the radioactive concentration of the ore-bearing rock body is very great. It is effective and forms an integral part of the general technological scheme.

The principal points of the proposed schemes are corroborated by many years of practical experience.

The scheme of radiometric work for each deposit is best planned when the projects for new ore mining undertakings are drawn up. Such planning, carried out with account taken of geological-morphological and practical mining factors, must ensure maximum efficiency of prospecting and exploitation, a reduction in their cost, and optimum location of the principal surface buildings of the mines.

HEAT-TREATMENT OF URANIUM

G. Ya. Sergeev, V. V. Titova, Z. P. Nikolaeva,
and A. M. Kaptel'tsev

Translated from Atomnaya Energiya, Vol. 8, No. 4, pp. 340-347,
April, 1960
Original article submitted April 20, 1959

This article describes one of the uranium heat-treatments, hardening, which makes it possible to obtaina fine-grained quasi-isotropic structure.

The possiblity of improving the strength characteristics of uranium by hardening in the β and γ-phase and the effect of hardening on the micro- and macrograins in dependence on the chemical composition is analyzed. Uranium creep in the α-phase temperature interval is considered.

The deformation resistance of uranium materials under the action of neutron fluxes depends on the composition, structure, and properties of the metal [1].

The composition and structure of the core metal must vary with the fuel element operating conditions. One of the methods for modifying the structure and properties of uranium is heat-treatment, conventionally called hardening.

By hardening, we shall designate the heating of uranium to the temperatures of the β and γ-phases with subsequent quenching in water or oil. In this, the fixing of high-temperature or intermediate phases does not occur at room temperature in uranium of usual purity.

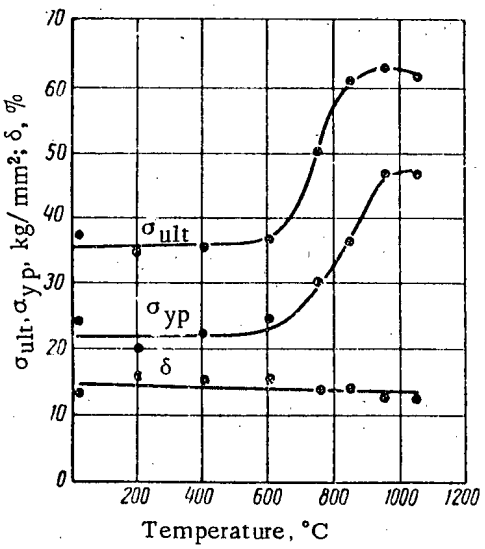

Fig. 1. Variation of the mechanical properties of hot-rolled uranium at 20°C with the hardening temperature. The specimens were tested at 20°C. Impurity content (% by weight): iron, $7 \cdot 10^{-3}$; silicon, $1.2 \cdot 10^{-2}$; carbon, 0.04; nitrogen, $7.4 \cdot 10^{-3}$.

However, as will be shown later, hardening produces a considerably finer macro- and microstructure, changes the texture, and improves the strength characteristics of uranium.

We investigated the effect of hardening on the macro- and microstructure and the mechanical properties of cast and hot-rolled uranium, which were determined at room and higher temperatures.

Tensile tests of proportional shortened specimens which had a diameter of 5 mm, were performed in an IM-4R machine with short-duration load application, and creep tests were performed in TsKTI-3 machines, which were specially modified and equipped according to the authors' specifications for the heating of readily oxidizable metals in an atmosphere of purified helium. Standard specimens (diameter: 10 mm, gauge length: 100 mm) were machined from rods 22 mm in diameter and 200 mm long.

The rods to be hardened were heated in a vacuum furnace. The heating of uranium specimens to 1000°C in tensile tests was performed in an atmosphere of chemically pure argon in a specially constructed adapter [2].

For the investigation of different changes in mechanical properties caused by hardening after heating in the α, β, and γ-phases (Fig. 1), rods of hot-rolled and then air-cooled uranium were heated over a period of 1 hr at temperatures from 200 to 950°C, after which they were quickly transported to the oil tank.

Hardening of uranium at the temperatures of the β- and γ-phases considerably improves its strength characteristics. The greatest change in ultimate strength and the yield point is observed after hardening in the γ-phase (a change of approximately 60%), when the ultimate strength increases from 35-40 to 60-65 kg/mm². A similar regularity in the ultimate

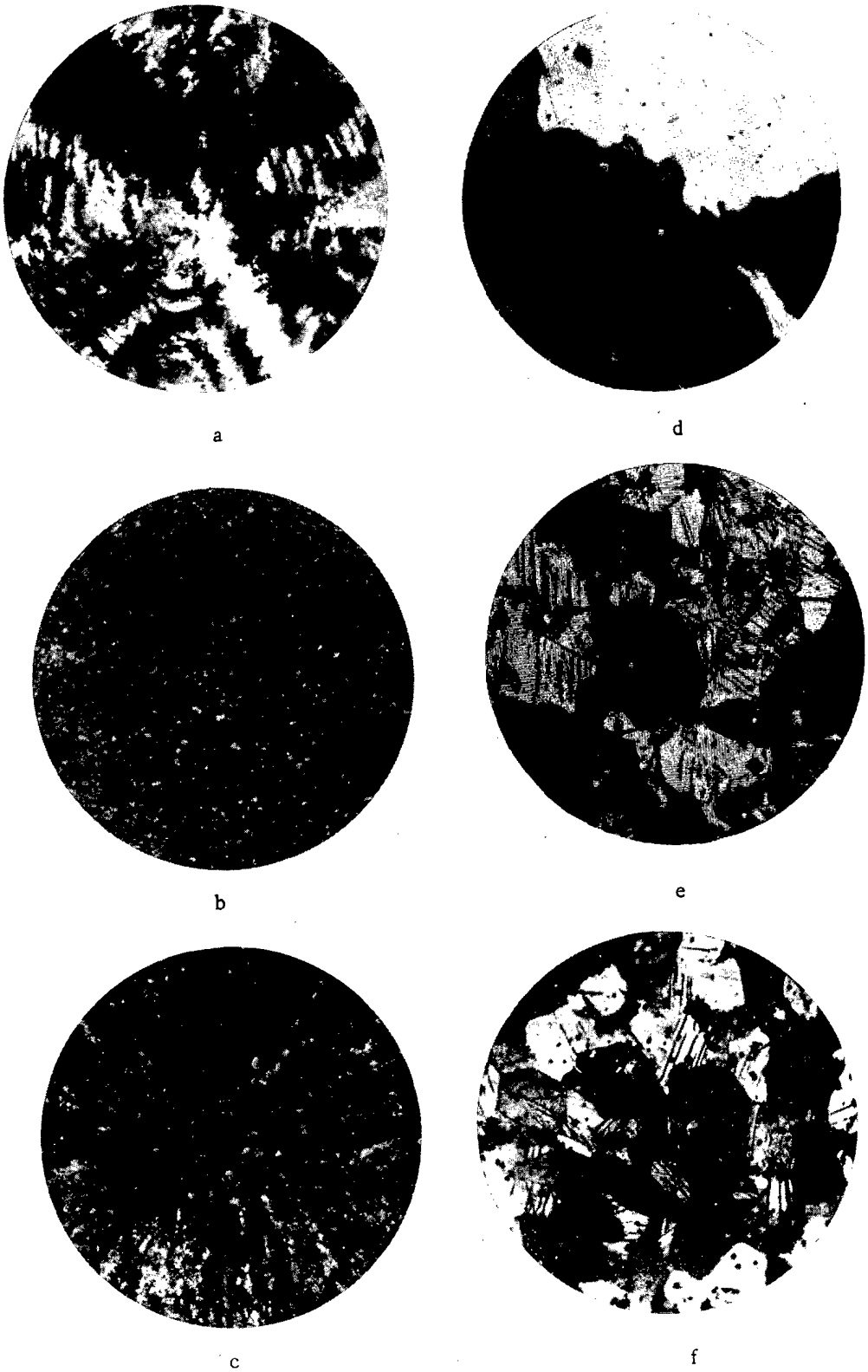

Fig. 2. Structural changes in uranium after hardening. a) Macrostructure of hot-rolled uranium; the over-all content of iron and silicon was $1.9 \cdot 10^{-2}$% by weight (× 2); b) macrostructure of uranium hardened in the β-phase (× 2); c) macrostructure of uranium hardened in the γ-phase (× 2); d), e), and f) microstructure of the a, b, and c specimens, respectively (× 135).

TABLE 1. Mechanical Properties of Uranium Hardened in Different Cooling Media[1]

Heat-treatment	Ultimate strength, kg/mm²	Yield point, kg/mm²	Strain, %	Relative reduction in area, %
Hot-rolled	37.9	26.0	6.8	10.8
Hardening[2] at 750° C in argon-stream	39.5	21.2	8.2	10.4
» at 750° C in oil	50.4	34.7	4.9	8.2
» at 750° C in water	51.6	31.2	6.3	8.4
» at 850° C in argon stream	39.5	23.1	6.6	9.7
» at 850° C in oil	55.6	39.3	6.5	8.4
» at 850° C in water	64.3	56.5	6.8	8.6

[1] The specimens were tested at room temperature.
[2] Exposure at the given temperatures lasted 60 min.

TABLE 2. Effect of the Water Temperature on the Mechanical Properties of Hardened Uranium.

Heat-treatment	Ultimate strength, kg/mm²	Yield point, kg/mm²	Strain, %	Relative reduction in area, %
Cast uranium with (% by weight): iron, $1.96 \cdot 10^{-2}$; silicon, $1.65 \cdot 10^{-2}$; carbon, 0.05	44.1	31.3	4.6	8.8
Harden. in water[1] (t=0° C)	68.6	50.7	4.1	4.7
» » (t=20° C)	68.7	51.6	2.4	5.6
» » (t=30° C)	68.7	50.6	4.0	4.8
» » (t=50° C)	64.4	47.1	3.3	5.2
» » (t=80° C)	55.4	45.9	2.6	6.0
» » (t=100° C)	49.9	45.4	2.4	5.0

[1] The hardening was performed in the γ-phase temperature range (850 °C), and the exposure time at this temperature was 60 min.

TABLE 3. Effect of the Billet Diameter on the Mechanical Properties of Hardened Uranium.

Billet diam., mm	Ultimate strength, kg/mm²	Yield point, kg/mm²	Strain, %	Relative reduction in area, %
22	55.6	39.3	6.5	8.4
18	60.9	37.2	7.3	7.7
14	61.0	44.5	6.9	6.7

strength variation is observed in hardening cast uranium [3]. The strain remains practically the same.

Cast or hot-rolled uranium has a coarse-grained dendritic macrostructure* (Fig. 2a). In large cast pieces, the size of individual macrograins attains 30 mm. Hardening in the β-phase region leads to the formation of a fine-grained disoriented structure with a macrograin size of the order of 0.8-2.0 mm (Fig. 2b). The grains become finer also in hardening in the γ-phase region, however, in this case, a radial orientation of grains is usually observed (Fig. 2c).

The microstructure† of cast or hot-rolled uranium consists of coarse grains, which, in turn, consist of a number of subgrains whose orientation differs by 5-10°, while uranium grains without texture can have the most diverse orientations. The size of micrograins in hot-rolled and cast uranium is of the order of 500-800 μ. Hardening in the β- and γ-phase regions reduces the grain size to 70-150 μ. However, beside fine grains, also large grains are observed, especially in uranium of higher purity. Beside the general refinement of grains, a strongly pronounced jaggedness of boundaries is also observed after hardening, and a large number of twins and slip lines appears (Fig. 2, d and e).

The degree of the reduction in size of grains in hardened uranium depends on the chemical composition and the ratio of impurities, in the first place, iron, silicon, nickel, and aluminum [1]. For a larger iron and silicon content in uranium, the macrograin size sharply decreases, however, beginning with a content of $3 \cdot 10^{-2}$% by weight, the changes are insignificant. Aluminum exerts a similar, but less intensive, influence.

In order to determine the effect of the exposure time before hardening on changes in mechanical properties, uranium billets were heated to 750 and 850°C; the exposure time at the hardening temperature varied from 15 to 120 min. The quenching was done in oil.

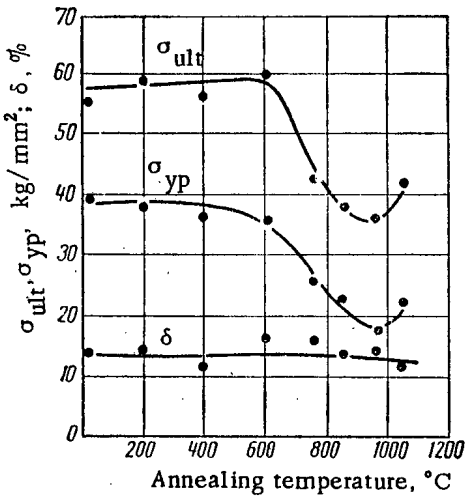

Fig. 3. Variation of the mechanical properties of uranium hardened in the γ-phase with the annealing temperature.

In many cases, good mechanical properties of hardened uranium were obtained after a 15-min. exposure. A futher increase in the exposure time in hardening in the β as well as in the γ phase did not result in substantial changes in strength characteristic values.

Table 1 shows the results of mechanical testing of specimens hardened in different cooling media (water, oil, and argon), and Table 2 shows the effect of changing the water temperature on the mechanical properties of uranium in hardening. These data indicate that the hardened uranium strength characteristics are the better, the higher the cooling rate.

Since the mechanical properties of hardened uranium depend on the cooling rate, they also depend on the diameter of the billet to be hardened (Table 3).

The hardenability of uranium must be taken into account if large products are to be subjected to heat-treatment.

Figure 3 shows the diagram of changes in the mechanical properties of hardened uranium in dependence of the annealing temperature. In comparison with unhardened uranium, hardened uranium exhibits higher ultimate strenght and yield point values after annealing at α-phase temperatures, and only after heating at the β-phase temperatures can we observe a sharp reduction of the strength characteristics to values obtained in testing the initial unhardened specimens. For the investigation of the effect of repeated hardening on the mechanical properties of uranium, rods 22 mm in diameter were hardened in water after an exposure time of 35 min at 740°C. The metal contained the following basic impurities (% by weight): iron, $1.07 \cdot 10^{-2}$; silicon, $3.4 \cdot 10^{-3}$; carbon, 0.09; nickel, $3.2 \cdot 10^{-3}$.

After the first ten hardenings, the ultimate strength increased by 17% (Fig. 4). If the number of hardenings is increased to 20, the ultimate strength drops to a certain extent, which is connected with the appearance of cracks. During the experiment, the rod was elongated by 4%. Metallographic investigations showed that repeated hardening leads to a reduction in size of macro- and micrograins in hardened uranium; this is in agreement with data from [4].

* The macrostructure was developed by immersing the section into the following reagent for a period of 3-5 min: 1 liter water solution of 53 g ammonium chloride, 85 g cuprous chloride, and 66 ml hydrochloric acid. The chilling was performed in concentrated nitric acid.

† The microstructure was developed by electrolytic etching in a reagent consisting of a water solution of chromic and acetic acid in 1 : 1 : 2 proportion.

TABLE 4. Results of Creep Tests of Cast and Hardened Uranium at 100, 300 and 500° C. Impurity content (% by weight): iron, 1.5×10^{-2}; silicon, 4.83×10^{-3}; carbon, 4×10^{-2}; nitrogen, 4.85×10^{-3}.

Test temp. °C	Metal state	Stress, kg/mm²	Deformation at the moment of loading, %	Creep rate, %/hr	Creep rate measurement interval, hr	Total creep deformation	
						hr.	Σε, %
100	Cast uranium	30	1.88	$1.6 \cdot 10^{-4}$	180—500	500	2.53
	Cast uranium with subsequent hardening in the γ-phase region	30	0.45	$2.9 \cdot 10^{-5}$	20—500	500	0.52
300	Cast uranium	25	3.50	$4.9 \cdot 10^{-4}$	220—540	540	5.00
	Cast uranium with subsequent hardening in the β-phase region	25	0.59	$1.1 \cdot 10^{-4}$	110—565	565	0.74
	Cast uranium with subsequent hardening in the γ-phase region	25	0.35	$7.6 \cdot 10^{-5}$	170—565	565	0.53
500	Cast uranium	4	0.04	$1.3 \cdot 10^{-3}$	40—520	520	0.87
	Cast uranium with subsequent hardening in the β-phase region	4	0.04	$7.7 \cdot 10^{-3}$	50—210	500	5.05
	Cast uranium with subsequent hardening in the γ-phase region	4	0.05	$7.3 \cdot 10^{-3}$	40—340	525	4.92

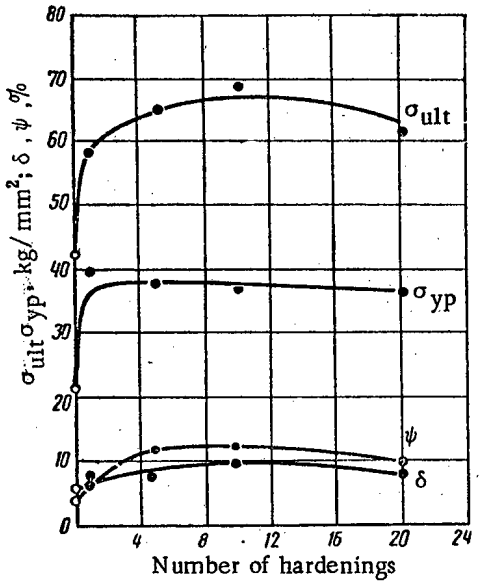

Fig. 4. Variation of the mechanical properties of uranium with the number of repeated hardenings; O) strength characteristics of hot-rolled uranium.

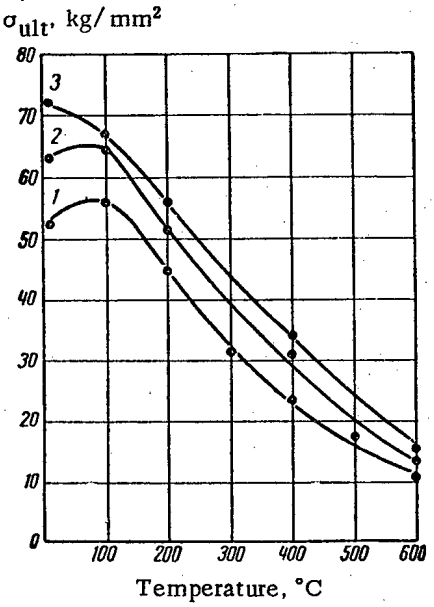

Fig. 5. Effect of test temperatures on the mechanical properties of uranium. 1) Cast uranium; 2) uranium hardened in the β-phase region; 3) uranium hardened in the γ-phase region.

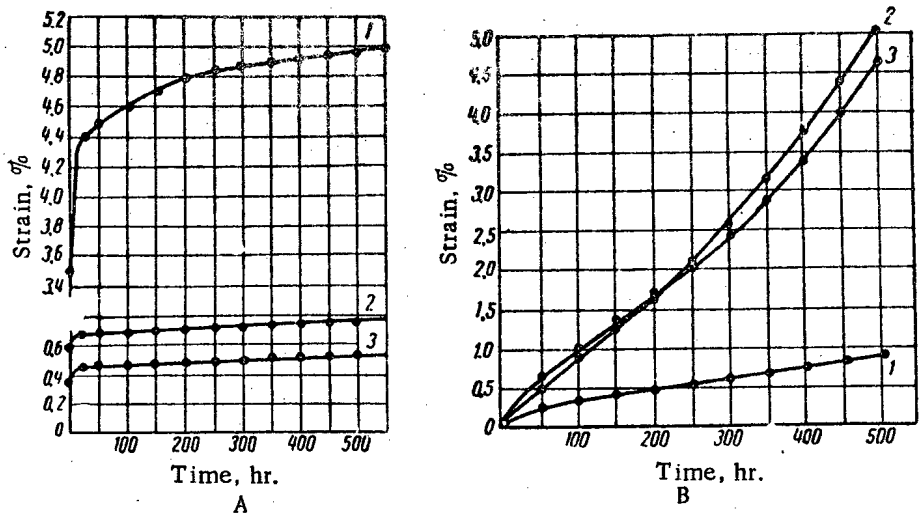

Fig. 6. Primary creep curves for uranium. 1) Cast uranium; 2) uranium hardened in the β-phase region; 3) uranium hardened in the γ-phase region. A) Test temperature: 300°C; stress: 25 kg/ mm²; B) test temperature: 500°C; stress: 4 kg/ mm².

For uranium hardened in the β and γ-phases, the strength characteristic values in short-duration tensile tests at higher temperatures become gradually lower, however, for all α-phase temperatures, they remain higher than the values of the same characteristics of the unhardened metal at the corresponding temperatures (Fig. 5).

The hardening of cast as well as hot-rolled uranium in the β- and γ-phase regions leads to a considerable increase in creep resistance. However, this is observed only in the case where the specimen under investigation is stressed at temperatures not exceeding 350-400°C. At higher temperatures, hardening produces the opposite effect, i.e., it reduces the creep resistance of uranium (Table 4 and Fig. 6). This effect was noted also in [5].

At temperatures exceeding 300-350°C, the grain flow at the boundaries begins to play an important role in the process of uranium deformation. In connection with this, the deformation of hardened uranium with fine crystals and large boundary surfaces occurs much more readily than the deformation of cast or hot-rolled uranium with large crystals. At low temperatures, when the deformation is caused mainly by twinning, uranium with fine crystals, which is strengthened by hardening, has a much greater deformation resistance.

Prolonged action of stresses in creep tests at temperatures exceeding 400°C causes recrystallization in the hardened metal, which also leads to a fine division of grains. The tendency to recrystallization in uranium hardened at a certain given rate during annealing without the application of additional stresses was demonstrated in [6,and 7].

In the technological processing of fuel elements, uranium is hardened in order substantially to reduce the anisotropy of its properties, which had an adverse effect on the stability of uranium cores in neutron fields and in in thermic cycles.

The structure of hardened uranium approaches the quasi-isotorpic structure as a result of fine grain division and the elimination of texture. This considerably improves the strength characteristics of uranium in short- and long-term tests (in the latter case, at temperatures not exceeding 400°C).

If a specimen having a certain given crystal orientation is heated to a temperature higher than the $\alpha \rightleftharpoons \beta$ phase conversion temperature, this and the subsequent conversion in cooling will cause a reduction in the thermal expansion anisotropy, and the specimen will approach the quasi-isotropic state.

The reduction in the anisotropic thermal expansion coefficient in a specimen or product depends on the time of the β- or γ-phase existence, the heating temperature, and the cooling rate. Figure 7 [5] shows the dependence of the linear anisotropic expansion coefficient (variation

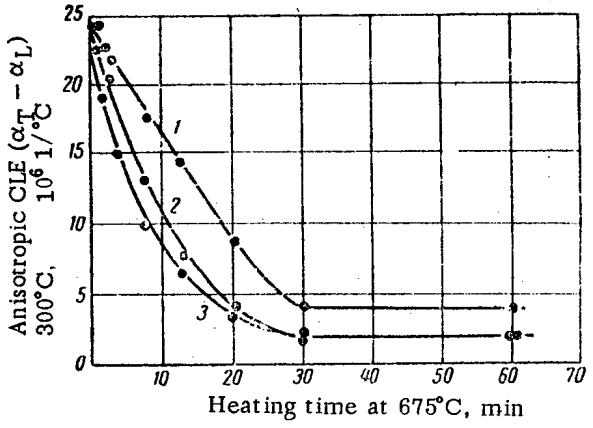

Fig. 7. Effect of the heating time at 675°C on the anisotropic linear expansion coefficient in uranium rods under different cooling conditions. 1) Air-cooling; 2) hardening in the β-phase region with subsequent annealing in the α-phase; 3) hardening in the β-phase region.

of the coefficient value along the rod axis and radius) on the heating time at 675°C under different cooling conditions.

From the above, the following conclusions can be drawn:

1. As a result of fast cooling of uranium heated to the β- and γ-phase temperatures (hardening), its structure and properties change.

2. Hardening reduces the uranium macrograin size from 10-30 to 0.8-2.0 mm and the micrograin size from 500-800 to 70-150 μ.

3. The ultimate strength of hot-rolled uranium after hardening at the β-phase temperature is raised by approximately 30% and, after hardening at the γ-phase temperature, by approximately 60%.

4. Hardening of uranium brings about a manifold increase in its creep resistance at temperatures not exceeding 400°C and a reduction of this resistance at higher temperatures of the α-phase.

5. The degree of changes in the macro- and microstructure and the strength characteristics after hardening depends on the uranium chemical composition; primarily, it depends on the content of iron, silicon, aluminum, and nickel.

6. The cooling rate in hardening uranium in the β- and γ-phase regions greatly affects its strength characteristics. The rise in the values of uranium strength characteristics is the greater, the greater the cooling rate in hardening.

7. At all α-phase temperatures, the strength characteristics of hardened uranium (in short-term tests) are higher than those of unhardened uranium at the same temperatures.

LITERATURE CITED

1. A. S. Zaimovskii, G. Ya. Sergeev, V. V. Titova, B. M. Levit-skii, and Yu. N. Sokurskii, Atomnaya Énerg. 5, 4, 412 (1958).‡
2. G. Ya. Sergeev, V. V. Titova, E. M. Savitskii, A. A. Zhul'kova, and Z. P. Nikolaeva, Atomnaya Énergiya 5, 6, 618 (1958).‡
3. A. A. Bochvar, S. T. Konobeevskii, A. S. Zaimovskii, G. Ya. Sergeev, et. al., Atomnaya Énergiya 5, 1, 5 (1958).‡
4. H. H. Chezwik, et al., Transactions of the Second International Conference on the Peaceful Use of Atomic Energy (Geneva, 1958). Selection of Reports by Foreign Scientists. Nuclear Fuels and Reactor Materials [Russian translation] (Atomizdat, Moscow, 1959) Vol. 6, p. 53.
5. R. Nichols, Nucl. Eng. 2, 18, 355 (1951).
6. W. Donell, "Kinetics of the beta transformation of uranium." Nuclear Engineering and Science Conference (Chicago, March, 1958).
7. H. Garder, and J. Riches, "The effect of transformation cooling rate on the activation energy required for recrystallization of beta-quenched uranium " Nuclear Engineering and Science Conference, (Chicago, March, 1958).

‡Original Russian pagination. See C. B. translation.

INVESTIGATION OF THE INTERNAL FRICTION INCREASE CAUSED BY TEMPERATURE CHANGES IN POLYCRYSTALLINE URANIUM SPECIMENS

Yu. N. Sokurskii and Yu. V. Bobkov

Translated from Atomnaya Énergiya, Vol. 8, No. 4, pp. 348-353,
April, 1960
Original article submitted May 30, 1959

The increase in the internal friction with time in heating at different rates was measured with respect to the damping of torsional vibrations during the heating of specimens. Specimens of γ-phase quenched, γ- and α-phase annealed, and recrystallized polycrystalline uranium were investigated. It is shown that the rate of the internal friction rise in specimens gradually decreases in time and that the internal friction increment attains a limiting value, the magnitude of which is approximately proportional to the specimen heating rate. The internal friction increment is related to stresses which arise in the specimen due to the anisotropic thermal expansion coefficient when the temperature changes. The reduction in internal stresses, which is either due to an increase in the grain size to a magnitude comparable to the diameter of the specimen under investigation or the formation of a predominant orientation in specimens, results in a reduction of the internal friction increment. During the heating process, also macroscopic shearing deformation occurs in the specimen. Such an increase in internal friction in heating was also observed in a thermally anisotropic metal, such as zinc; it was not observed in metals with isotropic thermal expansion coefficients – aluminum and molybdenum.

Introduction

During the investigation, a sharp increase in internal friction in uranium was observed at the moment when the specimen temperature changed. This phenomenon, indicating an intensification of relaxation processes in uranium when the temperature changes, is of considerable interest, since the temperature of uranium materials repeatedly changes during its utilization.

It is known that polycrystalline uranium specimens are greatly deformed in the case of cyclic temperature changes [1 and 2]. This phenomenon is explained by the effect of internal stresses which arise in polycrystalline thermally anisotropic metals when their temperature changes. As the grains of a polycrystalline aggregate expand anisotropically due to a temperature rise, they act on the neighboring grains and cause stresses and deformation. It was demonstrated that these stresses can accelerate creep [3], similar to the way in which stresses connected with radiation growth accelerate the creep of uranium which is being irradiated [1 and 4]. However, with the exception of a brief reference to an unpublished paper [5], there is no literature providing data on the effect of these stresses on such a sensitive parameter as internal friction.

It is known that internal friction increases during the plastic deformation process. In particular, in deformation at a rate of 0.08%/ min, internal friction in molybdenum increases six- to ten fold [6]. There were also reports on the intensification of internal friction in zinc in plastic deformation [7]. It was established in [8] that internal friction in a lead tube becomes approximately twice as large when the gas pressure in the tube rises. At the same time, if a constant pressure is applied, the internal friction magnitude is not affected. It was also reported [9] that internal friction in aluminum increases in slow extension at higher temperatures. In connection with this, the growth of internal friction in thermally anisotropic polycrystalline solids as their temperature changes is not unexpected: the increase in internal friction can be caused by deformations due to the anisotropic expansion of individual grains.

Investigation Method and the Material Tested

Internal friction was determined with respect to the damping of free torsional vibrations in a device similar to the Ke tester [10] (Fig. 1). A special feature of this tester is a device for heating the specimen by transmitting an electric current through it. Provision was made for a mercury switch to be switched on and off during experiments by means of a relay, 4. Investigations showed that this switch does not greatly influence the internal friction magnitude, and, therefore, the measurements could be performed directly during

the heating of specimens by current. The measurements were performed in a vacuum of $5 \cdot 10^{-6}$ mm Hg for a constant heating rate. The heating rate constancy was secured by manual regulation of current I according to a program determined beforehand. The experiments were performed for heating rates from ~2.5 to 20 deg/ / min.

Measurements performed by means of thermocouples 8 (see Fig. 1) showed that the temperature drop along the specimen length in heating usually did not exceed 3-4°C.

The internal friction was determined with respect to the time in which the oscillation amplitude was reduced to one-half of the initial value. The pendulum and the lower grip weight created stresses in the specimen which did not exceed 75 g/ mm^2. The maximum osicllation amplitude corresponded to a maximum specimen shear deformation of $1.2 \cdot 10^{-5}$. The measurements were performed visually for an oscillation frequency of ~2 cps. In a number of experiments, photographic records of oscillograms were obtained, which were used for calculating the internal friction.

Uranium specimens 1 mm in diameter and 220 mm long were obtained from rods 3 mm in diamter by drawing at 200°C with repeated intermediate annealing in the α-phase. These specimens had the following composition (basic impurities) % by weight:

Material composition designation	C	Fe	Si	Al
A	0.037	$2.1 \cdot 10^{-3}$	$4.5 \cdot 10^{-3}$	—
B	0.049	$8.3 \cdot 10^{-3}$	$1.4 \cdot 10^{-2}$	$1.4 \cdot 10^{-2}$

Specimens in the following states were investigated.

1. Specimens quenched in water after exposure in the γ-phase (at 850°C) over a period of 2 hr. The average grain size was 15-25μ.

2. Specimens annealed in the γ-phase at 850°C over a period of 2 hr with slow cooling and subsequent tempering at 600°C over a period of 4 hr; the specimen cross section usually contained three to five grains with a size of 0.2-0.4 mm.

3. Recrystallized specimens annealed at 600°C over a period of 4 hr. The grain size was 15-20 μ.

4. Recrystallized fine-grained specimens annealed at 500°C over a period of 10 hr. The grain size was 2-4 μ.

Before measurements, the specimens were kept in the device at room temperature in order to release cold-working stresses caused by straightening after hardening and by the operations in fastening the specimen in the device.

For a comparison of the heating rate effects on anisotropic and isotropic materials, we investigated internal friction in specimens of the same size made of zinc, technically pure molybdenum, and aluminum. Cast specimens of ChDA zinc were obtained, and some specimens of recrystallized "Kal'baum" aluminum were made. Before fastening in the device, all specimens were annealed at a temperature of the order of the recrystallization temperature, after which they were annealed in the device in order to release the cold-working stresses caused by mounting.

Experimental Results

Figure 2 shows the results obtained in measurements performed on uranium of A composition (state 1), and Fig. 3 shows the initial (A) and the final (B) portions of one of the oscillograms obtained in these experiments.

It is obvious from the figures that internal friction begins to increase immediately after the temperature starts to rise and that it drops almost simultaneously with the cessation of heating. In the initial heating stages, the internal friction rise rate gradually decreases and the internal friction itself attains a certain limiting value Δ_{li}. Similar curves for the increase in

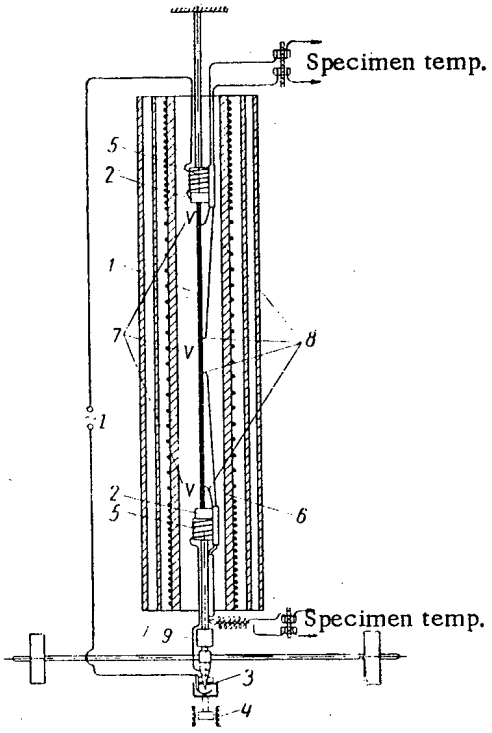

Fig. 1. Apparatus for measuring internal friction: 1) specimen; 2) draw-in clamps; 3) mercury contact; 4) switch; 5) heater for warming-up draw-in clamps; 6) tubular electric furnace; 7) thermocouples; 8) nichrome-constantan thermocouples, diameter 0.1 mm, welded to specimen; 9) mirror (distance from mirror to scale reading —2.5 m).

internal friction with time were obtained in heating within the 120-210 and 210-290°C temperature intervals. A similar increase in internal friction was observed in uranium specimens of B composition (states 2, 3, and 4).

It was demonstrated that even the low cooling rates secured in the tester (v = 1 deg/ min) causes a considerable increase in internal friction. A similar increase was also observed in heating the specimens in an electric furnace; consequently, it was not connected with the possible effect of the current used for heating the specimens.

If the temperature variation is arrested, a simultaneous sharp drop in internal friction is observed (see Figs. 2 and 3). If the specimen temperature remains constant after the heating has been stopped, the internal friction can be reduced in 2 to 5 sec to a magnitude corresponding to the given temperature. However, in the above-described device, it was difficult to ensure the temperature constancy along the entire specimen length immediately after the heating was discontinued. In a number of cases, the change in the temperature distribution along the specimen at this stage resulted in a gradually decreasing increment of internal friction, which can be seen in Fig. 2.

The dependence of the internal friction increment on the heating rate for three temperature intervals (for specimens in different initial states) is shown in Fig. 4. As a rule, the internal friction increment is proportional to the heating rate. The tendency to "saturation" was observed only in heating hardened specimens in the 120-210 and 210-290°C intervals.

The internal frication increment in coarse-grained uranium in state 2 is approximately equal to the internal friction increment in uranium in states 3 and 4, and it is 2 to 2.5 times lower than the internal friction increment in uranium in state 1. In heating to temperatures above 300°C, the effect of the internal friction increase was reduced, and in heating to temperatures above 350°C, it was almost completely absent.

During the heating process, also a macroscopic shear deformation of the specimen was observed, which led to the "zero drift", i.e., a shift of the oscillation equilibrium point (see Fig. 3). The rate of the "zero drift" in constant-rate heating was practically constant. It was at the maximum in the case of coarse-grained specimens (state 2). For a specimen heating rate of 10 deg/ min, it corresponded to the maximum shear deformation rate, which was $(0.1\text{-}0.3) \cdot 10^{-5}$ 1/ min.

Investigations of internal friction variations in molybdenum and aluminum in heating under the same conditions as in measuring the internal friction in uranium showed that the internal friction vs. temperature curves in these cases are practically independent of the heating rate. An additional increase in internal friction in connection with the heating process was not observed (Fig. 5). The internal friction variation in heating a zinc specimen with a strongly anisotropic thermal expansion coefficient is also shown in Fig. 5. This variation strongly depends on the oscillation amplitude in the temperature interval under investigation. Figure 5 shows the internal friction increment curve for the maximum amplitude $1.2 \cdot 10^{-5}$. It is obvious from the figure that internal friction sharply increases to a magnitude several times as large as the magnitude obtained in heating with prolonged exposures. If the heating is discontinued, the internal friction is reduced, however, in contrast to the case of uranium, the reduction is gradual and does not occur in jumps.

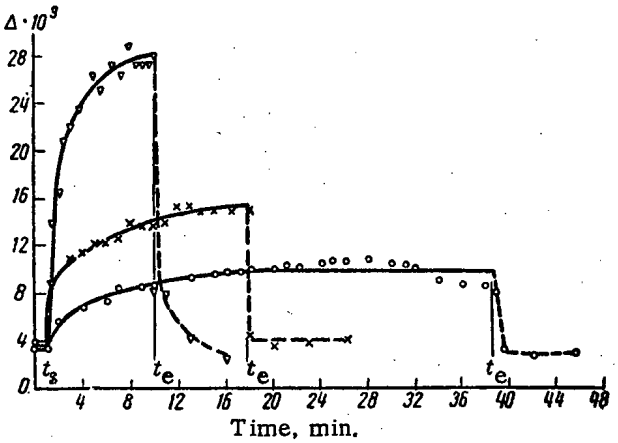

Fig. 2. Increase in internal friction of hardened uranium of composition A in dependence on the heating time for constant rates in the 20-120°C interval. Values of v (deg/ min): ▽) 13.55; ×) 5.75; ○) 2.83. Frequency: 1.9 cps; t_s) start of heating; t_e) end of heating.

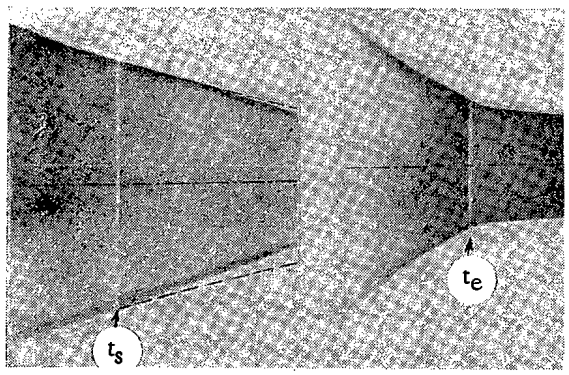

A B

Fig. 3. Oscillograms showing the variation of internal friction in hardened uranium of composition A. A) After start of heating (at the moment t_s). The dotted line indicates the change in the oscillation amplitude without heating; B) after end of heating (at the moment t_e). The dotted line indicates the change in amplitude if heating is continued. The dash-dot line in A) and B) denotes the position of the equilibrium point. The frequency was 1.9 cps.

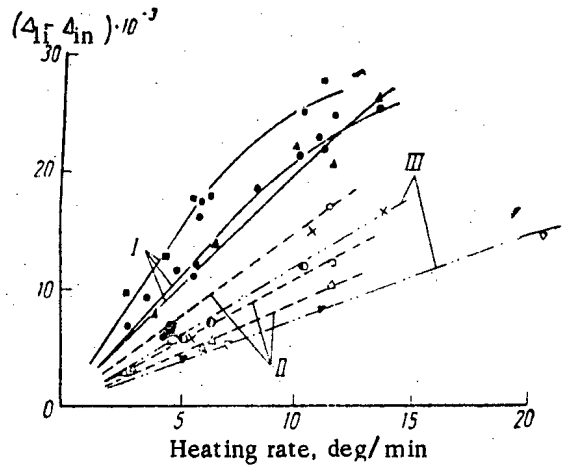

Fig. 4. Dependence of the internal friction increment in uranium ($\Delta_{li} - \Delta_{in}$) on the heating rate $\underline{v}$. The frequency was ≃ 2 cps. I) Specimens of composition A hardened in the γ-region [treatment 1: ●) 20-120°C; ■) 120-210°C; ▲) 210-290°C]; II) specimens of composition B hardened in the γ-region [treatment 2: Δ) 20-120°; □) 120-210°C; ○) 210-290°C]; III) recrystallized specimens of composition B [treatment 3: ▼) 20-120°C; ◐) 120-210°C; treatment 4: ∇) 20-120°C; ×) 120-210°C].

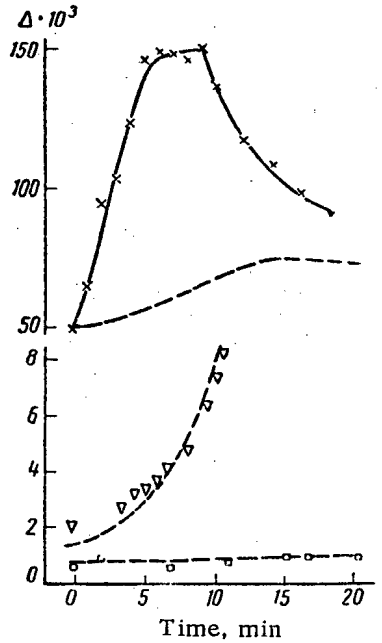

Fig. 5. Variation of internal friction in the heating of the following specimens: ×) zinc ($\underline{v}$ = 6.86 deg/min, f = 2.6 cps); ∇) aluminum ($\underline{v}$ = 6.7 deg/min, f = = 1.4 cps); □) molybdenum ($\underline{v}$ = 10.4 deg/min, f = 2.8 cps). The dotted line indicates the variation of internal friction for the zero heating rate, i.e., the variation after long constant-temperature exposures.

Discussion of the Results

A comparison of the results obtained in testing uranium, zinc, and thermally isotorpic metals clearly indicate that the increase in internal friction due to temperature changes is caused by internal stresses arising from the anisotropic expansion of grains when the specimen temperature changes.

During the testing process, the stresses in polycrystalline uranium grains are determined by the initial stresses (σ_{in}), internal stresses, which are caused by anisotropic lattice expansion, and the cyclic stresses due to the pendulum torsional oscillations. Figure 6 provides the graphic presentation (according to the method used in [8]) of the deformation of a grain under the action of the above stresses.

For a constant heating rate, ϵ_{heat} increases proportionally with time, and, therefore, the stress $\sigma = E(\epsilon_{heat} + \epsilon_{osc} + \epsilon_{in})$, where E is the elasticity modulus, will become equal to the critical shearing stress σ_{cr} at a certain instant of time. After this time t_1, the corresponding grain will be plastically deformed and the energy of elastic oscillations will be used up for this process; internal friction will increase. Plastic deformation will continue up to the time t_2, when the direction of the deformation due to torsional oscillations changes its sign and thereby causes the stresses to drop below the σ_{cr} value.

The plastic deformation in the first cycle will be equal to $\Delta\epsilon_0$, and, therefore, the plastic deformation in the second cycle will occur at the instant of time t_1', when the total deformation exceeds the level previously attained and the stresses become equal to σ_{cr}. Thus, the grain will experience plastic deformation during the time intervals $t_1 - t_2$, $t_1' - t_2'$, $t_1'' - t_2''$, etc.

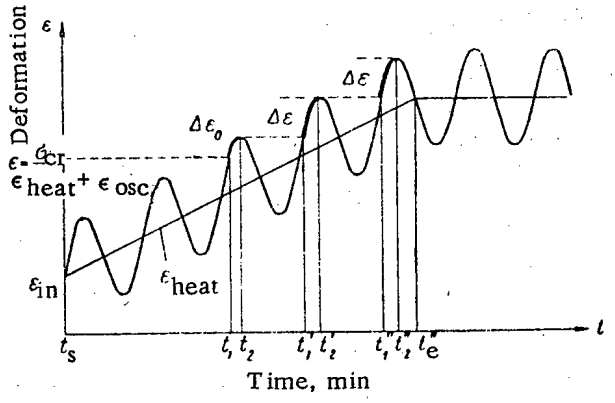

Fig. 6. Schematic diagram of the α-uranium grain deformation caused by the anisotropic expansion of crystals in heating and by the inertial pendulum oscillatory motion. ϵ_{in}) Deformation caused by initial stresses; ϵ_{heat}) deformation due to anisotropic expansion of grains in heating; ϵ_{osc}) periodic deformation due to the pendulum torsional oscillations.

The magnitude of deformation $\Delta\epsilon$ for one period and, consequently, the magnitude of the internal friction increment are proportional to the slope of the straight line characterizing the variation of ϵ_{heat} in time, which, in turn, is proportional to the heating rate. Figure 6 indicates that this conclusion basically agrees with experiments.

It is obvious from Fig. 6 that the cessation of heating must cause a simultaneous drop in the internal friction magnitude, since the interruption of heating at the time t_e causes the plastic deformation per single period ($\Delta\epsilon$) to drop to zero. This conclusion is also in good agreement with experiments.

The increase in internal friction begins immediately after the heating starts. This signifies that the internal stresses in polycrystalline uranium grains are very large and that they attain $\sigma_{cr} - E\epsilon_{osc}$ values. The gradual increase in internal friction with time in the first stages of heating at a constant rate is connected with the accumulation of internal stresses and an increase in the number of grains where the total stresses exceed σ_{cr}. The limiting value of internal friction corresponds to the state for which deformation occurs in the majority of grains with an orientation favorable to the development of deformation.

If the grain size is increased to dimensions comparable to the specimen diameter, internal stresses decrease, since a considerable portion of the surface of grains in this case emerges on the specimen surface, and the shape of grains changes more freely in heating. The internal friction increment correspondingly decreases.

The internal friction increment is small also for recrystallized specimens, regardless of the fact that the grains in these specimens are small. This is explained by the influence of the predominant orientation, which appears as a result of the preceding deformation. If some of the grains are favorably oriented, the internal stress accumulation rate in heating is lower and the internal friction increment is correspondingly smaller. The more regular polygonal form of recrystallized grains also contributes to the reduction in internal stresses, while grains in hardened and annealed uranium have an irregular form and very jagged boundaries.

The plastic deformations of individual grains are mutually compensated, but not completely so. Due to this a macroscopic shearing deformation appears, which is manifested in the "zero drift" detected in experiments. The larger the grain, the greater the probability that the magnitude of this uncompensated deformation will be large. Actually, a large "zero drift" was usually observed in coarse-grained materials.

In the temperature intervals for which the measurements were performed (20-290°C), the relaxation at the grain boundaries apparently did not play an important role, since the internal friction increment would otherwise strongly depend on the grain size and the over-all surface area of the boundaries. Experiments performed on hardened and annealed uranium indicate that an increase in the grain size by one order of magnitude (i.e., an approximately hundredfold increase in the grain boundary surface area) causes a reduction in internal friction by only one-half, while this reduction can be explained by a decrease in internal stresses in the grains.

The influence of grain boundaries must become noticeable at higher temperatures [11]. It is possible that the vanishing of the internal friction rise effect during heating in the 300-350°C interval is connected with an increase in the plasticity of grain boundaries.

LITERATURE CITED

1. S. T. Konobeevskii, N. F. Pravdyuk, and V. I. Kutaitsev, Transactions of the International Conference on the Peaceful Use of Atomic Energy, (Geneva, 1955) [in Russian] (Goskhimizdat, Moscow, 1958) Vol. 7, p. 526.
2. Chizuik and Kelman, Transactions of the International Conference on the Peaceful Use of Atomic Energy (Geneva, 1955) [Russian translation] (Goskhimizdat, Moscow, 1958) Vol. 9, p. 184.
3. McIntosh and Hill, Transactions of the Second International Conference on the Peaceful Use of Atomic Energy (Geneva, 1958). Selection of Reports by Foreign Scientists: Nuclear Fuels and Reactor Materials [Russian translation] (Atomizdat, Moscow, 1959) Vol. 6, p. 187.
4. A. Roberts and A. Cottrell, Philos, Mag., 47, 711 (1956).
5. A. Holden, Physical Metallurgy of Uranium. (New York, Addisson-Wesley Publ. Corp., 1958).
6. R. Maringer, J. Appl. Phys. 24, 1525 (1953).
7. G. Alerst, Phys. Rev. 97, 863 (1955).
8. R. I. Garber and T. T. Mogil'nikova, Doklady Akad. Nauk SSSR 118, 479 (1958).
9. G. Brook and A. Sully, Acta Metallurgica, 3, 460 (1955).
10. Kĕ Ting Sui, Phys. Rev. 71, 533 (1947).
11. S. T. Konobeevskii, A. S. Zaimovskii, V. M. Levitskii, Yu. N. Sokurskii, et al., Transactions of the Second International Conference on the Peaceful Use of Atomic Energy (Geneva, 1958). Reports by Soviet scientists: Nuclear Fuels and Reactor Metals [in Russian] (Atomizdat, Moscow, 1959) Vol. 3, p. 396.

METHODS OF RADIOACTIVITY METROLOGY IN USSR

K. K. Aglintsev, V. V. Bochkarev, V. N. Grablevskii, and F. M. Karavaev

Translated from Atomnaya Énergiya, Vol. 7, No. 4, pp. 354-359, April, 1960
Original article submitted October 27, 1959

The article gives a review of the present state of the problem of standardization of radioactive sources and of the methods for measuring radioactive radiations. The general principles for organizing systems of radiometric measurements based on the use of a single unit system, of standard methods and equipment, and of relative measurements involving standard sources are illustrated. A scheme is reported for the verification of radioactive sources graduated in activity units: a standard method for reproducing the Curie unit is taken as the basis of this scheme. The fundamental characteristics of standard and check radioactive sources are briefly described.

The fundamental problem of radiometry consists in the measurement of the activity of radioactive preparations. The practical use of isotopes requires, in addition to a solution of this basic problem, the development of metrological methods for finding all the dosimetric characteristics of the preparations, determined by the composition of the emission spectrum, by the activity, by the parameters of the measured preparations (size, chemical composition, weight), and by the data concerning the container in which the preparation is enclosed.

The activity of a preparation and the emission spectrum of an isotope determine the total emission of a preparation; this total emission differs from the external emission important for practical purposes because of the absorption and sacttering of the radiation in the preparation and in its container. For this reason activity measurements are essentially connected with measurements of emission intensity, and very often a preparation cannot be used without a knowledge of its external emission.

The necessary starting points for a metrology are the unification of measure units, the definition of standards or of standard methods corresponding to the unit, and the elaboration of a system and method of transfer of the unit values from the standards to the working preparations and to the measuring equipment.

The following units have been accepted officially in the USSR: the Curie, the milligram-equivalent of radium, the roentgen, the rad. The reproduction of the Curie unit is made in the USSR with the help of 4π-counters, calorimeters, and ionization cameras. The 4π-counters are used for measuring α- and β-active preparations having an activity of 10^{-7}– 10^{-11} C with an accuracy of 1-3 % [1].

The activity of preparations decaying by e capture [2] is defined as the difference of the number of countings by a 4π-counter when filled with methane, when only electrons and noise are recorded, and upon addition in the counter of xenon for recording the characteristic emission. The limits of measurement of e capture activities are 10^{-10} – 10^{-6} C, and the accuracy of the measurements is 6-8%.

In order to measure the activity of preparations wit with α, β, and γ radiations in the region above 0.01-0.05 C, the following standard apparatuses are used: differential γ calorimeters [3], isothermal β and γ calorimeters and a differential α calorimeter. The calorimeters of this type give the possibility of measuring activities in the limits 0.05-3 C with an accuracy of 3-5%.

The isothermal β calorimeter is based on the principle of evaporation of liquid nitrogen [4]. A γ calorimeter of the same type differs from the corresponding β calorimeter by the presence of a special tungsten-mercury absorber and by the larger sizes of the Dewar vessels. The calorimeters of this type give the possibility of measuring activities above 0.01 C with an accuracy of 3-6%.

The differential α calorimeter is used for measuring the activity of preparations with respect to α radiation and consists of two identical silver containers placed within a copper block thermostat. The sensitivity of the calorimeter is sufficient for measuring radium preparations containing no less than 1 mg of radium element; with an accuracy of 1-2%.

The ionization method for reproducing the Curie is based on the measurement of the ionization produced by the γ radiation of the preparation in an ionization camera. In this method the effectiveness of the camera must be known, i.e., one must know the ionization current referred to the unit of activity of the given radioactive isotope.

The slit ionization camera prepared for these purposes with a solid angle of 4π [5] consists of two concentric aluminum spheres with external diameters of 230 and 260 mm and with walls having a thickness of 5 mm. The preparation to be measured is placed in the center of the internal sphere. The calculation of effectiveness requires a knowledge of the energy of the quanta and of their number per decay act for the γ-spectra of the isotopes under study, and also of the value of the ionization work in air for γ rays. This quantity is known at present with an accuracy of $\pm 5\%$, and therefore the accuracy of the determination of the activity from the data of the method is equal to 7-8%. The measurements limits are 10^{-4}– 10 C.

The external γ radiation of radioactive sources is often characterized nowadays by the value of the radium γ equivalent. This quantity corresponds to an amount of radium (closed in a platinum shell having a thickness of 0.5 mm), whose γ radiation produces in the air-equivalent camera the same ionization as the γ radiation of the given source.

The reproduction of the radium γ equivalent (1 mg-eq Ra) unit is made by the State radium standard. So far the standard sample No. XI has been used as the standard radium sample of the USSR, compared with the old primary international standard radium sample (1911). Sample No. X prepared and measured simultaneously with sample No. XI was used as a standard copy. At present work for preparing a new sample No. 5427 from 20 preparations prepared by O. Khenigshmidt in 1934 is being carried out. The transfer of the radium γ equivalent unit from the standard sample to the practical radium sources is made on standard devices with an ionization camera. The accuracy of the results of the measurements is 0.5%, for sources with a γ equivalent of 10 mg-eq of Ra, and increases to 1.5%, for sources with a γ equivalent of 1000 mg-eq Ra. Sources with γ equivalents of 1-0.001 mg-eq Ra, which produce an ionization of the same order as that of the noise, are measured in an appratus including a so-called compensation camera [6]. The accuracy of the results lies in the limits of 1 , for sources with a γ equivalent of 1 mg-eq Ra, and 5-8%, for sources with a γ equivalent of 0.001 mg-eq Ra.

The reproduction of the roentgen for γ radiation with a quantum energy of 0.3-3 Mev is performed on a standard apparatus [1, 7, 8] having an ionization camera with a high pressure (up to 20 atm). Taking into account all the errors, the accuracy of the measurement is $\pm 3\%$.

The sequence of operations for transferring the size of the unit from the standard sample or the standard equipment to the practical apparatuses or working sources is described by the calibration scheme. The standard methods for reproducing the Curie unit is taken as the basis of this scheme.

In the USSR sources of two types are mass produced and commonly used: standard sources, intended for the verfification of radioactive preparations and for the graduation of radiometric and dosimetric equipment; check sources, intended solely for control of the work and verification of the reproducibility of various devices. The application of this type of check sources was required by the presence of a large number of different dosimetric and radiometric apparatuses used in this country [9], and by the necessity of ensuring a control of their operation on the place and of having comparable data from their indications.

Preparations prepared according to special technical conditions and accurately measured on one of the standard devices are considered as the first class standard sources. Preparations compared with first class standard sources are called second class standard sources and serve for the graduation of dosimetric and radiometric equipment and for verifying control and other working sources [10].

In the calibration scheme (see accompanying scheme) the four horizontal dotted lines correspond to standard samples and apparatuses, to first and second class standard sources, and to working preparations. The rectangles represent measuring apparatuses, the squares measure methods. Thus, the scheme in question shows the connection between any preparation of measuring apparatus usable in practice and the State standard sample.

The check scheme includes a provision for the verification of counters with the help of ionization cameras, in connection with the measurements of the γ equivalents of preparations in milligram-equivalents of radium. The application of "slipping", i.e., decaying, radon preparations is avoided. The verification scheme for the measurement in roentgens is based on a standard method of reproduction of the roentgen with the help of an air ionization camera. The transfer of the size of the unit is obtained by means of sample dosimeters or of standard γ sources.

In the calibration of dosimeters by means of γ sources, it is very important to choose correctly the distance and the method of diaphragming of the beam, because these two factors affect in a very important way the radiation field of the source [11].

The reproduction of the unit of neutron flow is obtained by standard methods by means of which the sample neutron sources of the first class are calibrated. These sources are preparations in which beryllium is irradiated by α particles or by γ quanta from different sources (radium, polonium, plutonium).

Abroad, for similar measurements, it is customary to use:

1) 4π– β-counters, working with a proportional or Geiger operation (USA, England, Canada, France, German Federal Republic, Sweden, Japan, Portugal,

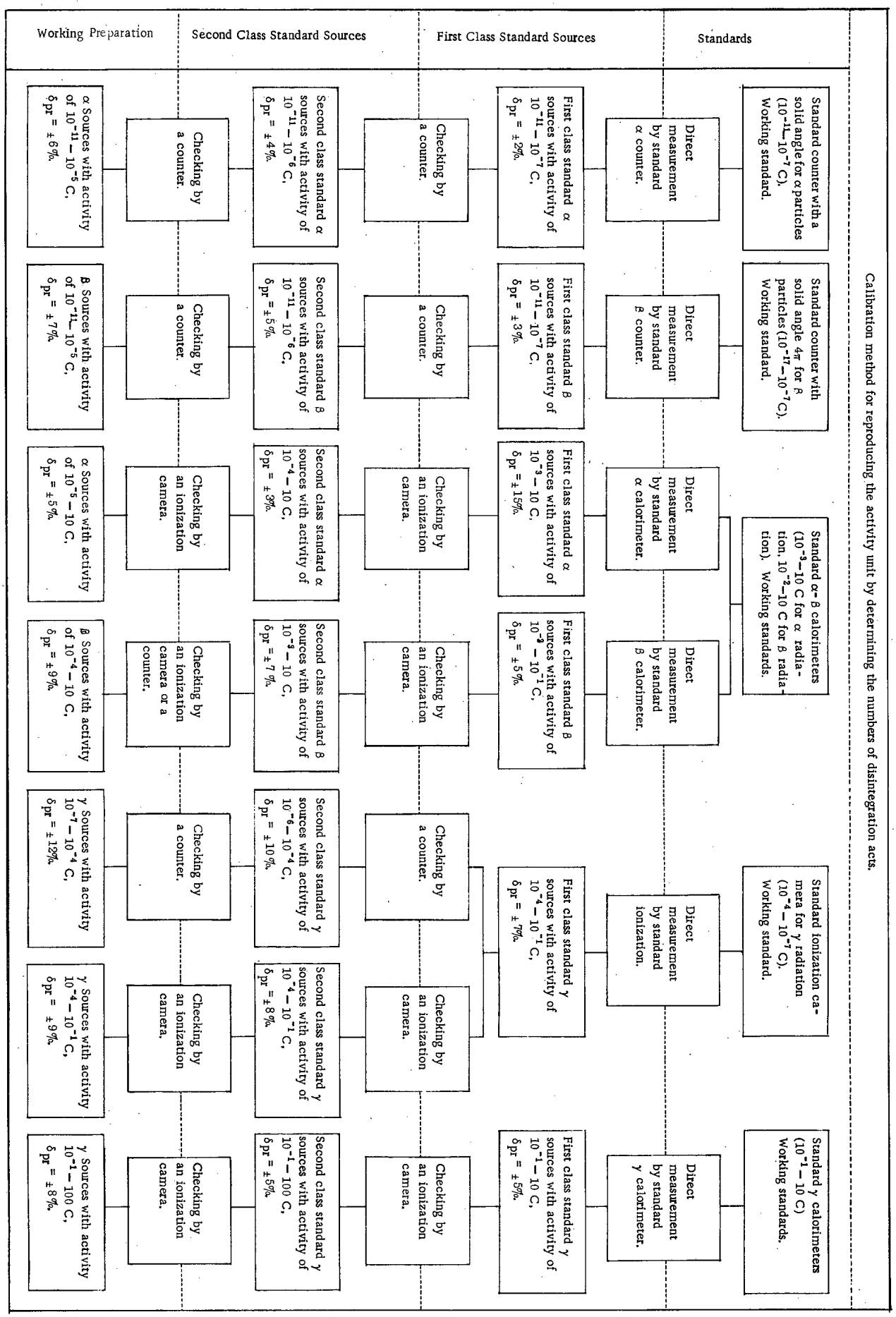

TABLE 1. Standard α sources.

Source activity decays/min	U^{233}	U^{235}	Natural uranium	Pu^{239}
30	+	+	+	+
100	+	+	+	+
300	+	+	+	+
1000	+	+	+	+
3000	+	+	+	+
10 000	+	—	—	+
30 000	+	—	—	+
100 000	+	—	—	+
300 000	—	—	—	+
1 000 000	—	—	—	+
3 000 000	—	—	—	+
10 000 000	—	—	—	+

etc.); a great attention is given to the technique for preparing the samples and to the method for introducing the necessary corrections in the results of the measurements;

2) 4 π-counters of β−γ coincidences (USA, England, German Federal Republic, Canada, etc.);

3) Calorimeters for the measurement of α and β sources (USA);

4) Liquid scintillation counters, in particular 4 π-counters for the measurements of H^3 and C^{14} (England, USA, etc.);

5) Counters with a filling of active gas (England, USA, Canada, German Federal Republic, etc.).

It is interesting to know that, abroad, the method of measuring the activity of γ sources by means of γ calorimeters is apparently used quite seldom, whereas in the USSR this method is successfully applied. It is also necessary to remark that in the USSR the connection between activity measurements and dose measurements is appreciably deeper than in foreign metrological institutions; this gives well known advantages in the standardization of radioactive preparations and in the graduation of dosimetric apparatuses.

An essential part of the check schemes, as has been already noted, is given by standard sources. Below we shall give a short description of the various types of sources.

The standard α sources serve for determining the counting coefficients of α devices used for checking α preparations. The absolute α activity of the preparations under study is determined from these coefficients. In order to prepare standard α sources, U^{233}, natural uranium and Pu^{239} are used.

An active substance is deposited electrolytically in the form of a spot having a diameter of 10 mm on a platinum disc having a diameter of 15 mm.

Table 1 shows the fundamental types of mass produced standard α sources. The Table shows that only part of the various types of α sources are produced with a complete range of scaling (cases not denoted by the sign +).

The electrolytical preparations of α sources ensures the obtainment of stable, homogeneous, thin layers, well linked to the base. The intensity values of the standard α sources may differ from the nominal values not more than ±10%, as it is indicated in the rating plate.

The comparison of first and second class standard sources is made by means of a pulse ionization camera with an electronic circuitry. Activities up to 30,000 decays/min are measured in the ionization camera, knowing the value of the solid angles 4π or 2π. Activities above 30,000 are measured with small values of the solid angle (α beam method). The accuracy for measurements with 4π or 2π solid angles must be 0.5-1%.

Each standard α source is provided with its rating plate where the activity (expressed by the number of decay acts per minute), the isotope composition, the quantity of radioactive impurities, data concerning the half life period, the assumed decay scheme, the surface density and the weight contents of active substances, the size of the active spot, the material, the thickness, the weight, the diameter of the base, the method of the date of measurement are given.

Check α sources. The activity of check α sources is expressed as a rule by the number of α decays/min. Sometimes the activity is expressed as the number of α particles in an angle 2π or 4π with a correction for particle reflection from the base and for the absorption of them by the active layer.

All check α sources in the USSR (except the sources prepared for special requirement) are made with plutonium. Pu^{239} corresponds most completely with its properties to the requirements characteristic of radioactive isotopes used for the preparation of standard and check sources.

The deposition of plutonium on the base is carried out most often electrolytically, since this method, due to the high specific activity of plutonium (0.06 C/g), gives a sufficiently thin (down to 0.7 mg/cm^2) plutonium dioxide layer, which is also very strongly linked to the base.

For all check sources prepared, definite time limits for use are established depending upon the activity of the source and the conditions of use.

At present, sources having an activity of 10, 20, 40, 60, 80, 100, 200, 400, 600, 800, . . . up to 10^8 decays/min are mass produced; they have found a wide application for the control of the work of various types of dosimetric apparatuses.

Twenty types of α source series are prepared. The sources entering each series have different active surfaces (1-200 cm^2) and different bases (12 forms).

Standard β sources are mass produced from different isotopes in order to cover a wide range of energies,

since the effectivness of counting apparatuses depends essentially upon the energy of the radiation under study. For these purposes the following isotopes with comparatively long half-lives and, as a rule, with a simple spectrum, are prepared: H^3, C^{14}, S^{35}, Ca^{45}, Co^{60}, Tl^{204}, Ra(D + E), P^{32}, Sr^{90}+ I^{90}, UX_1 + UX_2.

It should be noted that in the latter time also promethium has started to be used. Such sources are prepared with different activities in the range 10^4-10^6 decays/ min.

First class sources are prepared with a practically weightless layer deposited on a thin plate, for measurements with the help of a 4π counter. Second class standard β sources are prepared by depositing a thin uniform layer of a radioactive preparation on a base, usually an aluminum base, with an active spot diameter of 10 mm; such samples are mechanically stable, chemically stable, nonhygroscopic, and are protected from the possiblity of an isotope exchange with the external medium.

As for α sources, the rating plates accompanying the β sources show the assumed decay scheme, the value of the half life period, data concerning radioactive impurities and indications about the measurement method. The term within which the rating plate is valid is one year for longlived sources (more than 5 years); for the shortlived sources it is one half life period (but not more than one year). The radioactive impurities do not exceed 0.5% in activity during the use terms of a standard source. The accuracy of the rating values for the sources in question lies in the limits 2-7%, depending upon the energy of the β source and the nominal activity.

Check β Sources. These sources are prepared basically with Sr^{90}, which is in equilibrium with Y^{90} and partially with Tl^{204} and Pm^{147}. The activity of control sources is expressed by means of the number of β decays per min. Sources are prepared either by applying a salt of Sr^{90} on a base of a phenolformaldehyde resin, or by laying an oxide plate on aluminum. Promethium and tallium are layed on the base by an electrolytic process. Some sources are closed in aluminum foil in order to protect the active layer against mechanical influences.

The check β sources are prepared in a large range of activities (20-10^9 decays/min), which corresponds to a specific surface activity per 1 cm^2 from 0.2 to $2 \cdot 10^8$ decays/min. The scale of activities of β sources is established in the same way as that of check α sources.

The 25 different series of check β sources are prepared on different bases of 13 types. These sources have an active surface of 0.1-300 cm^2.

The deviations from uniformity is determined by means of a measurement of a part of the active surface of the source with a size of 1 cm^2 in some places (from 3 to 12 depending upon the geometric size of the source) by means of an appropriate diaphragming of the active surface.

Standard γ sources are prepared with radium, Co^{60}, and Cs^{137}. The assembly of the sample sources consists of preparation with the following values of radium γ equivalents (in g-eq of Ra): 5, 2, 1, 0.500, 0.200, 0.100, 0.025, 0.010, 0.005, 0.001, 10^{-4}, 10^{-5}, 10^{-6}, 10^{-7}, 10^{-8}, 10^{-9}, 10^{-10}, 10^{-11}. The value of the radium γ equivalent may differ from its nominal value by not more than $\pm 20\%$: this is shown in the rating plate.

Standard γ sources made of Co^{60} are prepared in the form of small spheres or cylinders having the size of 1-2 mm. Each source is enclosed in a tight aluminum shell with walls having a thickness of 0.2 mm.

Standard γ sources of Cs^{137} (1 mg-eq Ra and less) are a spherical ampoule of rustproof steel having a wall thickness of 1.2 mm within which Cs^{137} layed on a small sphere having a diameter of 0.25-1 mm is placed. Sources having a γ equivalent larger than 1-mg-eq Ra are realized in the form of cylindrical ampoules of rustproof steel having diameters up to 10 mm and lengths up to 15 mm.

Radium standard sources containing 10^{-7}-10^{-11} g of radium have the form of a water solution of radium chloride containing a determined impurity of barium chloride and enclosed in a cylindrical glass ampoule.

Standard radium sources containing radium in amounts of $5 \cdot 10^{-11}$, $n \cdot 10^{-10}$, $n \cdot 10^{-9}$, $n \cdot 10^{-8}$, and $n \cdot 10^{-7}$ (where n is any given number from 1 to 9) are produced in ampoules having a length of 5-12 cm and a diameter of 0.6-1.5 cm.

The radium contents in the ready preparation is determined by the preparer by counting on the basis of the weight of the starting solutions and of its concentration. The starting solution is measured with an accuracy of 0.7%. The rating plate of a source gives the following data: radium content (in grams), preparation date, barium content, data concerning the ampoule (diameter, length, wall thickness).

Standard radium sources containing 0.2-10^6 g of radium consist of radium bromide placed in a glass ampoule. The ampoule is enclosed in a container made of an alloy (90% platinum and 10% iridium), with a wall thickness of 0.5 mm. A short summary of the characteristics of the γ sources prepared with radium is reported in Table 2. The ampoules are prepared with glass of the mark TS-32 which does not contain boron.

The rating plates of sample γ sources indicate the weight of anhydrous radium bromide, the content of radium in the sources (in grams), the accuracy of the determination and the date of measurement.

Check γ sources are prepared with the same isotopes as in the case of the sample sources, and in a large range of activities. In addition to the forms mentioned above, Co^{60} check sources are produced as cylinders having sizes of 1 x 1, 2 x 2, and 5 x 5 mm (in an aluminum shell) and in the form of wire pieces having diameters of 0.7-0.9 mm. The Cs^{137} sources are produced in the same types as standard sources. In

TABLE 2. Characteristics of radium γ emitters.

Radium content, g	Permitted deviation in radium content, %	Size of the external glass ampoule, mm	
0.2	± 5	6.9—7.8	40±2
0.1	± 5	6.9—7.8	40±2
0.025	±10	6.9—7.8	40±2
0.010	±10	6.9—7.8	40±2
0.005	±10	6.9—7.8	40±2
0.001	±10	6.9—7.8	40±2
10^{-4}	±20	6.9—7.8	40±2
10^{-5}	±20	6.9—7.8	40±2
10^{-6}	±20	6.9—7.8	40±2

addition a large number of control γ sources of the most different forms and sizes is produced for application to special devices.

Standard neutron sources. A combination of Ra-α--Be sources, containing 1000, 300, 100, 30, 10, and 1 mg radium, and also a combination of Pu-α-Be sources containing 15, 1, 0.5, 0.1 and 0.01 g plutonium are used as sample neutron sources.

The former sources are a compressed mixture of radium bromide with powdered beryllium, enclosed in a tight double shell having a cylindrical shape. The ratio of the weight quantities of radium and beryllium in the mixture must be 1 : 6. The latter sources are metal-metal compounds of plutonium and beryllium ($PuBe_{13}$).

The yield of neutrons per 1 mg of radium in the angle 4π is not less than $1 \cdot 10^4$ neutrons/sec. The radium must be purified from mesothorium and should not contain more than 5% of barium.

In a number of foreign countries standard sources are systematically produced. In England sources of 60 different isotopes are produced; among them a large number serves for international cross comparisons. In the USA a large variety of standard sources are produced: they have a large range of activity, and are in particular sources made of P^{32}, K^{42}, Co^{60}, I^{131}, Ta^{182}, Au^{198}, Sr^{90} + + Y^{90}, Tl^{204}, Na^{22}, H^3, C^{14}, Cs^{137}, S^{35}, Kr^{85}, Hg^{203}, preparates of Ra^{226}, etc. In the German Federal Republic standard sources of some long lived isotopes are prepared, although there is a project of production for 1960 also of shortlived isotopes.

A great importance must be ascribed to the international comparisons of standard sources with different isotopes that are made in large numbers. Many countries participate in these comparisons.

LITERATURE CITED

1. K. K. Aglintsev, et al., Atomnaya Énerg., No. 2, 55 (1956)*
2. A. A. Konstantinov, Pribor. i Tekh. Éksp., No. 1, 67 (1959).
3. K. Al Aglintsev and E. A. Khol'nova, Trudy VNIIM, 30 (90), 25 (1957); Doklady Akad. Nauk SSSR 98, 357 (1954).
4. E. A. Khol'nova, Trudy VNIIM, 30 (90), 18 (1957); Doklady Akad. Nauk SSSR 98, 357 (1954).
5. F. M. Karavaev, Izmeritel'naya Tekh., No. 5, 60 (1959).
6. F. M. Karavaev, Trudy VNIIM, 30 (90), 53 (1957).
7. K. K. Aglintsev, G. P. Ostromukhova, and M. F. Yudin, Trudy VNIIM, 30 (90), 109 (1957).
8. K. K. Aglintsev and G. P. Ostromukhova, Atomnaya Énerg. 6, 1, 63 (1959).*
9. Handbook on Dosimetric, Radiometric, and Electro-Physics Instruments, Meters, Scintillators, and Photomultipliers [in Russian] (Atomizdat, Moscow, 1959).
10. K. K. Aglintsov, M. A. Bak, V. B. Bochkarev, et al., Proceedings of the Second International Conference on the Peaceful Uses of Atomic Energy (Geneva, 1958). Reports of Soviet Scientists. Obtaining and Usage of Isotopes [in Russian] Vol. 6, p. 227.
11. Z. P. Balom, et al, Imeritel'naya Tekh., No. 12, 47 (1959).

*Original Russian pagination. See C. B. translation.

CROSS SECTION FOR THE REACTION Th^{232} (n, 2n)Th^{231} AT 14.7 MEV NEUTRON ENERGY*

Yu. A. Zysin, A. A. Kovrizhnykh, A. A. Lbov, and L. I. Sel'chenkov

Translated from Atomnaya Energiya, Vol. 8, No. 4, pp. 360-361, April, 1960
Original article submitted October 21, 1959

The cross section for the reaction Th^{232}(n, 2n) at 14.7 Mev neutron energy was determined† by measuring Th^{231} activities and fission fragments of Mo^{99} and Ba^{140}. It was thus unnecessary to know the absolute value of the neutron flux although the fission cross section σ_f and the corresponding fragment yields γ_{Mo} and γ_{Ba} had to be known.

The 14.7 Mev neutrons were obtained from a low-voltage deuteron linear accelerator ($E_d \simeq 150$ kev) using the reaction d(T, n)He^4. A uniform mixture of thorium nitrate [$Th(NO_3)_4 4H_2O$] (~0.2 g) and uranoso-uranic oxide [U_3O_8](~0.6 g) free of $UX_1 + UX_2$ was irradiated. Six irradiations were performed (time of irradiation 3-11 hr) and the total number of emitted neutrons in each of them was $(2\text{-}6) \cdot 10^{14}$.

The mixture was hermetically sealed in a cylindrical container which was placed with its axis along the neutron beam and at a distance of ~7 mm from the center of the tritium target.

The large amount of U_3O_8 was introduced into the container because the fission cross section and the yield of Mo^{99} and Ba^{140} fragments in the case of fission of U^{238} at 14 Mev neutron energy is well-known ($\sigma^U_f = 1.1$ barns, $\gamma^U_{Mo} = 0.063$, $\gamma^U_{Ba} = 0.047$). The amount of Mo^{99} or Ba^{140}, which are formed during the fission of Th^{232} for a given ratio of the amounts of Th^{232} and U^{238}, were less than 5% ($\sigma^{Th}_f = 0.35$ barns).

After irradiation the container was opened and the mixture was dissolved in hydrochloric acid to which nitric acid had been added. The required isotopes were then extracted from the solution by a chemical method. A 4π-counter was used for β-measurements so that no corrections were necessary for conversion electrons.

Decay curves and absorption in aluminum were used to check the purity of the separated specimens. Corrections were made in the calculations for disintegrations during the time of irradiation, and for Tc^{99m} and La^{140}. The increasing activity of the natural decay products of Th^{232} was also taken into account.

All the calculations were based on the formula

$$\sigma^{Th}_{n,\,2n} = \frac{N_{Th} T_{1/2\,Th}}{N_{Mo} T_{1/2\,Mo}} \times \times \left(\sigma^U_f \gamma^U_{Mo} \frac{232 P_U}{238 P_{Th}} + \sigma^{Th}_f \gamma^{Th}_{Mo} \right),$$

where N_{Th}, N_{Mo} are the numbers of Th^{231}, Mo^{99} (Ba^{140}) disintegrations per unit time at the end of the irradiation time and referred to the total amounts of Th^{232} and U^{238} in the container; $T_{\frac{1}{2}Th}$, $T_{\frac{1}{2}Mo}$, are the half-lives of Th^{231}, Mo^{99}(Ba^{140}); σ^U_f, σ^{Th}_f are the fission cross sections of U^{238}, Th^{232} at 14 Mev neutron energy; γ^U_{Mo}, γ^{Th}_{Mo} are the fragment yields during the fission of U^{238}, Th^{232} at 14 Mev neutron energy; and P_{Th}, P_U are the weights of Th^{232} and U^{238} in the container.

The following value was obtained for the cross section for the reaction Th^{232}(n, 2n)Th^{231} at 14.7 Mev:

$$\sigma^{Th}_{n,\,2n} = 0.65 \pm 0.15) \text{ barn.}$$

The error includes both the scatter in the experimental quantities and the systematic error in the fission cross sections and fragment yields.

Later, in connection with the determination of Mo^{99}, Ce^{141} yields ($\gamma^{Th}_{Mo} = 0.020$, $\gamma^{Th}_{Ce} = 0.059$) as well as the yields of other fragments emitted during the fission of Th^{232} at 14.3 Mev neutron energy, it became possible to irradiate pure thorium nitrate without the addition of U_3O_8. The results obtained from these control experiments turned out to be in agreement with those obtained earlier.

In conclusion, we wish to thank V. A. Vlasov, A. S. Kovaldov, V. M. Lartsev, V. R. Negina and N. D. Osyaev for taking part in the present work.

* This work was carried out in 1956-1957.

† See G. P. Antropova et al, Atomnaya Énergiya 5, No. 4, 456 (1958).

* * *

γ RADIATION EMITTED BY U^{238} UNDER THE ACTION OF 14 MEV NEUTRONS

A. I. Veretennikov, V. Ya. Averchenkov, M. V. Savin, and Yu. A. Spekhov

Translated from Atomnaya Énergiya, Vol. 8, No. 4, pp. 361-363, April, 1960
Original article submitted October 12, 1959

The γ-ray spectrum and the number of γ-rays per neutron-U^{238} interaction have been determined at 14 Mev neutron energy. The time-of-flight method was used to separate effects due to γ-rays and neutrons.

The geometry of the experiment and a block diagram of the apparatus are shown in Fig. 1. Neutrons from the reaction $d(T, n)He^4$ at $E_d \simeq 125$ kev were employed. The diaphragm D defined a solid angle of $\omega_a = 4 \cdot 10^{-3}$, which corresponded to a neutron beam having an energy of 14 Mev. The specimen was in the form of a disc made from natural uranium. It was placed at an angle of 45° to the axis of the beam and covered the beam completely. The γ-rays emitted by the specimen were detected by a stilbene crystal, 56 mm in diameter and 28 mm long, mounted on a FÉU-33 photomultiplier. In order to reduce the background due to the inelastic scattering of 14 Mev neutrons, this detector was at an angle of 90° to the beam axis. The detector was screened from the neutrons emitted directly from the target by a brass cone. The α particles were recorded by a thin film scintillator [1] covered by an aluminum foil 2 μ thick. This foil served as a screen against scattered deuterons and β particles from tritium.

Pulses from the α and γ detectors were fed into a time analyzer [2]. The distribution of the time intervals between pulses from the α and γ detectors for a U^{238} specimen, 100 mm in diameter and 11 mm long, is shown in Fig. 2 (curve 1). The flight path was 65 cm. The background of random coincidences, measured under the working conditions by introducing an additional delay of $\Delta t_1 = 75$ nanosec, is shown by curve 2.* The half-width of the α-n coincidence curve, obtained by placing the γ-detector in the beam (curve 3), is a measure of the resolving time of the analyzer ($2\tau = 4$ nanosec).

Pulses from the twelfth dynode of the photomultiplier of the γ-detector were fed through an amplifier and a linear gate controlled by the time analyzer into a fifty-channel kicksorter. The gate was open only for pulses appearing during a time interval of 0-10 nanosec after the interaction of neutrons with uranium (in the above geometry 14 Mev neutrons from the specimen reached the detector after ~13 nanosec).

In time operation, a loss of low-amplitude pulses from the γ detector was observed and was largely due to deterioration in the pulse shaping of low-amplitude pulses in the input stages of the time analyzer [2]. Corrections for this effect were introduced by comparing the amplitude distribution of pulses due to the 14 Mev neutrons obtained directly from the γ-detector, and the amplitude distributions due to the same neutrons obtained from α-n coincidences.

The energy callibration of the kicksorter was carried out using Cs^{137}, Co^{60}, and RaTh γ rays. In order to take into account higher energy γ rays, a limitation was introduced on the pulse amplitude at the kicksorter input so that a 'pulse limit peak' appears in the last channels of the kicksorter.

The spectra were corrected by subtracting the background of random coincidences and by allowing for counting losses in the region of small amplitudes. The spectrum was divided into equal energy intervals with $\Delta E = 60$ kev. The amplitude disbribution of γ rays in each of these intervals was assumed to be rectangular [3]. (This approximation was justified by measurements of amplitude distributions for Cs^{137} and Co^{60}). The number of γ rays per interval was determined with due allowance for the efficiency of the crystal (assumed equal to the efficiency of anthracene [4]) and the self-absorption in the specimen (energy losses were not allowed for).

Three uranium specimens were investigated (100 mm diameter, 3.8 and 11 mm thick respectively). The results obtained for the three specimens were in good agreement. The γ ray spectrum in the range 0.4-0.8 Mev, averaged over the data for the three specimens, is shown in Fig. 3. The average energy of the γ radiation, corrected for the 'amplitude limit peak', was found found to be 0.98 Mev. (The limit peak was replaced by a triangular distribution defining an area equal to the area of the peak and corresponding to about 10% of the total number of γ-rays.) The energy resolution in the measurement of the γ-spectra was approximately 30% at $E_\gamma = 662$ kev, and approximately 15% at $E_\gamma = 2.62$ Mev.

* The background of random coincidences was also measured by placing the specimen outside the beam but at the same distances from the γ detector and the target as under the conditions of the main experiment. The results were found to be the same as in the case of the 75 nanosec delay.

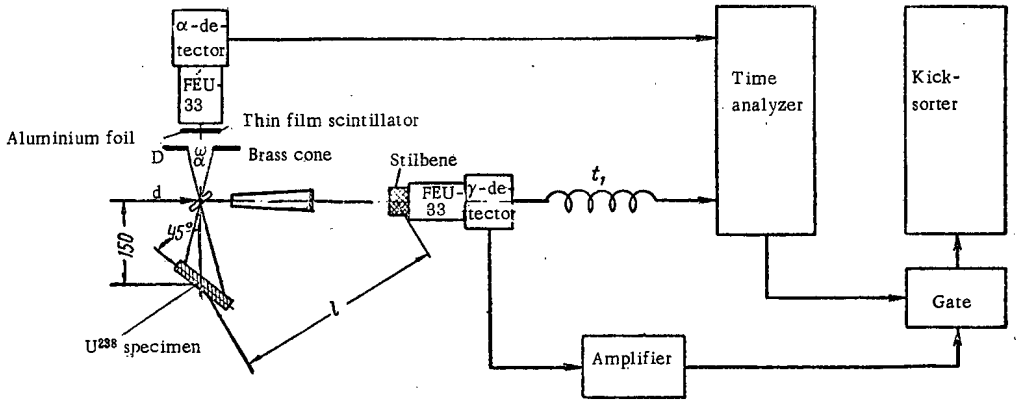

Fig. 1. Geometry of the experiment and block diagram of the apparatus.

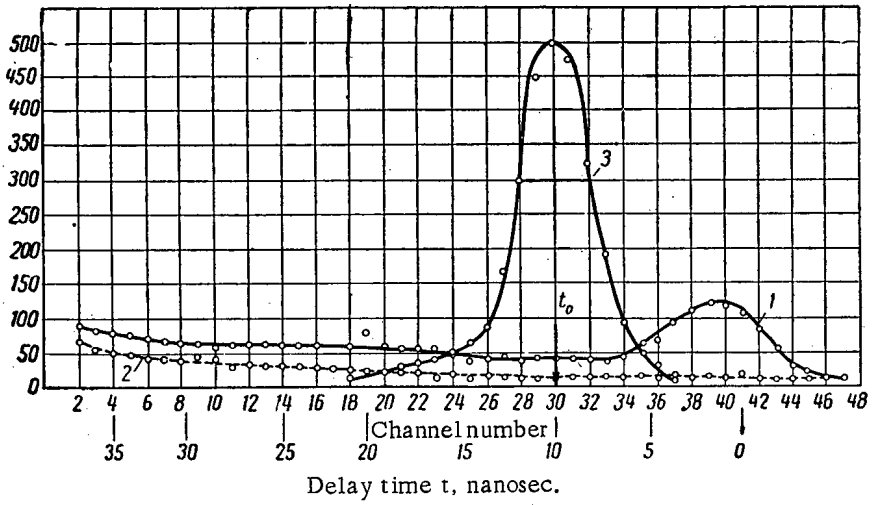

Fig. 2. Time distribution of γ rays and secondary neutrons emitted from the U^{238} specimen.

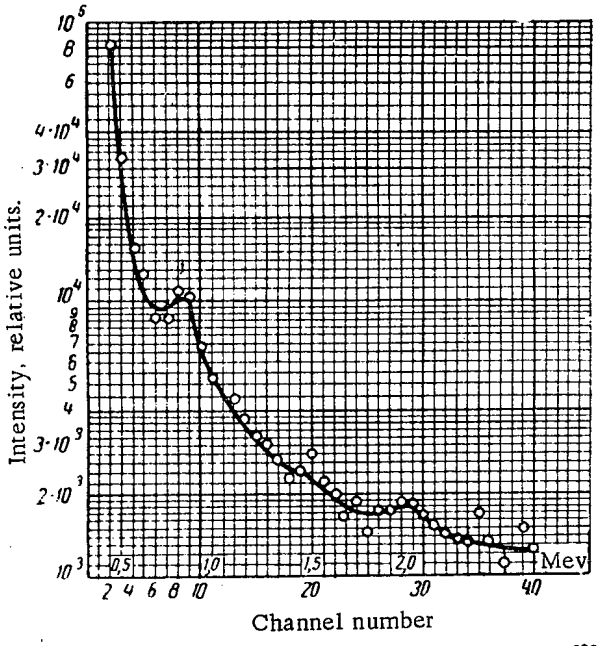

Fig. 3. The spectrum of γ-radiation emitted by U^{238} under the action of 14 Mev neutrons.

The mean number of γ-rays per interaction is given by

$$\bar{\eta}=\frac{N_\gamma}{AN_n[1-\exp(-\sigma n_0 h)]},$$

where N_γ is the number of γ rays in the entire spectrum, A is a geometrical constant, N_n is the total neutron flux at the specimen, determined from the number of α-particles, n_0 is the number of nuclei per cubic centimeter, $\underline{h}$ is the effective thickness of the specimen, and σ is the total cross section for inelastic neutron-U^{238} interactions giving rise to the emission of γ rays. For σ = 2.85 barns the quantity η was found to be equal to 6 ± 1.2. Corrections were introduced for γ rays due to the interaction of secondary neutrons with the specimen and for the replacement of the true amplitude distribution of pulses due to monoenergetic γ rays by a rectangular distribution. The error in the values obtained for η includes contributions due to errors in the energy callibration of the γ spectrometer, errors in the determination of the geometrical parameters, and errors involved in the estimation of the number of γ rays in the 'amplitude limit peak'.

The authors express their deep gratidude to Yu. S. Zamyatnin for valuable discussions and V. G. Kokoulin for the preparation of the large crystal of stilbene.

LITERATURE CITED

1. V. M. Gorbachev and M. I. Kazarinova, Pribor. i Tekh. Éksp. No. 4, 20 (1957).
2. A. I. Beretennikov and V. Ya. Averchenko, Pribor. i Tekh. Éksp. No. 3, 48 (1958).
3. I. Sharpe, Nuclear Radiation Detector (London, Methuen Co. LTD, 1955) p. 18.
4. J. B. Birks, Scintillation Counters [Russian translation] (IL, 1955), p. 89.

* * *

A STUDY OF SCINTILLATIONS IN HELIUM AT LIQUID HELIUM TEMPERATURES

B. V. Gavrilovskii

Translated from Atomnaya Énergiya, Vol. 8, No. 4, pp. 363-365, April, 1960
Original article submitted October 12, 1959

The use of high-pressure helium scintillators was suggested in [1] as a method for measuring the polarization of fast neutrons. In this connection the light output of helium scintillators was measured in helium mixed with other gases at pressures up to 80 atm. In practice it is difficult to increase the gas pressure in the scintillator considerably above 100 atm, which is necessary in order to produce an efficient polarimeter. Moreover, the most effective mixture (helium and nitrogen) studied in [1] gives rise to scintillations whose amplitude strongly depends on the purity of the gas, and decreases when the pressure is increased to a value which makes it difficult to record neutrons having an energy less than 5 Mev [1]. The density of the scintillating gas can be considerably increased by cooling the scintillator to low temperatures. A description of a helium container which can be cooled down to liquid nitrogen temperatures at a pressure of a few tens of atmospheres was described in [2].

A helium scintillator which can be cooled to liquid helium temperatures is described in the present paper. The density of such a scintillator at pressures below the critical pressure for helium (2.2 atm) can be varied in a very wide range, right up to the condensation point of the scintillating gas. Moreover, at these temperatures all impurities, including gas activators, are frozen out, and highly pure helium can be obtained. The mechanism responsible for the luminescence of very pure helium in a wide density interval is of considerable interest in its own right.

The scintillations were studied using the apparatus illustrated schematically in Fig. 1. The principal elements of the cryostat were made of glass, which enabled visual control of the relative disposition of the photocathode, container, light reflector and α-source, and also visual inspection of the condensation of helium in the container. The vacuum chamber of the cryostat is formed by the cyclindrical steel chamber 1, the glass cylinder 3 and the helium dewar [7] introduced into the cylinder on a conical seal. The demountable construction of the cryostat ensured a rapid replacement of the helium dewar and facilitated the use of containers of different types. The preliminary purification of technical helium was carried out with the aid of an apparatus consisting of three copper U-tubes having an internal diameter of 25 mm and filled with activated charcoal. The apparatus was placed in a nitrogen dewar. The scintillations produced by α particles in the container were recorded by a FÉU-14 photomultiplier. Pulses from this photomultiplier were fed into a a scaling unit and an oscillograph which was used to measure the amplitudes. The photocathode was inside a nitrogen jacket and was therefore gradually cooled to liquid nitrogen temperature. (The photocathode of the FÉU-14 photomultiplier retains its sensitivity on cooling down to $-190°C$ [3].) The amplification coefficient of the photomultiplier was controlled during the measurements with the aid of light flashes produced by a neon lamp (MTKh-90) included in the circuit of a relaxation oscillator. The amplitude of these light pulses was calibrated by comparing it with the amplitude of pulses due to scintillations produced by α-particles in a CsI crystal.

The helium scintillations were investigated at room temperature, at liquid nitrogen temperature and at liquid helium temperature. The amplitude of pulses in the first two cases have the following values: 1) for technical helium at room temperature the pulses were of the same order as the noise of the FÉU-14 photomultiplier, 2) for a mixture of technical helium and

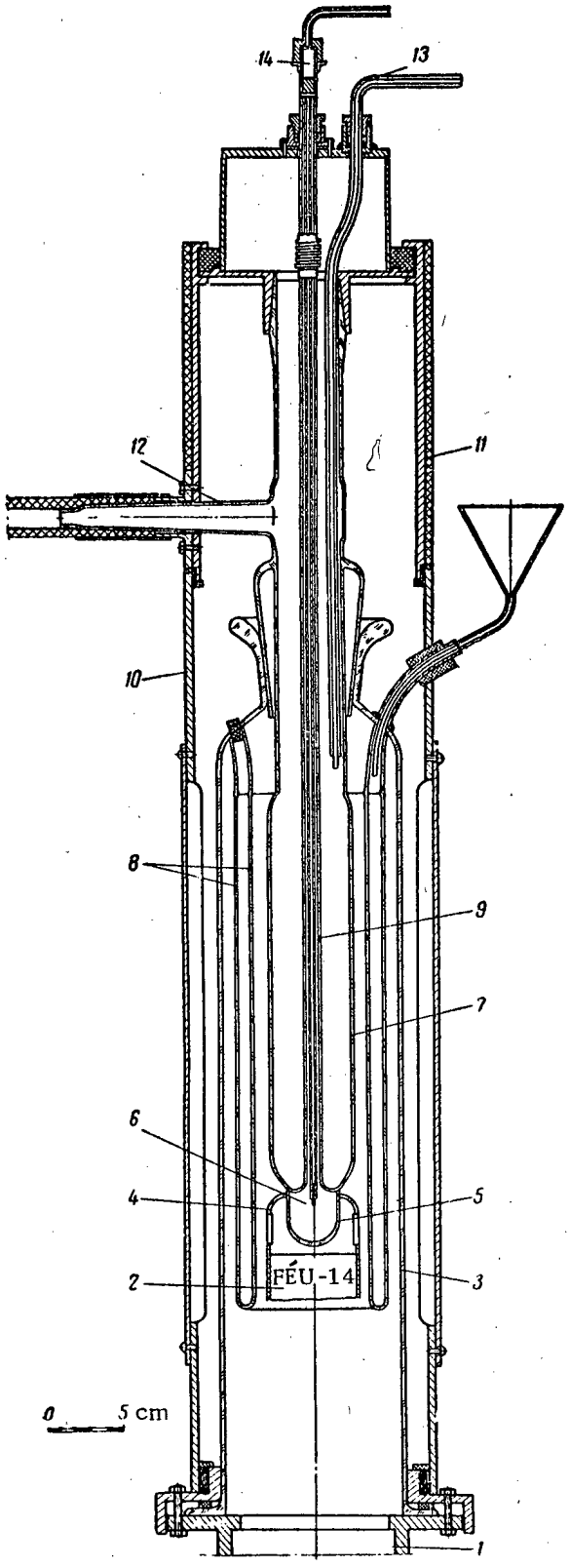

Fig. 1. Diagram of the apparatus. 1) Steel chamber; 2) FÉU-14 photomultiplier; 3) glass cylinder; 4) reflector; 5) scintillator container; 6) point α source; 7) helium dewar; 8) nitrogen dewar; 9) tube for supplying gas into the scintillator and for introducing the α source; 10, 11) demountable light screen for the FÉU-14 photomultiplier; 12) pumping line for removing helium vapor; 13) liquid helium supply line; 14) steel rod for introducing the source into the the container with the aid of a magnet.

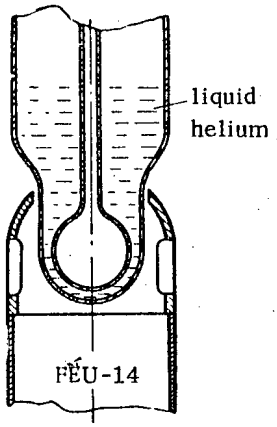

Fig. 2. Scintillator container (second form).

nitrogen (0.1% N_2) it was 5-10 times greater than the noise level, which corresponds to 2% of the output for CsI, 3) for pure helium at room temperature it was 1.5%, 4) for a mixture of pure helium and nitrogen (0.1% N_2) - 3%, 5) for a mixture of pure helium and nitrogen at liquid nitrogen temperature - 3%. At room temperature the results were not always reproducible but at −190°C the reproducibility was good. The amplitude of the scintillations produced in pure helium and in helium-nitrogen mixtures did not vary very much as the pressure was reduced. At a pressure of 15-20 mm Hg the light output was 30-50% of the light output at 760 mm Hg. This effect is particularly well defined at liquid nitrogen temperatures. The mean distance of the the α source from the walls of the container was 1.5 cm. Thus, at low helium pressures, α particles lose only a small fraction of their energy inside the container. At pressure corresponding to energy losses of 10-30 kev, the amplitude of the scintillations was 2-3% of the amplitude of CsI pulses produced by 5.5 Mev α particles. Thus, the specific light output of a helium-nitrogen mixture at pressures below 760 mm Hg reaches values which are not less than those for the light output of CsI, and may even exceed it. Gas scintillators with low energy losses may be useful in the recording of short-range particles and recoil nuclei.

At liquid helium temperatures, the gas pressure was increased up to 1000 mm Hg. In the container shown in Fig. 1 the condensation of helium took place very slowly, and in order to accelerate this process it was necessary to reduce the temperature by pumping out vapors from the dewar. The container was in the form of a glass sphere surrounded by liquid helium (Fig. 2) and was more convenient from the point of view of thermal conditions. The light collection was worse by a factor of ~2.5 as compared with the first container because of the greater number of glass surfaces.

The density of gaseous helium cooled down to liquid helium temperatures reached a value equivalent to a pressure of ~100 atm. In this region the light output had a wide maximum at ~20-30 atm (5% of CsI) and was reduced by a factor of 1.5-2 when the maximum density was reached. In liquid helium, the amplitude of the scintillations did not exceed the noise level of the photomultiplier. When the point source was raised above the level of the liquid to a distance of a few millimeters the scintillations in the saturated vapor were the same as in the cooled gas prior to condensation. In the case of technical helium (2% impurity) the amplitude of the scintillations was almost the same as for pure gas. Clouding of the windows of the container due to the condensation of impurities on the inner surface was frequently observed. Thus, the light output is not very dependent on the purity of the original gas.

An investigation was made of the effect of the light converter on the amplitude of the scintillations. In these experiments the spherical container shown in Fig. 2 was employed. A thin film of quaterphenyl was deposited (by evaporation in a vacuum) on the inner surface. The thickness of this film was a few hundreds of $\mu g/cm^2$. Under the action of α-particles the quaterphenyl film in an evacuated container gave rise to scintillations, and the amplitude of these scintillatillations exceeded the noise level of the FÉU-14 photomultiplier and remain unaltered on cooling below the λ point of helium. At helium temperatures the use of quaterphenyl led to a rapid increase in the amplitudes of the scintillations. Thus, the amplitude of scintillations of gaseous helium was greater by a factor of 2.5-3, and was 15-20% of the amplitude of CsI scintillations (in the maximum).

The most interesting result is that the scintillations observed in liquid helium have roughly the same amplitudes as in the cooled gas. The light output remains the same on cooling the condensed helium below the λ point. Thus, excitations giving rise to the emission of ultraviolet radiation play a dominating and roughly the same role both in liquid and in gaseous helium, while the direct emission of visible light in liquid helium is very much reduced.

The above method was also used to investigate scintillations in gaseous and liquid He^3. A gas cylinder containing purified He^3 was attached to the apparatus. Condensation of He^3 was achieved by removing helium vapor in the dewar. A modified form of the container shown in Fig. 2 was employed. The He^3 scintillations at nitrogen and helium temperatures had roughly the same amplitude as the scintillations in He^4, both with and without the light convertor. He^3 scintillations are of interest in connection with experiments using both slow and fast neutrons.

In conclusion, I wish to express my gratitude to F. E. Chukreev and A. F. Prokoshin who took part in the initial stages of the experiment, A. G. Petrov for considerable help in the building of the apparatus, N. A. Belov who produced the glass parts of the cryostat, and K. S. Mikhailov in whose laboratory the quaterphenyl light converter was prepared.

LITERATURE CITED

1. S. A. Baldin, B. V. Gavrilovskii, and F. E. Chukreev, Atomnaya Énergiya 3, 10, 331 (1957).*
2. S. A. Baldin and B. V. Gavrilovskii, Pribor. i Tekhn. Éksp., No. 1, 144 (1960).
3. S. A. Baldin, B. V. Gavrilovskii, and F. E. Chukreev, Paper read at the VII Conference on Radio Electronics [in Russian] (Moscow, 1959).

* Original Russian pagination. See C. B. translation.

* * *

MASS-SPECTROMETRIC ANALYSIS AND THE IDENTIFICATION OF TECHNETIUM

G. M. Kukavadze, R. N. Ivanov, V. P. Mexhcheryakov, Yu. G. Sevast'yanov, B. S. Kir'yanov, V. I. Galkov, and A. P. Smirnov-Averin

Translated from Atomnaya Énergiya, Vol. 8, No. 4, pp. 365-367, April, 1960)
Original article submitted January 18, 1960

Technetium, which has a mass number 43, is of major interest [1, 2]. This is due to the fact that it may be used as an inhibitor in reactors, and also in other industrial applications [3, 4].

Small quantities of technetium for radiochemical studies are usually obtained by irradiating molybdenum with neutrons, protons or deutrons. Technetium has a number of known isotopes. Isotopes with mass numbers, 97, 98, and 99 are long-lived. The last of these has a half-life of $2.2 \cdot 10^5$ years [5, 6] and is produced in reactors as a fission product of uranium and plutonium with a relatively large yield (approximately 6.5%) [7]. In view of this, considerable quantities of technetium are accumulated in the heat liberating elements of a reactor.

In the analysis of technetium it is very important to distinguish it from the neighboring elements which are also produced on fission, namely, zirconium, niobium, molybdenum and ruthenium. Chemical, radiometric and spectroscopic methods of analysis (on their own) cannot give an unambiguous result at the present time. Mass-spectrometric methods on the other hand, used in conjunction with the above methods, do give an unambiguous result.

During experiments concerned with the isotopic composition of the spent heat-producing element of the reactor of the First Atomic Power Station, technetium was separated by an extraction method.*

The technetium specimens were identified not only by spectrophotometric, radiometric and spectroscopic methods, but also by a mass-spectrometric method.

The present paper describes an original method developed by the authors for the mass-spectrometric analysis of technetium.

The work was carried out on a mass spectrometer (type MS) with a 60° sector magnetic field and a chamber bent along a circular arc of radius 150 mm. The ion currents were detected with a 100% feedback dc amplifier capable of measuring currents down to 10^{-14} amp and an electron multiplier having aluminum-magnesium alloy dynodes. The use of this alloy increased the sensitivity of the ion detector by more than two orders of magnitude. The ion source was in the form of a thermionic emitter based on surface ionization of the substance under investigation at a hot high-melting point wire [8]. This source was chosen because the surface ionization effect is not accompanied by a considerable background such as usually appears in mass-spectrometers due to the degassing of source components and also contamination by previous specimens and residual gases. This avoids the overlapping of spectral lines and ensures good resolution. However, experiments showed that technetium ions are not formed at hot tungsten emitters such as are normally used in thermionic sources. Clearly, the affinity of electrons for technetium atoms is greater than for tungsten, and this leads to the re-evaporation of technetium in the form of atoms rather than positive ions.

Some authors [9, 10] have used iridium emitters. The use of iridium in our case did not lead to a positive result because the iridium foils were found to disintegrate at a lower temperature than the evaporation temperature of technetium.

In the present work we used tungsten emitters, carrying a 0.1 μ layer of iridium which was evaporated onto tungsten by electron bombardment.

Technetium in the form of a water solution of ammonium pertechnetate was deposited from a micropipette on to the emitter prepared as above. Next, technetium was brought to its metallic state by heating to red heat for a few minutes in a hydrogen stream.

The ion source, with the specimen prepared in the above way, was then placed in the mass spectrometer. Technetium ions (Tc^+) appeared at temperatures of 1600-1800°C.†

Figure 1 shows the mass spectrogram of technetium (mass number 99) and rubidium (mass number 87 and 85). Rubidium was present in the emitters as an iridium impurity and was used as a marker.

Figure 2 shows the mass spectrogram obtained in a control run. In this run a mixture of all the reagents which were used in the main experiment was deposited

* Yu. B. Gerlit and D. S. Kapustin took part in the separation of technetium.

† The temperature was measured in a separate vacuum system using an optical pyrometer.

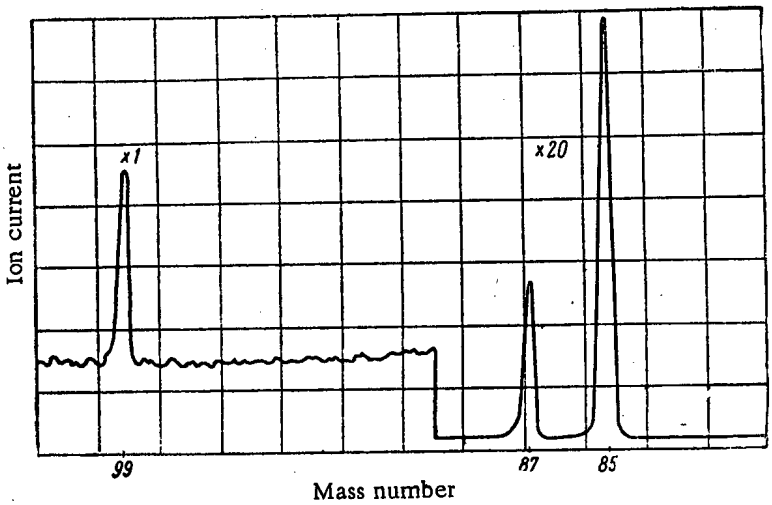

Fig. 1. Mass spectrogram of technetium and rubidium with emitter at 1900°C.

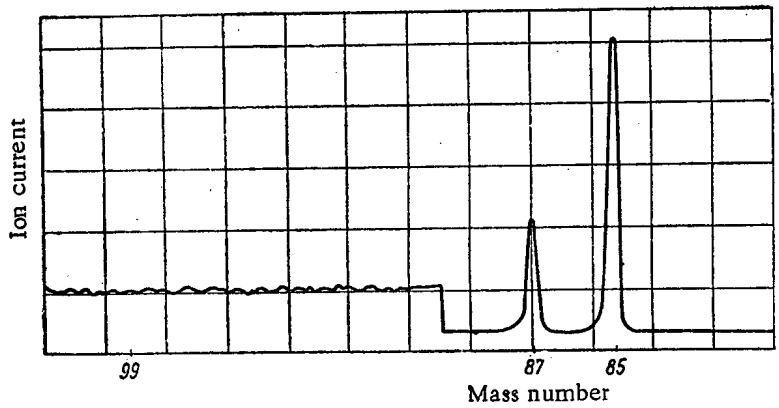

Fig. 2. Mass spectrogram obtained in the control experiment with emitter at 1900°C (same mass range as in Fig. 1).

on the emitter and the procedure used in the chemical separation of technetium was repeated. The emitter was then subjected to treatment in a hydrogen stream.

The above method, together with the isotopic dilution method [11-13] and the integral mass-spectrographic method of determining the concentration of elements [14], can be used in the quantitative determination of technetium. It can also be used to study a number of chemical compounds of technetium, and to determine some of its thermodynamic constants.

The authors consider it their pleasant duty to thank V. G. Zhuravleva for preparaing the emitters us used in this work.

LITERATURE CITED

1. Yu. B. Gerlit, Proceeding of the Second International Conference on the Peaceful Uses of Atomic Energy (Geneva 1955) [in Russian] (Goskhimizdat, 1958) Vol. 7, p. 183.
2. Vikt. I. Spitsyn and A. F. Kuzina, Atomnaya Énerg. 5, 2, 141 (1958)‡
3. G. Cartledge, J. Phys. Chem. 59, 979 (1955).
4. R. Rympson and G. Cartledge, J. Phys. Chem. 60, 1037 (1956).
5. S. Fried, A. Jaffey, N. Hall and L. Clendenin, Phys. Rev. 81, 741 (1951).
6. G. Parker, ORNL-870 (March, 1951).
7. H. Fickel and R. Tomlinson, Canad. J. Phys. 37, 916 (1959).
8. R. N.Ivanov and G. M. Kukavadze, Pribor. i. Tekh. Éksp. No. 1, 106 (1957).
9. G. Boyd, J. Sites, Q. Larson and C. Baldock, Phys. Rev., 99, 1030 (1955).
10. M. Smith, Electromagneticity, Enriched Isotopes and Mass Spectrometry. Proceedings of the Conference Held in the Cockroft Hall (Harwell, 1955) p. 152.
11. M. Inghram, J. Phys. Chem. 57, 809 (1953).
12. G. M. Kukavadze, M. P. Anikina, L. L. Gol'din, and B. E. Ershler, Session of the Academy of Sciences of the USSR on the Peaceful Uses of Atomic Energy (Department of Chem. Sci.) [in Russian] (Izd. AN SSSR, Moscow, 1955) p. 205.
13. G. M. Kukavadze, Zhur. Fiz. Khim. 33, 1436 (1959).
14. V. K. Gorshkov, Pribor. i Tekhn. Éksp. No. 2, 53 (1957).

‡Original Russian pagination. See C. B. translation.

* * *

HEAT TRANSFER TO SODIUM AT LOW Re NUMBERS

M. S. Pirogov

Translated from Atomnaya Énergiya, Vol. 8, No. 4, pp. 367-368, April, 1960
Original article submitted October 5, 1959

The present paper reports results of experiments on heat transfer to sodium flowing through a circular copper tube (d_{ext} = 28 mm, δ_{wall} = 4 mm) in the range Re = = 17-416.

The apparatus employed is shown schematically in Fig. 1. Thermocouples set up on the experimental section were calibrated in situ against a platinum-rhodium thermocouple. The apparatus was set up vertically, the sodium flowing in the upward direction. The oxygen impurity in the sodium was 0.0056% by weight.

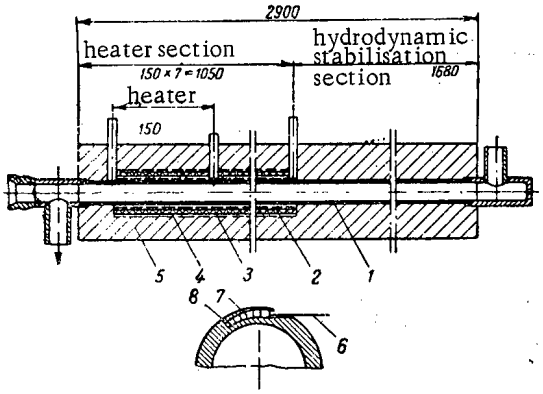

Fig. 1. Experimental section. 1) Copper tube, 2) heater, 3) heat-meter, 4) compensating heater, 5) insulation, 6) thermocouple, 7) porcelain tube, 8) copper wedge.

The following quantities were measured in steady state: the emf's produced in the thermocouples attached to the walls of the tube, the electrical power dissipated in the heater, and the amount of sodium flowing through the tube. Heat losses were compensated by special heaters. The temperature of sodium at the input and output of the apparatus (t_{in} and t_{out}) was measured by the thermocouples attached to the walls of the tube before and after the heated region.

Special measurements, carried out with the aid of a temperature probe, showed that the temperature distribution in the current of sodium in these two positions is uniform. The coefficient of heat transfer from the wall of the tube to the flowing sodium over the region of stabilized heat transfer was calculated from the formula

$$\alpha_x = \frac{q_x}{(t_w - t_{Na})_x}. \qquad (1)$$

The temperature of the sodium across a distance x was determined from the expression

$$\bar{t}_{Nax} = t_{in} + \frac{\pi q d_{ex}}{GC_p} x + \left[\frac{\Delta t}{\Delta l}\right]_w \left(\frac{\pi d_{ex}^2 \lambda_{Na}}{4GC_p} + \frac{\pi d_{av} \delta_w \lambda_w}{GC_p}\right), \qquad (2)$$

where $[\Delta t/\Delta l]_w$ is the temperature gradient in deg/m

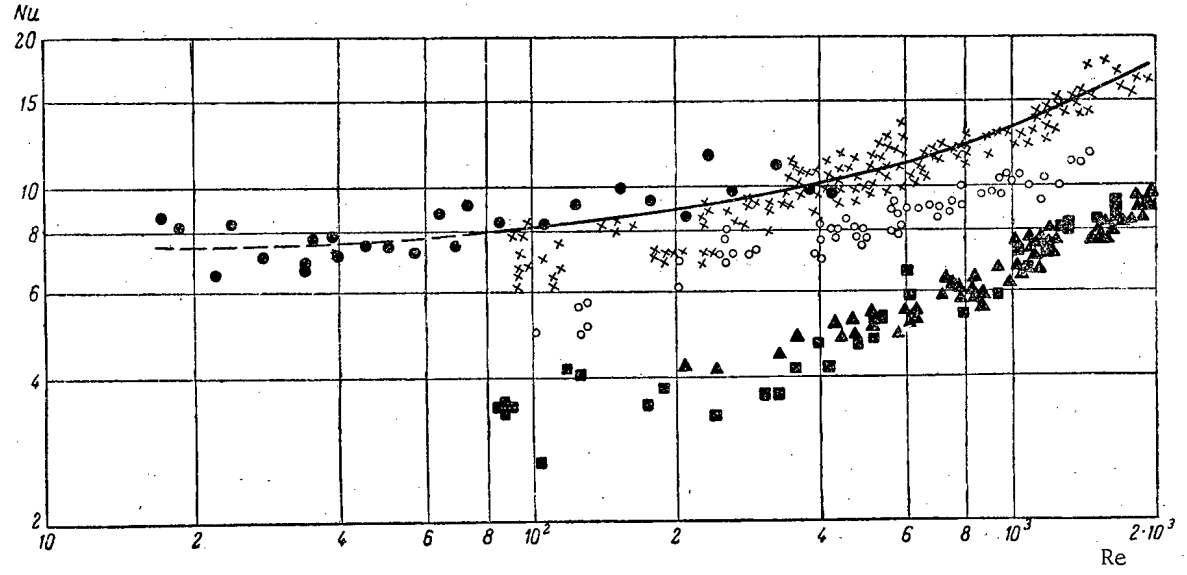

Fig. 2. Comparison of experimental data (the curve represents the Martinelli-Lyon theory with ϵ = 1): x) data of [2] (Na–K, Hg), ▲) data from the Power Institute, AS USSR, (Na), ■) data from the Central Boiler-Turbine Institute (Na), O) data from the Technical Physics Institute (Na) [1], ●) present data.

along the axis of the tube over the stabilized heat transfer region, as determined from measurements of the temperature of the wall.

The specific heat flow through the experimental tube was ~80,000 kcal/ m^2·hr. The rate of flow of sodium in the tube was varied between 0.04 and 1 m/sec, the Re number between 2300 and 70,000, the temperature drop $(t_w - t_{Na})_x$ between 5 and 3.5°C, and the heat transfer coefficient between 16,000 and 28,000 kcal/ / m^2·hr·deg.

Experimental data were analyzed on the basis of the similarity criterion Nu = f(Re) and are shown in Fig. 2, together with the data obtained by other workers [1, 2].

In the above range of Re numbers, the experimental data are in agreement with the Martinelli-Lyon formula with ϵ = 1:

$$Nu = 7 + 0{,}025\,(Pe\varepsilon)^{0{,}8}. \qquad (3)$$

They are also in agreement with the results reported by P. L. Kirillov, V. I. Subbotin et al [2] for Re > 100.

The results obtained in the present investigation do not confirm the suggestion put forward by a number of authors that there is a rapid deterioration in heat transfer in the region of low Re numbers.

LITERATURE CITED

1. S. S. Kutateladze, V. M. Borishanskii, I. I. Novikov, and O. S. Fedynskii, "Liquid-metal heat carriers," Atomnaya Énerg. (Atomizdat, 1958) Suppl. No. 2.
2. P. L. Kirillov, V. I. Subbotin, M. Ya. Suvorov, and M. F. Troyanov, Atomnaya Énerg. 6, 4, 382 (1959).*

*Original Russian pagination. See C. B. translation.

* * *

SEPARATION OF LITHIUM ISOTOPES ON A SIMPLE ION-EXCHANGE COLUMN

G. M. Panchenkov, E. M. Kuznetsova, and L. L. Kozlov

Translated from Atomnaya Énergiya, Vol. 8, No. 4, pp. 368-370, April, 1960
Original article submitted November 5, 1958

In the study of isotope separation by ion-exchange, after the determination of the single-stage separation factor, it is advantageous to check the operation of a simple ion-exchange column. Both frontal analysis and displacement elution have been used in such experiments [1]. In the first case a 3% lithium chloride solution was passed at 2-3 ml/ min through a 10-meter column with sodium zeolite. The maximum ratio of lithium isotopes in the head fraction was 13.3 instead of the original 11.6. In the second case, better results were obtained on a 30-meter column of sodium zeolite. in the head fraction the ratio of Li^7/Li^6 equaled 14.1 and in the tail, 8.8.

A theoretical analysis of the conditions affecting the separation process was given in [2]. One of the experiments was carried out on a column 90 cm long with the cationite Zeocarb with a grain size of $1.5 \cdot 10^{-3}$ cm; 1 N lithium acetate solution was passed through the column at $4 \cdot 10^{-4}$ ml/ sec. Analysis of the first enriched fractions for Li^7 gave an isotopic ratio of 199 instead of 12.2. Nobody has been able to repeat these results. Thus, in the elution of the lithium band in a 1.5-meter column, the content of the isotope Li^7 was found to equal 94.6 weight % in the head and 89.6 weight% in the tail fractions instead of the original content of 92.47 weight % [3]. Preliminary experiments on the separation of lithium isotopes in 80% acetone on a 40-cm column with the cationite Zeocarb with the lithium band eluted with potassium chloride solution led to an insignificant change in the isotopic composition [4]. The ratios of isotopes in the head and tail fractions were 11.62 ± 0.03 and 11.23± 0.03, respectively, in comparison with the starting ratio of 11.52.

In later work on the separation of lithium isotopes by ion-exchange [5], a study was made of the elution of the lithium band on a column with the resins Dowex-50 and IRC with solutions of sulfuric and hydrochloric acids, ammonium chloride, and ammonium ethylenediaminetetraacetate. Unfortunately, the over-all separation factor was not given in this work. The theoretical factor for single-stage separation of the isotopes lay within the range of 1.001-1.002 [6].

The data presented show that with the normal ion-exchange process it is impossible to obtain any appreciable amount of enriched material.

The countercurrent ion-exchange process is of great interest, but it involves very great experimental difficulties. The theoretical analysis of this method and also

TABLE 1. Separation of Lithium Isotopes in an Ion-Exchange Column.

Solution	Column length, cm	Critical volume, ml	Isotopic ratio of samples	Total enrichment factor
LiCl	230	115	13.3	1.13
$Li_3C_6H_5O_7$	227	375	14.4	1.23
$LiC_7H_5O_2$	225	420	14.1	1.20
LiOH	231	695	14.2	1.21

the operation of a column for the separation of elements has been described in [7, 8].

For studying the separation of lithium isotopes in a simple ion-exchange column we used solutions of various lithium salts and also lithium hydroxide. The filtration rate in the experiments was varied from $1.5 \cdot 10^{-3}$ to $5 \cdot 10^{-3}$ ml/sec. The starting concentration of the solutions was the same, namely, 0.5 N. The isotopic ratio of these solutions was 11.7. The ion-exchange material was sulfocarbon in the hydrogen form with a grain size of $(1.7\text{-}2.5) \cdot 10^{-2}$ cm. The data obtained are given in Table 1.

In the filtration of solutions of lithium salts through the column, the first traces of lithium ions appeared when different volumes of the starting solution had passed, depending on the salt used. The solution volume up to the appearance of the first traces of lithium increased in the series chloride–citrate–benzoate–hydroxide. A plot of the negative logarithm of the dissociation constant of the acid formed against the critical volume of solution required for the appearance of the first traces of lithium gave an approximately straight line. Such a graph (Fig. 1) can evidently be used to determine the critical volume for solutions of various lithium salts under the same conditions. The critical volumes are given in Table 1.

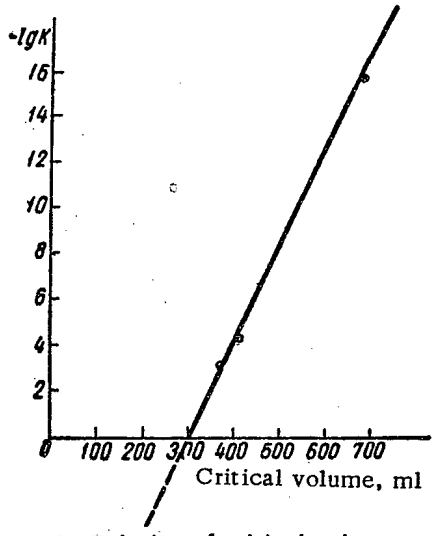

Fig. 1. Relation of critical volume to dissociation constant K of acid formed.

TABLE 2. Displacement of Lithium by Acids.

Acid	Column length, cm	Filtration rate ($\times 10^{-3}$) ml/sec	Isotopic ratio of samples	Total enrichment factor
$H_2C_2O_4$	214	5	14.0	1.19
$H_2C_2O_4$	214	1.5	13.2	1.13
$H_2C_2O_4$	100	5	13.5	1.15
HCl	220	1.5	14.3	1.22

It is interesting to note that in all the experiments presented in Table 1, the solution was enriched in the heavy isotope of lithium (Li^7). When the filtration rate was changed from $1 \cdot 10^{-3}$ to $5 \cdot 10^{-3}$ ml/sec, the total separation factor was practically unchanged.

Replacement of the aqueous medium by butanol did not have an appreciable effect on the enrichment factor. When lithium chloride in 80% butanol was used on a column 224 cm long, the total enrichment factor increased from 1.11 to 1.13 with a change in the solution flow rate from $5 \cdot 10^{-3}$ to $1.5 \cdot 10^{-3}$ ml/sec.

In addition to the experiments described, we also carried out experiments by means of displacement chromatograms. For this purpose we used 1.2 N solutions of hydrochloric and oxalic acids. The data obtained are presented in Table 2. As a comparison of the data in Tables 1 and 2 shows, the results of displacement chromatography were similar to those of frontal chromatography.

The column illustrated in Fig. 2 was made countercurrent ion-exchange. Moist sulfonated charcoal in the hydrogen form was loaded at the top of the column into bunker 1. Lithium chloride solution was introduced from the bottom through tube 3 under a pressure of 1.2 atm and its input rate was controlled with clip 7 and de-

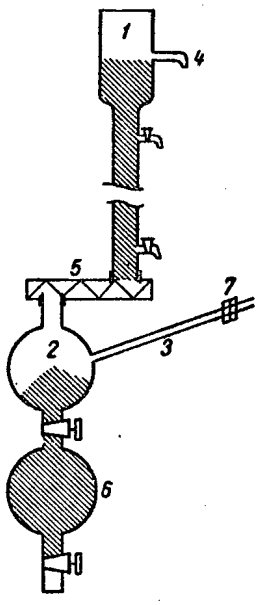

Fig. 2. Countercurrent ion-exchange column.

termined with a flow meter. The solution passed through the column and emerged through side-arm 4 at the top of the bunker. The sulfocarbon, whose level at the top of the column was kept constant, passed downwards under gravity and its speed was regulated by the rotation rate of the screw 5. The spent carbon fell into bunker 2 and when necessary it was transferred to bunker 6. Analysis samples were withdrawn from four taps along the column.

In the experiment described, the working 0.0125 N solution of lithium chloride was introduced at 0.25 ml/sec, counter to the ion-exchange material, which was moving at $1.9 \cdot 10^{-2}$ ml/sec.

A stationary state was established after 2-hr operation and as a result of this the distribution of lithium ion concentration along the column remained constant. The stationary state was not disrupted for 5 hr. Samples for mass spectrometric analysis of the lithium isotopes were withdrawn at distances of 70 and 100 cm from the beginning of the column. The Li^7/Li^6 ratios were 12.6 and 13.3, respectively, instead of 11.7.

The column was operated by the residues method and therefore only 3% of the starting material was separated.

We consider it most advantageous to operate the column under the following conditions: Lithium is introduced at the bottom of the column and the eluent moves upward through the column, while the resin moves downward. The result obtained in the stationary state on a small section of the column corresponds to the result which could be obtained on a column of infinite length.

From a comparison of experimental data on the single-state separation factor [9] and the operation of the column, the enrichment of the solution in the heavy isotope in experiments with lithium hydroxide and benzoate may be explained by the inverse concentration dependence of the single-stage separation factor.

In actual fact, in these experiments carried out by the frontal analysis method there was a decrease in the solution concentration with passage through the column due to irreversible reactions with the formation of water and sparingly soluble benzoic acid. This also explains the comparatively low enrichment factors. Data from experiments with lithium chloride agree completely.

LITERATURE CITED

1. T. Taylor and H. Urey, J. Chem. Phys. 6, 429 (1938).
2. E. Glueckauf, K. Barker, and G. Kitt, Disc. Faraday Soc. 7, 199 (1949).
3. J. Grosse, AECD Report No. 295229 (1950).
4. C. Davies and B. Owen, J. Chem. Soc. 6, 1676 (1956).
5. F. Menes, E. Saïto, and E. Roth, Proc. Symp. Separ. (Amsterdam, 1957).
6. S. Mayer and E. Tompkins, J. Amer. Chem. Soc. 69, 2869 (1947).
7. G. Dickel and K. Becker, Chem. Ing-Tech. 28, 529 (1956).
8. G. Dickel, Z. Elektrochem. 54, 353 (1950).
9. G. M. Panchenkov, E. M. Kuznetsova, and O. N. Kaznadzei, Atomnaya Énerg. 7, 6, 556 (1959).*

*Original Russian pagination. See C. B. translation.

* * *

SOME ASPECTS OF AERIAL γ-RAY PROSPECTING OVER FORESTED REGIONS

G. N. Kotel'nikov and N. I. Kalyakin

Translated from Atomnaya Énergiya, Vol. 8, No. 4, pp. 370-372, April, 1960
Original article submitted May 30, 1959

Due attention is not always given to the screening effect of the forest plant growth when aerial γ-ray surveys are carried out. This results in the overlooking of uranium deposits and in mapping of an annoying number of spurious anomalies.

In this letter, we shall cite examples of established uranium mineralization and discuss the effect of the screening capacity of the forest cover on the results of airborne γ-ray prospecting of the uranium bodies.

1. The deposit is located in a region of absolute elevations ranging 400-450 m and relative elevations 100-150 m. The region is covered with dense stands of mixed flora and thick shrub growth. Denuded patches of land are sufficient to facilitate the work.

The airborne γ-ray surveys (using AN-2 airplanes with ASGM-25 equipment) were carried out on a 1 : 25,000 scale at flying atitude 60 m. A narrow local anomaly peaking at 17 μr/hr (background: 4 μr/hr) was detected

Absorption of Gamma Radiation by Forestal Flora

Tree species	Age of wood, years	Number trees per hectare	Total weight of wood mass per hectare, tons	Total thickness of screen, g/cm²	Value of $\Phi(\mu,h)$ at $\mu = 0.04$, in cm²/g	Absorption of γ-radiation, %
Spruce . .	40	3123	8844	89.7	$0.56 \cdot 10^{-2}$	99.5
	60	1509	3996	41.2	$6.0 \cdot 10^{-2}$	94.0
	100	700	2934	30.5	$10.9 \cdot 10^{-2}$	89.1
Pine . . .	40	3000	3560	36.8	$7.5 \cdot 10^{-2}$	92.5
	60	1200	2485	26.0	$13.8 \cdot 10^{-2}$	86.2
	100	560	1737	18.6	$22.2 \cdot 10^{-2}$	77.8

on one prospecting sortie. Detailed surveying carried out on a 1 : 10,000 scale at 30 m altitude on two routes pinpointed an anomaly with peaks at 17-18 μr/hr and a third at 7 μr/hr.

On the map compiled from the aerial survey data, the anomaly was found to extend 300 m with a width of 30-40 m. Subsequent ground sorties using γ-ray equipment revealed, on the site of the unique anomaly discovered from the air, three ore zones running parallel at 300-500 m separation from each other (Fig. 1). The principal ore zone, part of which was exposed as an outcropping seen from the air, was traced for 2000 m. Surface uranium mineralization is manifested in the form of discrete patches of surface area ranging from 1 m wide to 1200 m² in area, at a γ-emission intensity of 50-1500 μr/hr (against the background noise of 6-7 μr/hr from neighboring interfering rocks). The areal ore-bearing coefficient of the anomaly is about 30%. Aside from the outcropping of bedrock, bodies of ore material (blocks up to 10 cm³ with γ intensity from 50 to 1500 μr/hr) extend over an area of about 80,000 m² in the principal ore zone. These ore runs, like the flanks of the principal ore zone, went unnoticed in the aerial survey, and yet were well exposed except that they were hidden in a dense forest stand. The anomalous sector detected was distinguished by absence of forest growth, lesser shrubbery, and heightened relief.

The fact that areas considerable in extent and of high radiation intensity were not spotted in the aerial γ-ray survey is to be explained by the high screening ability of the forest wood. This supposition was con-

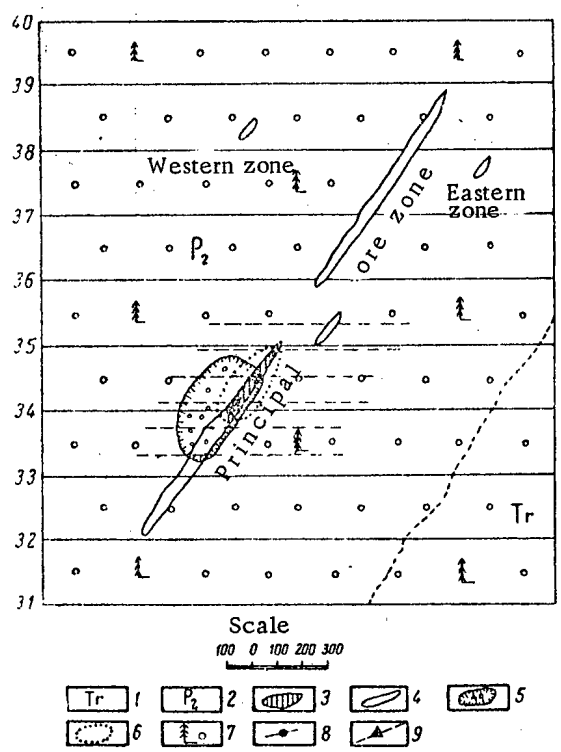

Fig. 1. Base map for anomaly No. 1: 1) tertiary coarse-grained sandstone; 2) carbonaceous clayey shales of Upper Permian; 3) ore zone with contours traced according to aerial survey data; 4) ore zone with contours traced according to ground sortie data; 5) ore dump zone; 6) deforested zone; 7) softwoods (spruces, pines); 8) aerial survey intineraries and anomalies, scale 1 : 25,000; 9) itineraries and anomalies in detailed work, scale 1 :10,000.

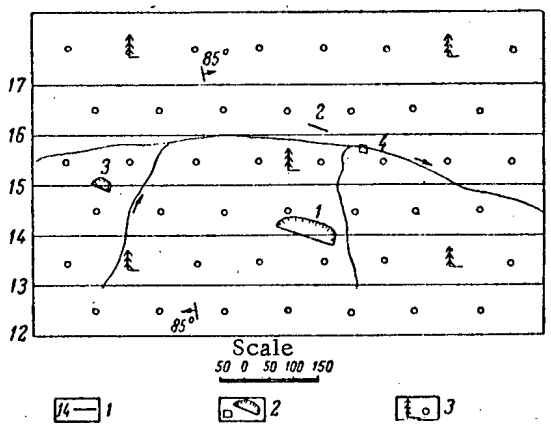

Fig. 2. Base map for anomaly No. 2: 1) aerial survey itineraries; 2) contours of ore zones; and dumps; 3) conifers.

firmed by empirical data. When the tree height over the area l = 33 m, the trunk diameter H = 36 cm, the specific weight of the wood timber is 0.8, the weight of the crown, brushwood, pine needles in the case of conifers, is equal to the weight of the trunk, the total weight of the wood is $P_1 = (v_1 \cdot 0.8) \cdot 2 = (g_m H l \cdot 0.8) \cdot 2 =$ = 2.705 m [1, 2] (where v_1 is the trunk volume, g_m is the species number of the tree; 2 is the corrective factor for the weight of the crown, deadwood, needles or cones). When the density of a forest stand presents us with one tree per 10 m^2, the distributed density is $d = 2705/10 = 270.5$ kg/m^2 = ~27 g/cm^2.

Absorption of the broad beam of γ radiation on its path to the radiation detectors aboard the surveying airplane is expressed by the formula

$$I = I_0 \Phi(\mu d),$$

where $\Phi(\mu d)$ is King's function, and I_0 is the radiation intensity at ground level.

The effective mass attenuation coefficient of γ radiation for wood μ = 0.04 cm^2/g [3]; so that $\Phi(\mu d) =$ = 0.13 and $I = I_0 \cdot 0.13$, i.e., 13% of the unscreened γ radiation.

Consequently, 87% of the γ radiation is absorbed entirely on account of the screening ability of the forest cover. Taking into account the decline in intensity of γ radiation, at an altitude of 50 m and for an area of 1200 m^2, to 4% of the ground-level intensity, and introducing an ore-bearing coefficient of 30%, we obtained the minimum intensity value required to ensure recording, viz. 1540 μr/hr. The intensity of gamma radiation at ground level did not actually exceed 1500 μr/hr for the flanks of the zone and the ore dumps, and the fact that they went unnoticed in the aerial survey is to be expected.

2. γ-Surveying on the ground, scale 1 : 25,000, and aerial γ surveying at scale 1 : 10,000 with subsequent crowding-in of flights over promising areas were carried out over a region of absolute elevation 1100-1600 m and relative elevation 300-500 m. The region is covered with dense softwood stands. Because the conifers are grouped together in clumps, the relative amount of barren exposed land is favorable.

A hydrothermal uraniferous deposit consisting of four patches 500 by 300 m in area was detected in ground sorties. Over three of these patches, mineralization was in the form of veins, the fourth being a bedded structure. The area of the active patches was found to be 150, 800, and 4,000 m^2 according to an isogamma of 300 μr/hr (outcroppings and ore dumps). The activity of discrete ore blocks and ore lumps exceeded 10,000 μr/hr.

In the surveying flight carried out crosswise (AN-2 aircraft with SGM-10 equipment, at flight altitude 70-80 m) over the breadth of the ore structures, not one of these patches was located by air. Several flights coming in from different directions directly over the centers of the ore sectors also yielded negative results.

Calculations by R. M. Kogan (using a transparent overlay with divisions by squares), where the screening ability of spruce wood was taken into account, indicate that the mean intensity required for a confident location of ore zones No. 1 and No. 3 (in Fig. 2) from the air comes to 1450 and 8000 μr/hr, respectively. Since the intensity actually ranged 300-500 μr/hr, it is understandable that the anomaly escaped detection.

3. In aerial γ-ray surveys on a 1 : 25,000 scale over a wooden region structured of Precambrian gneisses and paleozoic intrusives with an increased clarke of uranium (background of 15-40 μr/hr at ground level, 6-7 μr/hr from the air), a grouping of narrow local anomalies of 12-15 μr/hr intensity was detected. Photographs of the anomalous areas were used to interpret the phenomenon. All of the anomalies were located near forest clearings and cuttings or thinnings with 200-400 m drift on the course (due to instrument inertia), and were due to absence of the forest screen. Verification by a ground sortie proved the anomaly to be barren of ores.

As an example, we furnish in the accompanying table the results of the calculation of γ-radiation absorption by the forestal flora present. Reference data characterizing the volume and weight of the timber mass, the number of trees per hectare, etc. were used in the calculations [1, 2, 4]. The screening effect of deadwood, windfallen trees, and shrub undergrowth is left out of account. The pronounced anisotropy of the medium, due to the distribution pattern of the tree trunks, is also neglected. In calculating the distributed density of the timber for several regions, the wood mass of the trunks may even be ignored, preference being given to calculations of the more evenly distributed mass of tree crowns, needles and cones, and forest floor, which contribute 30-60% of the total mass.

Even when the corrective factors mentioned above (0.3-0.6) are introduced, the density of the timber screen remains high for particular timber age groups, and and the percentage absorption of γ radiation will fluctuate from 25% to 60%, which may lead in the case of airborne surveys over wooded regions to the failure to locate ore bodies of industrial interest.

LITERATURE CITED

1. N. F. Lyashenko, Lumber and Logging Handbook [in Russian] (Izd. Akad. Arkhitektury Ukr SSSR, Kiev, 1955) pp. 32, 68.
2. Forester's Handbook [in Russian] (Izd. AN Belorus. SSR, Minsk, 1954) p. 180.
3. Radiometry Handbook, edited by V. I. Baranov (Gosgeoltekhizdat, Moscow, 1957) pp. 111, 184.
4. G. F. Morozov, Lectures on the Forest [in Russian] Izd. Goslesbumizdat, Moscow-Leningrad, 1949) Vol. 7.

* * *

ON THE ACCURACY OF CALCULATION OF THE BUILD-UP FACTOR FOR γ RAYS IN THIN ABSORBING AND SCATTERING MEDIA

A. V. Bibergal' and N. I. Leshchinskii

Translated from Atomnaya Énergiya, Vol. 8, No. 4, pp. 372-373, April, 1960
Original article submitted November 13, 1959

It is considered at the present time that the following is the most satisfactory formula for calculating the build-up factor for γ rays in absorbing and scattering media

$$B_0(h\nu, \mu_0 x, z) = A_1 e^{-\alpha_1 \mu_0 x} + A_2 e^{-\alpha_2 \mu_0 x}, \quad (1)$$

In this formula α_1, α_2, A_1, A_2 are coefficients which must be suitably chosen for different γ-ray energies ($h\nu$) and atomic numbers (z) of the absorbing and scattering media as shown in [1], μ_0 is the linear absorption coefficient for a narrow beam of γ rays in the given medium, and x is the thickness of the medium.

It was shown [2] that in the case of water, the use of Eq (1) in conjunction with the coefficients given in [1] leads to results which are in sufficiently good agreement with experimental data [2, 3] for Co^{60} γ-rays. However, for Cs^{137} γ-rays, calculations using the data reported in [1] lead to results which are much higher than the experimental results.

The figure shows plots of $f(x) = e^{-\mu_0 x} B(h\nu, \mu_0, x, z)$ calculated using Eq (1) with the coefficients as given in [1], and the data reported in [4, 5]. The latter papers report data on the attenuation of Co^{60} and Cs^{137} γ rays in water, aluminum, steel and lead. It is clear from the figure that for materials having high atomic numbers, the calculations lead to good agreement. For water, the agreement is good only for $x > 60$ cm. For $x < 60$ cm, the values of $f(x)$ calculated from Eq. (1) (dotted curves) are considerably higher, particularly for Cs^{137}, than those determined from the data reported in [4, 5].

The reason for the discrepancy between the data taken from [1] and the experimental data for thin layers with low atomic numbers is the incorrect choice of the coefficients in Eq. 1. This is due to the fact that these coefficients were originally chosen for use with relatively thick layers of screening materials.

In calculations of the attenuation of Cs^{137} γ-rays in thin layers and, in particular, in the calculation of the radiation fields due to high-activity sources, it is convenient to use the data reported [2], or to calculate $f(x)$ on the basis of the results given in [6] which lead to agreement with experiment to within ±5%. Equation 1 can also be used provided the coefficients are chosen so that the formula applies to thin media.

Direct calculations based on [4, 5] are very complex, although they do lead to good agreement with experiment.

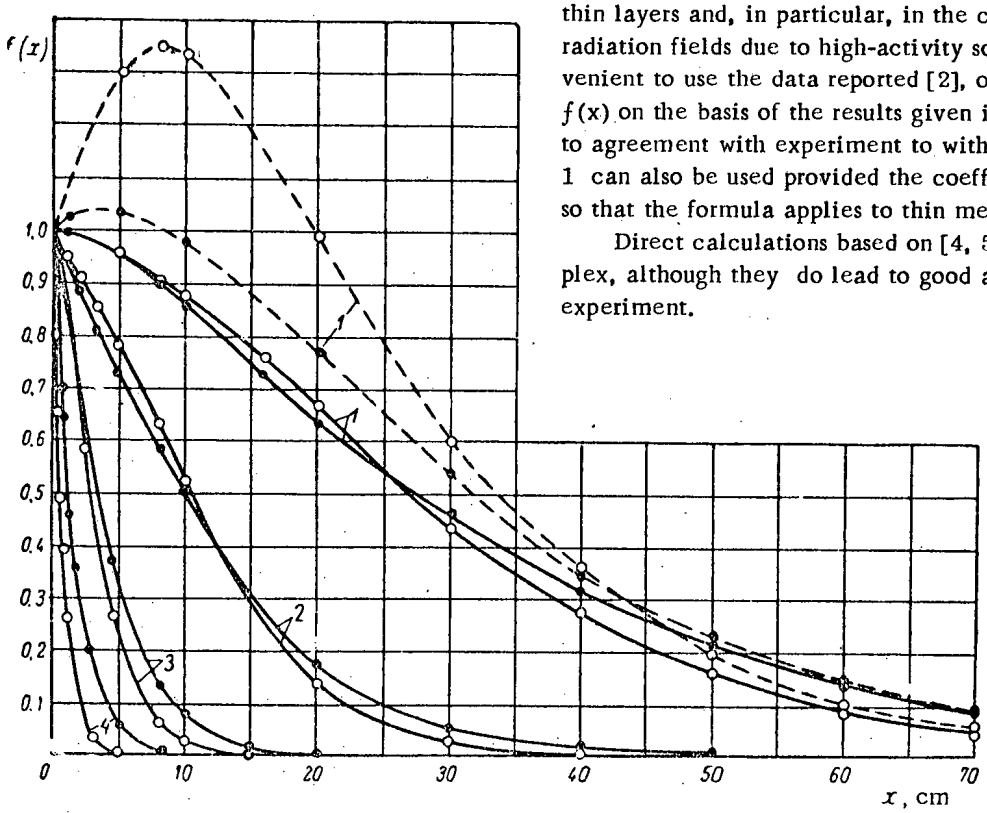

Attenuation of radiation due to absorption and scattering in a medium. 1) Water; 2) aluminum; 3) steel; 4) lead; (– – – – – – calculation on the basis of Eq. (1) and the data of [1]; ——— calculation on the basis of [4, 5]; O – Co^{60}; ●) Cs^{137}.

LITERATURE CITED

1. T. Rockwell (ed.), Reactor Shielding Design Manual [Russian translation] (IL, 1958) p. 300.
2. A. V. Bibergal', M. M. Korotkov and I. G. Ratner, Atomnaya Énerg. 7, 3, 244 (1959).*
3. G. White, Phys. Rev. 80, 2, 154 (1950).
4. U. Fano, Nucleonics 11, 53 (1950).
5. C. Davisson and R. Evans, Rev. Mod. Phys. 24, 79 (1952).
6. N. I. Leshchinskii, Atomnaya Énerg. 8, 1, 62 (1960).*

* Original Russian pagination. See C. B. translation.

* * *

RADIATION FIELD DUE TO A CYLINDRICAL SOURCE PLACED BEHIND A PLANE SCREEN

D. P. Osanov and E. E. Kovalev

Translated from Atomnaya Energiya, Vol. 8, No. 4, pp. 374-376, April, 1960
Original article submitted August 5, 1959

Usually, the derivation of equations describing the absorption of γ rays emitted by a cylindrical source is based on the replacement of the complex source by a simpler one. Clearly, such a replacement cannot be of universal validity.

The absorption of γ-rays leaving a cylinder in the radial direction can be treated as follows. The dose rate at the point A (Fig. 1) is given by

$$P = 2P_\gamma qR \int_0^k dn \int_0^1 m\,dm \int_0^\pi \frac{d\varphi}{m^2 + n^2 + p^2 - 2mp\cos\varphi} \times$$

$$\times e^{-\sqrt{m^2+p^2+n^2-2mp\cos\varphi}\left(\mu_1 R \frac{m^2 - mp\cos\varphi + \sqrt{m^2+p^2-2mp\cos\varphi - m^2p^2\sin^2\varphi}}{m^2+p^2-2mp\cos\varphi} + \frac{\mu_2 d}{p - m\cos\varphi}\right)} = \quad (1)$$

$$= 2P_\gamma qRS\,(p,\ k,\ \mu_1 R,\ \mu_2 d).$$

In this expression $z = nR$, $\rho = mR$, φ is the integration variable in a cylindrical system of coordinates with the 0, P_γ is the γ-constant, λ is the specific activity, μ_1 and μ_2 are the absorption coefficients in the source and the screen respectively, $k = H/R$ and $p = b/R$.

The above expression is based on the assumption that the radioactive material is distributed uniformly through the cylinder, and the γ rays emitted by the elementary sources are isotropic and monochromatic.

Mathematically, the problem is reduced to the evaluation of the integral $S(s, k, \mu_1, R, \mu_2 d)$ over the volume of a right-circular cylinder. This integral cannot be expressed in terms of elementary functions, and hence it was evaluated with the aid of the electronic computer "Strela". In most cases the total computational error did not exceed 2%. The computations were carried out for the following values of the parameters: $1.25 \le p \le 10$; $0.5 \le k \le 10$; $0 \le \mu_1 R \le 10$ and $0.5 \le \mu_2 d \le 10$. The total number of computer values of the integral $S(p, k, \mu_1 R, \mu_2 d)$ was more than 4300. Some of them are given in the table.

Comparison of our results with the data reported in [1] shows that the latter results are too high by up to 100% or more for large thicknesses of the screen.

This is of particular importance when the weight and size of the screen, or economic considerations, are

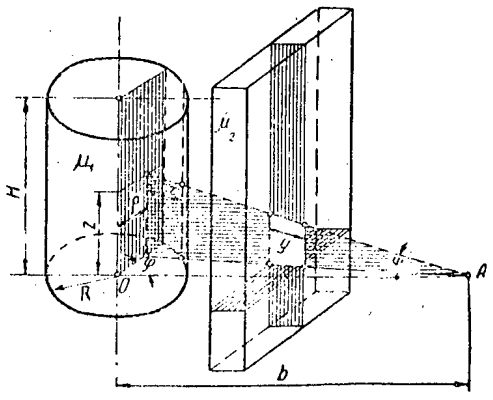

Fig. 1. Calculation of the γ-radiation field due to a cylindrical source behind a plane screen.

The values of the integral $S(p, k, \mu_1 R, \mu_2 d)$ for $\mu_1 R = 1$.

p	Magnitude of $\mu_2 d$						
	0.5	1	2	3	5	7	10
				$k=0,5$			
1,5	$1.38 \cdot 10^{-1}$	$7.84 \cdot 10^{-2}$	$2.5 \cdot 10^{-2}$	$8.41 \cdot 10^{-3}$	$9.30 \cdot 10^{-4}$	$1.05 \cdot 10^{-4}$	$4.18 \cdot 10^{-5}$
2	$7.06 \cdot 10^{-2}$	$4.16 \cdot 10^{-2}$	$1.45 \cdot 10^{-2}$	$5.04 \cdot 10^{-3}$	$6.14 \cdot 10^{-4}$	$7.53 \cdot 10^{-5}$	$3.27 \cdot 10^{-5}$
3	$2.89 \cdot 10^{-2}$	$1.73 \cdot 10^{-2}$	$6.23 \cdot 10^{-3}$	$2.24 \cdot 10^{-3}$	$2.90 \cdot 10^{-4}$	$3.77 \cdot 10^{-5}$	$1.76 \cdot 10^{-6}$
5	$9.84 \cdot 10^{-3}$	$5.95 \cdot 10^{-3}$	$2.17 \cdot 10^{-3}$	$7.93 \cdot 10^{-4}$	$1.06 \cdot 10^{-4}$	$1.41 \cdot 10^{-5}$	$6.86 \cdot 10^{-7}$
				$k=1,0$			
1,5	$2.14 \cdot 10^{-1}$	$1.17 \cdot 10^{-1}$	$3.60 \cdot 10^{-2}$	$1.13 \cdot 10^{-2}$	$1.17 \cdot 10^{-3}$	$1.27 \cdot 10^{-4}$	$4.83 \cdot 10^{-6}$
2	$1.24 \cdot 10^{-1}$	$7.15 \cdot 10^{-1}$	$2.39 \cdot 10^{-2}$	$8.02 \cdot 10^{-3}$	$9.17 \cdot 10^{-4}$	$1.07 \cdot 10^{-4}$	$4.36 \cdot 10^{-6}$
3	$5.49 \cdot 10^{-2}$	$3.26 \cdot 10^{-2}$	$1.15 \cdot 10^{-2}$	$4.08 \cdot 10^{-3}$	$5.13 \cdot 10^{-4}$	$6.46 \cdot 10^{-5}$	$2.90 \cdot 10^{-6}$
5	$1.94 \cdot 10^{-2}$	$1.17 \cdot 10^{-2}$	$4.23 \cdot 10^{-3}$	$1.54 \cdot 10^{-3}$	$2.03 \cdot 10^{-4}$	$2.67 \cdot 10^{-5}$	$1.28 \cdot 10^{-6}$

the decisive factors. On the other hand, for thin screens and sources with small self absorption, the data in [1] lead to results which are too low, and this in turn may lead to a serious underestimate of radiation hazards.

The above results were obtained without taking in into account multiple γ-ray scattering in the source and screen.

Multiple scattering of γ rays in extended sources cannot be rigorously taken into account. However, one can use approximate methods and estimate their accuracy by comparison with experimental data. The following method may be used in this way. Radiation produced as a result of scattering in the source is a small fraction of the total radiation after the screen, provided the screen is sufficiently thick. This is true when the primary radiation of the source is the most penetrating component. In such cases it is sufficient to take into account the scattering of the primary component in the screen in order to calculate the radiation dose after the screen. In order to simplify the calculation of the scattering, it is also convenient to introduce the equivalent absorption length in the screen $\mu_2 l$ for the γ radiation emitted by an extended source, which is defined by

$$\mu_2 l = \ln \frac{S(p, k, \mu_1 R, \mu_2 d = 0)}{S(p, k, \mu_1 R, \mu_2 d)}. \qquad (2)$$

The equivalent absorption length is defined as that thickness of the screen $\mu_2 l$ in which the absorption of γ radiation due to a point source is equivalent to the absorption of the γ radiation due to an extended source in a screen thickness $\mu_2 d$. The radiation dose due to a cylindrical source placed behind the screen can then be determined from the formula

$$P = 2P_\gamma q R S(p, k, \mu_1 R, \mu_2 d) B(\mu_2 l), \qquad (3)$$

where B is the dose build-up factor for a point source [2].

Figure 2 gives a comparison between the calculated and the experimental attenuations of γ radiation in a cyclindrical source of lead and iron as a function of $\mu_2 d$ (R – radius of the cylinder, b – distance from the center of the cylinder to the point at which the radiation is observed).

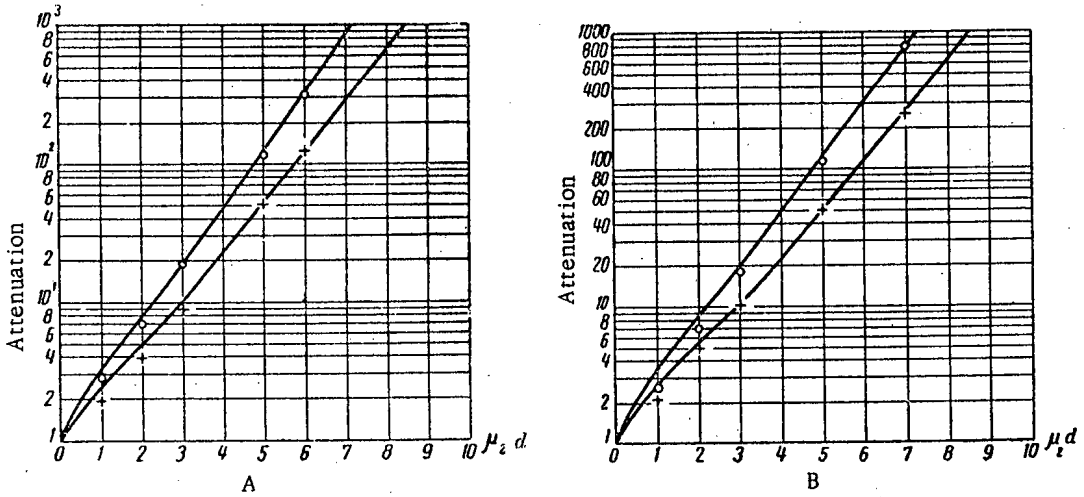

Fig. 2. Comparison of calculated and experimental attenuations for cylindrical sources. A – R = 25. b = 75 cm; B – R = 50, b = 150 cm; measured values: O) lead; +) iron. Both curves are theoretical.

In the experimental part, the sources were in the form of water solutions of cobalt sulfate. The theoretical curves were obtained by the method described above. Both the experimental and the theoretical attenuations were calculated using the experimental values for the γ-ray yield. As can be seen, calculations based on Eq. (3) give an entirely satisfactory agreement with experiments for $\mu_2 d \geq 2$-2.5. The following conclusions can be drawn on the basis of this result:

1) Radiation produced as a result of multiple scattering in the source for $\mu_2 d \geq 2$-2.5 is, in practice, a small fraction of the total radiation after the screen.

2) The radiation dose corrected for multiple scattering in the screen may be calculated using the equivalent absorption length and the dose build-up factors for a point source.

3) The maximum difference between the calculated and the experimental results for $\mu_2 d < 2$ to 2.5 does not exceed 30%.

It should be emphasized that in our experiments we used the strongest-scattering medium, i.e., a water solution of cobalt sulfate. Clearly, in all other cases the effect of multiple scattering in the source will be even smaller.

LITERATURE CITED

1. T. Rockwell (ed.), Reactor Shielding Design Manual [Russian translation] (IL, 1958).
2. H. Goldstein and J. Wilkins, "Calculation of the penetration of gamma rays" US AEC, Report NYO-3075 (1954).

* * *

AN INVESTIGATION OF CERTAIN ARTIFICIALLY RADIOACTIVE ISOTOPES AND THEIR USE IN MEDICAL γ RADIOGRAPHY

I. A. Bochvar, V. E. Busygin, and U. Ya. Margulis

Translated from Atomnaya Energiya, Vol. 8, No. 4, pp. 376-377, April, 1960
Original article submitted July 18, 1959

Among the artificially radioactive isotopes known at the present time, the most suitable for medical γ radiography (both as regards the spectrum of the γ radiation and the half-life) are the isotopes Tu^{170} and Eu^{155} It has been suggested in the literature [1] that the bremsstrahlung radiation of Sr^{90}– Y^{90} could be used for this purpose.

It is already possible to obtain Tu^{170} sources and most attention is therefore devoted to this isotope. Moreover, certain comparative characteristics of Eu^{155} and Sr^{90}– Y^{90} have been obtained. Since the γ ray yield from Tu^{170} is not more than 3%, and the maximum energy of Tu^{170} β-particles is 0.968 Mev, the bremsstrahlung radiation should play an important role. It is therefore useful to investigate the spectrum of Tu^{170} radiation and estimate the dose output of the different components in the spectrum.*

Figure 1 shows the spectrum of Tu^{170} radiation obtained experimentally at the end of a cylindrical source 0.7 cm in diameter and 1.4 g/cm^2 thick. The active specimen was contained in an aluminum filter 1.3 mm thick which completely absorbed Tu^{170} β rays.

Experiments show that the radiation dose due to the soft component of the spectrum (0.03-0.1 Mev), which is the most important for medical γ radiography, constitutes 41.4% of the total dose. The hard compoent of the spectrum gives rise to a deterioration in the quality of the image and the resolution. It must, however, be remembered that as the thickness of the object examined by γ radiation increases, the fraction of hard radiation reaching the film will also increase, so that the image contrast will be reduced. The Eu^{155} isotope is more convenient from this point of view, since its γ-ray spectrum is contained in the energy interval 0.06-0.132 Mev, and the output of bremsstrahlung radiation is negligible. The maximum energy of the latter does not exceed 0.25 Mev.

Comparison of γ-constants, which are equal to 0.045 r/hr for Tu^{170} [2] and 0.51 r/hr for Eu^{155} [3], shows that the radiation dose produced by 1 C of Eu^{155} is higher by a factor of 11.3 than the dose due to Tu^{170}.

The maximum energy of Sr^{90}– Y^{90} bremsstrahlung radiation is 2.2 Mev (with a maximum at about 0.074 Mev) when the source is surrounded by a lead filter 0.1 mm thick. Calculations show [4] that the dose rate

*Spectral analysis of Tu^{170} was carried out in collaboration with I. E. Konstantinov.

due to the bremsstrahlung is approximately 0.02 r/hr per 1 μC at a distance of 1 cm from the source. Thus, $Sr^{90} - Y^{90}$ is inferior to Eu^{155} and Tu^{170}, both as regards the spectrum of the radiation and the output.

In order to determine the possibility of detection of bone defects in the presence of foreign inclusions, use was made of aluminum dummies of various forms which imitated the bone. These were placed between perspex plates of various thickness (10-160 mm). The photographs were taken on Agfa films using standard medical intensifying screens (focal distance F = 45 cm).

These experiments show that in Tu^{170} and Eu^{155} γ radiography it is possible to detect metallic inclusions of 1 x 1 x 1 mm, located in the middle of a 160 mm thick phantom, and also cracks in bone structures of objects up to 160 mm thick, provided the width of the cracks is not less than 0.6 mm and their depth is 5 mm. Finer cracks (0.3 mm wide) can be detected for thicknesses not exceeding 80 mm.

It should be noted that the quality of photographs obtained with $Sr^{90} - Y^{90}$ is worse than in the case of Tu^{170} and Eu^{155}. The contrast of the image for Eu^{155} and Tu^{170} is roughly the same, although in the case of Eu^{155} the photographs are slightly clearer.

Although the use of Tu^{170} and Eu^{155} isotopes leads to satisfactory results as far as detectability of bone structure defect is concerned, the exposure time requires further consideration. Experiments show that in order to obtain photographs of the elbow joint, the hip, or the spine, the exposure time for a Tu^{170} source equivalent to 1 g Ra is 2-3 min, while for the wrist it is about 24 sec (the photographs were obtained on Agfa films with standard intensifying screens). In the case of photographs of bony tissues, exposures of the order of 15-20 sec may be acceptable in medical practice. It is therefore, necessary to reduce the above exposure time by a factor of at least 10 to 15.

Two methods are known for reducing the exposure time. They are: 1) use of more sensitive films and intensifying screens, and 2) higher source activity. By increasing the sensitivity of the film and of the intensifying screens, the exposure time may be reduced by a factor of 2 or 3. It follows that in order to produce a practical Tu^{170} source which could be used in medical γ radiography, it is necessary to use activities equivalent to 5-6 g Ra (1000-1200 C). The activity of the source should be increased by increasing the specific activity, since the dimensions of the source cannot be made too large owing to self-absorption.

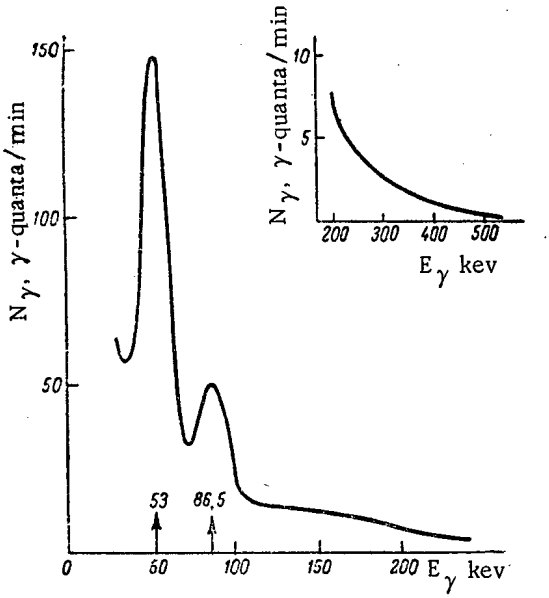

Fig. 1. Spectral distribution of characteristic bremsstrahlung and γ-radiations of a Tu^{170} source 1.4 g/cm^2 thick.

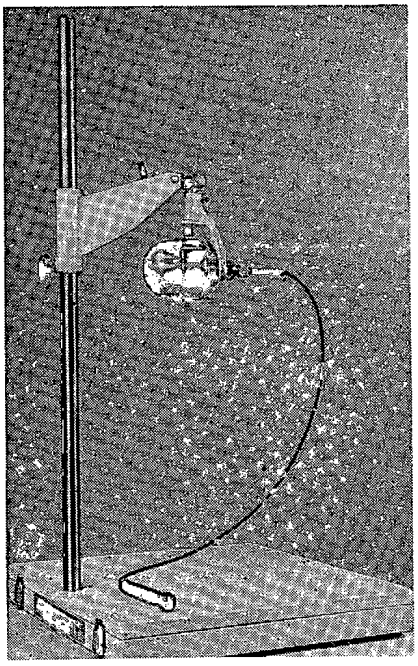

Fig. 2. Photograph of the portable source designed for γ radiography.

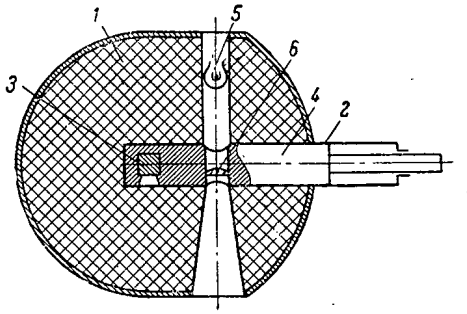

Fig. 3. Design of the source: 1) lead block contained in a duralumin jacket, 2) brass tube, 3) Tu^{170} source, 4) rod for displacing the source, 5) electrical lamp, 6) lens for projecting the image of the lamp filament on the object.

The exposure time for Eu^{155} (recalculated for a 1 g-eq Ra source) is approximately four times smaller than for Tu^{170} in the case of thin objects (wrist) and 1.5 times smaller in the case of relatively thick objects (hip, shoulder).

For Sr^{90} – Y^{90} the exposure time recalculated for a source of 1 g-eq Ra is greater by a factor fof 4-12 than for Tu^{170} and 16-17 than for Eu^{155}. Bearing in mind the poor quality of the image, and also the difficulties in obtaining high specific activity Sr^{90} – Y^{90} sources, it is clear that Sr^{90} – Y^{90} is not a convenient source of bremsstrahlung radiation for the purposes of medical γ-radiography.

The apparatus whose photograph shown in Fig. 2 was designed for γ radiography under field conditions. Its weight is 23 kg.

Figure 3 shows the design of the source. The device is based on the displacement of the source of radiation into the channel for the time of the exposure.

The experimental radioactive specimen of Tu^{170} was was designed to have a strength of 250 mg-eq Ra.

In the shielded position the thickness of the screen on the side of the adjusting device is 7 cm, and on the opposite side 5 cm. Calculations show that a 6.5 cm lead screen for the above source reduces the dose rate at the surface of the unit to the maximum permissible. For a lead screen 5 cm thick, one tolerance dose is produced at a distance of 17-20 cm from the surface.

Operation of the unit under laboratory conditions showed that it is entirely satisfactory and safe.

LITERATURE CITED

1. L. Reiffel, Nucleonics 13, 3, 22 (1955).
2. R. West, Nucleonics 11, No. 2, 20 (1953).
3. N. G. Gusev, Radioactivity and Shielding Manual [in Russian] (Medgiz, 1956).
4. I. A. Bochvar and U. Ya. Margulis, Med. Radiologiya, 2, 70 (1957).

* * *

TENTH ALL-UNION CONFERENCE ON NUCLEAR SPECTROSCOPY

The Tenth All-Union (annual) Conference on Nuclear Spectroscopy met January 19-27, 1960, at Moscow State University.

Nine years ago, at the First All-Union Conference on Nuclear Spectroscopy, which also took place in Moscow, 12 reporters faced an audience of seventy. In this year's gathering, over 400 were in attendance to hear over 180 papers read.

The scope of the topics discussed has been greatly expanded: the reports delivered at the Conference dealt with theoretical and experimental research on the widest range of problems in nuclear structure.

Beta decay. The overall problem of β decay was discussed in a review paper presented by V. A. Lyubimov (Institute of Theoretical and Experimental Physics of the USSR Academy of Sciences) taking up advanced problems in β decay and formulating the problems now being tackled by experimental physicists. A report delivered by Ya. A. Smorodinskii (Atomic Energy Institute of the USSR Academy of Sciences) touched on questions related to the value of the constant of universal four-fermion interaction. Experimental data showed that the values of this constant as found from μ-meson decay and from β decay, are slightly different. This circumstance may be fraught with great significance in probing β interactions.

The experimental papers dealing with β decay may be sorted out into two groups.

The first includes papers dealing with the study of β-γ-polarization correlations, circular polarization of internal bremsstrahlung, etc. All of these papers have something in common: the idea of finding experimental conditions such that the chief aspects of β decay would come through with particular clarity.

The second group of papers would include papers by P. E. Spivak and L. A. Mikaélyan (Atomic Energy Institute of the USSR Academy of Sciences) on measurement of the degree of longitudinal polarization of electrons in β decay, and a paper by Ch'ing Ch'eng-ju and L. S. Novikov (Nuclear Physics Research Institute (NIIYaF), Moscow State University) on a study of the shape of the β spectrum of P^{32}. These papers were devoted to various aspects of decay problems, but are united by a common tendency, an effort to improve on precision in measurements. At the present stage, this is an urgent requirement for further development of β decay theory.

To date, the prevailing opinion has held that polarization of electrons for all radioactive isotopes is equal to v/c, the quantity predicted by theory. The sole exception, firmly established in experimental work, is Ra ϵ, where a special explanation was devised for the discrepancy.

Experiments conducted by Spivak with increased precision have however demonstrated that polarization of electrons in P^{32}, In^{114}, Sm^{153}, Lu^{177}, Au^{198}, and Ho^{166} is different in each particular case, with the differences sometimes reaching 10%. The maximum polarization, (96 ± 4)% of v/c, was found for P^{32}.

These experiments thus showed that the deviation of the observed polarization from the value of v/c is more likely a general rule than an exception, a fact which calls for some explanation.

The paper presented by Ch'ing Ch'ĕng-ju and L.S. Novikov was devoted to careful research on the form of the P^{32} β spectrum. On the basis of the Gell-Mann hypothesis, some weak magnetism should be expected to appear in all weak interactions, leading to a deviation from the allowed shape of β spectra in nuclei with low Z and high energy of decay. With this in mind, the authors studied the forms of the β spectrum of P^{32}, where this effect is expected, and those of the β spectrum of In^{114}, where it is ruled out theoretically. Measurements performed on a double-focusing β spectrometer showed the Curie plot of the β decay spectrum of P^{32} in the 1000-1700 kev energy region to be 3-5% off linearity, which was not the case for In^{114}.

Nuclear reactions. Inelastic scattering of protons of of 6.8 Mev energy by chromium and nickel nuclei with excitation of levels of 1-1.5 Mev energy was investigated in the laboratory of M. V. Pasechnik (Institute of Physics of the USSR Academy of Sciences). The angular distributions demonstrated that, in the energy region of interest, the mechanism of formation of the compound nucleus plays the principal role in the process of inelastic scattering.

Many papers were presented by the laboratory headed by A. K. Val'ter (Physics and Engineering Institute (FTI) of the Academy of Sciences of the Ukrainian SSR Kharkov). A number of levels were established for the Na^{21}, Cl^{35}, and K^{41} nuclei, in studies reported on reactions of the (p, γ) type.

A highly interesting paper representing work done at the laboratory of N. A. Vlasov (Atomic Energy Institute of the USSR Academy of Sciences) discussed research on the (d, t) reaction for several light, intermediate, and heavy nuclei. In this reaction, a neutron is removed from the nucleus and the neutron binding energy is learned from the energy of the triton. By re-

moving neutrons of different binding energies from the nucleus, a clear picture may be had of the neutron shells in the nucleus.

Several of the sessions of the Conference were devoted to the nuclear spectroscopy of light, intermediate, and heavy nuclei. A large amount of experimental material has been accumulated in this area during the past year, existing decay schemes have been brought up to date and new decay schemes have been compiled for a broad selection of radioactive nuclides.

Quite a few papers appeared on research dealing with the neutron-deficient isotopes of osmium, platinum, and iridium, authored by the team working under A. V. Lavrukhina and T. V. Malysheva (GEOKhI, Geochemical Institute of the Academy of Sciences of the USSR, and Joint Institute for Nuclear Research). The combined effort of these chemsts and physicists bore fruit in the discovery of two new isotopes: Ir^{184} and Pt^{187}.

Theory of deformed nuclei. A review article on this topic was presented by A. S. Davydov.

Developing further the theory of the existence of nonaxial deformed nuclei, A. S. Davydov and G. F. Filippov (Moscow State University) extended the theory to odd nuclei. A comparison of the conclusions derived from the theory of nonaxial even nuclei with experimental results, effected by E. P. Grigor'ev and M. P. Avotina (Leningrad State University), led these workers to the conclusion that the consequences of this theory are not at variance with experimental data. Still other new facts and correlations of data are required if the existence of nonaxial nuclei is to be considered proven.

Over 10 papers were devoted to various problems in the theory of axial nuclei.

Neutron-deficient isotopes of the rare earths. This year saw a sizable number of papers presented on neutron-deficient isotopes. This field of work was discussed by researchers from 11 institutes: Joint Institute for Nuclear Research, eight other institutes in the Soviet Union, and corresponding bodies in Poland and Czechoslovakia. Some 50 papers representing original research, and 8 review papers were read. B. S. Dzhelepov delivered some introductory remarks constituting a survey of the results obtained in this area of work. He noted that, as a result of the combined efforts and creative cooperation of chemists and physicists in this field of spectroscopy, much new work had been successfully performed. Spectroscopists have penetrated into the region of remote neutron-deficient nuclei, have discovered several new isotopes: Ho^{155}, Ho^{158}, Er^{158}, Th^{150}, etc. An enormous amount of new experimental material, which introduced substantial changes in previously established decay schemes, was accumulated.

Gamma-ray Processes. Among the papers devoted to the study of γ-ray processes, we should like to note the experiments conducted by the group under D. G. Alkhazov and I. Kh. Lemberg (Leningrad Physics and Engineering Institute (LFTI) of the USSR Academy of Sciences) on coulombic excitation of nuclei of heavy ions. The most interesting aspect of these experiments was the observation of cascade excitation of nuclear levels. In investigations of the spectra of γ photons emitted in response to bombardment of the already separated isotopes W^{182}, W^{184}, W^{186} by Ne^{20} ions accelerated to an energy of 27.8 Mev, γ lines corresponding to the transitions from the second excited levels with spin 4+ to the first excited levels with spin 2+ were observed. Since there is very low probability of direct excitation of levels with spin 4+ in even-even nuclei, it is obvious that the observed exitation had to be the result of a cascade process. In this process, excitation of the level with spin 4+ takes place as a result of an initial electric quadrupole transition to the level with spin 2+, with a subsequent transition from that level to the level with spin 4+.

Some highly intriguing and promising experiments on resonance scattering of γ rays were explained by A. I. Alikhanov and V. A. Lyubimov (Institute of Theoretical and Experimental Physics of the USSR Academy of Sciences). They performed some experiments similar to the Mössbauer experiments on resonance scattering of γ rays, working with the nuclide Sn^{119} at the temperature of liquid nitrogen.

The effect of the appearance of an undisplaced line ($h\nu$ = 23.8 kev) observed by the authors was expressed much more sharply than in the Mössbauer experiments dealing with the γ emission of Ir^{191} ($h\nu$ = = 129 kev). The width of the resonance line was $\sim 5 \cdot 10^{-8}$ ev, i.e., approximately 130 times narrower than the line width observed in the Mössbauer experiment. The authors detected a considerable influence exerted by microscopic motions of the source, due to vibration and noise, on line intensity. They also observed a decline in the intensity of the resonance line as the source was placed in a magnetic field, the decline being due to Zeeman splitting of nuclear levels in lead. According to preliminary measurements, the magnetic moment of the first excited level of Sn^{119m} does not exceed 0.8 of the Bohr magneton.

A research paper on γ emission in E0-transition, delivered by V. A. Krutov (of Leningrad State University) aroused much interest. Nuclear transitions of the type $0_{\pm} \rightarrow 0_{\pm}$ are viewed as radiationless. It is shown in this paper that electrons belonging to a shell or to the electron background lead to a possible single-photon deexcitation of the excited state of the nucleus. In the process, the atom emits γ protons of multipole order M1. The author derived formulas for the ratio of the number of γ-photons emitted in an E0-transition to the number of internal-conversion electrons or conversion pairs (inverse conversion coefficient).

Calculations demonstrated that, for known E0 transitions in light and intermediate nuclei (C^{12}, O^{16},

Ca^{40}), the inverse conversion coefficient is, by order of magnitude, 10^{-4}–10^{-5}.

Techniques in nuclear spectroscopy. Many of the papers read at the sessions devoted to α, β, and γ-spectroscopy discussed new spectrometer designs. The most interesting newcomers this year were two new instruments with excellent spectral characteristics.

One was a large prismatic β spectrometer designed by V. M. Kel'man, B. P. Pereguda, and V. I. Skopina (of the Leningrad Physics and Engineering Institute), and capable of achieving a resolution of from 0.013 to 0.15% at a transmission of from 0.005 to 0.8%, respectively. The instrument employs a magnetic prism and a lens of new design. Control of the spectrometer and recording of measurement results are automatic.

The other was a high-resolution magnetic γ spectrometer designed by L. V. Groshev, A. M. Demidov, V. N. Lutsenko, and A. F. Malov (of the Atomic Energy Institute). The spectrometer is an improved Compton spectrometer with 0.23% resolution at energy E_γ = 1 Mev. This spectrometer can be used to measure the spectrum of γ rays accompanying the capture of thermal neutrons by chlorine. The measurements were performed over the range of energies extending from 0.3 to 9 Mev.

In his concluding remarks, B. S. Dzhelepov drew attention to the fundamental successes achieved in nuclear spectroscopy during the past year.

The proceedings of the conference will appear in the journal "Izvest. Akad. Nauk SSSR, Ser. Fiz." during 1960, viz., in numbers 3, 7, 9, and 10.

O. Kraft

* * *

AT THE INSTITUTE OF PHYSICS OF THE ACADEMY OF SCIENCES OF THE UKRAINIAN SSR

(A conversation with the vice-director of the Institute of Physics in charge of scientific research, O. F. Nemets)

A 10,000 kw reactor, the VVR-M, was started up during February 1960, at the Institute of Physics of the Academy of Sciences of the UkrSSR. The following research projects will be carried out on this reactor:

1) a study of resonance scattering of slow neutrons by the time-of-flight technique (for which purpose a mechanical chopper and a 1024-channel time-of-flight analyzer were built). This research will be carried out by M. V. Pasechnik, V. P. Vertebny, and R. G. Ofengenden;

2) a study of the spectra of capture γ rays (for which purpose a wide-angle γ spectrometer with acceptance angle variable up to 80° has been built). This research will be carried out by M. V. Pasechnik and M. F. Barchuk;

3) study of the lifetimes of short-lived nuclides.

Besides the investigations enumerated above, work in radiation chemistry and radiation biology will be performed using this reactor.

Studies of angular distribution in stripping reactions, involving 11 isotopes, were carried out during 1959, using the cyclotron which has been in operation at the Institute since 1957. O. F. Nemets and N. I. Zaika, workers at the Institute, obtained values for energy levels, spin, and parity. The angular distributions of deuterons subjected to elastic and inelastic scattering were also obtained, as well as those for

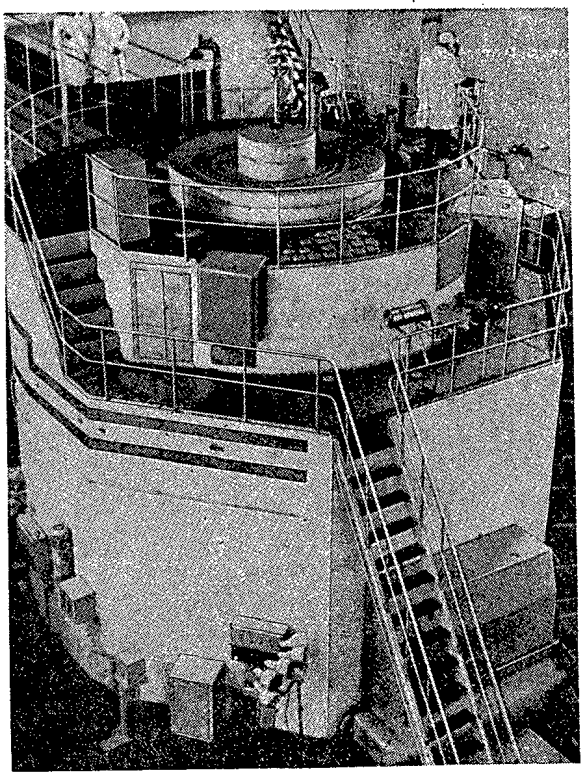

General view of the VVR-M reactor, 10,000 kw power, in use at the Institute of Physics of the Academy of Sciences of the UkrSSR.

deuterons and tritons derived from the (p, d) and (d, t) reactions. Conclusions were arrived at as to the mechanism involved in nuclear reactions. This work was conducted by O. F. Nemets, L. S. Saltykov, and M. V. Sokolov. The angular distributions of protons experiencing elastic and inelastic scattering were measured. A study of inelastic scattering on isotope targets Ni^{58}, Ni^{60}, Ni^{62} showed a sharp difference in the character of the angular distributions, which remained without explanation within the framework of the optical model. M. V. Pasechnik and N. N. Pucherov measured proton polarization in elastic scattering.

Plans for 1960 include extending these measurements. In addition to expanding the scope of research at the Institute, proton polarization in stripping reactions, angular (d, p) γ- correlations, and (d, n) and (d, α) reactions will be studied. The necessary equipment and accessories for these tasks have been developed and partially checked out.

During 1959, V. I. Strizhak studied angular distributions of elastically scattered neutrons of 3 and 14 Mev energies, using an electrostatic generator and low-voltage neutron generators. This research is to be extended into 1960, as is work on neutron polarization.

Research on the theory of nuclear matter and nuclear dynamics has undergone further development. Collective excitations of nuclear matter have been s studied on the basis of the superconductivity theory of N. N. Bogolyubov. On the basis of the same theory, B. B. Dotsenko and Yu. V. Tsekhmistrenko calculated the energy of the ground state in elementary excitations of a superfluid nucleon gas.

A. M. Korolev has developed a theory of stripping reactions based on the unified model of the nucleus for even-even nuclei.

The design of various types of laboratory equipment is also conducted at the Institute. In particular, work is in progress on building a multichannel pulse-height analyzer incorporating a magnetic memory, on low-voltage neutron generators, a binary-to-decimal scaler, scintillation γ-spectrometers, a neutron spectrometer, and charged-particle spectrometers.

V. Parkhit'ko

* * *

BRIEF COMMUNICATIONS

Bulgaria. The Academy of Sciences is building a research center with a nuclear reactor of the IRT type, with the assistance of the Soviet Union. Neutron physics research will be conducted with the aid of this reactor.

East Germany. Agreements were reached at Berlin, in early February, between representatives of the German DemocraticRepublic and the Polish Peoples Republic, on the basis of the governmental agreement dating back to 1957, regarding further collaboration in the area of the peacetul uses of atomic energy. Talks ended up in the signing of a plan for collaboration between the two countries for 1960.

Czechoslovakia. The nation's first cyclotron went into operation on February 19. The materials and equipment for the machine were delivered by the Soviet Union. The Soviet Union also provided assistance in the assembly and adjustment operations. Scientific research work in nuclear physics and production of artificial radioactive isotopes will be carried out with the cyclotron.

Yugoslavia. An agreement was reached between the Yugoslav atomic energy commission and IAEA on staging a dosimetric experiment at the Boris Kidric Institute near Belgrade. The experiment will be set up to get an accurate determination of the doses of neutron and gamma irradiation received by workers of the Institute in the criticality accident on October 15, 1958, when the Institute's critical facility went out of control.

The experiment and preliminary steps will be supervised by IAEA, while the critical facility involved will be turned over by the Yugoslav commission. During the experiment, the critical facility will be brought up to criticality and operated at 5 watts power for 4 hours, and later at 500 watts power for 1 hour. Carefully controlled dosimetric measurements will be performed at the same time.

The experiment is slated for conclusion by the end of May 1960. Results will be made public later.

* * *

NEW LITERATURE

Books and Symposia

I. E. Starik, Elements of Radiochemistry [in Russian] (Izd. AN SSSR, Moscow-Leningrad, 1959) 459 pages. 21 rubles, 80 kopeks. Reviewed by T. V. Malysheva.

This book is of special interest, being written in the spirit of the founder of the Soviet school of radiochemistry, V. G. Khlopin, with the author a close collaborator and student of the former over the course of many years' work.

The monograph presents for the first time a systematic exposition of the laws of behavior of radioactive isotopes as the result of a study of the laws of behavior of matter in vanishingly small concentrations.

The author approaches radiochemistry as an independent scientific discipline, serving as a theoretical foundation for work on the uses of atomic energy and applications of radioactive isotopes as labeled atoms. Primary attention is accorded to the state of trace amounts of radioactive isotopes in liquid, gaseous, and solid phases. A systematic rundown is given of the distribution of trace amounts of radioactive isotopes in heterogeneous systems. A new classification is proposed for adsorptive processes affecting radioactive isotopes.

A special section is devoted to the electrochemistry of radioactive materials which are of prime importance both from the practical and the purely scientific point of view.

Each chapter ends with a copious literature reference related to the subject matter of the chapter.

The book will be of interest to research workers engaged in the field of radiochemistry and related areas of science, and may prove useful as a textbook or manual for undergraduate and graduate students.

Articles from the Periodical Literature

I. NUCLEAR POWER PHYSICS

Voprosy Istorii Estestvoznaniya i Tekhniki, No. 8 (1959).

A. A. Vorob'ev, pp. 33-47. From the history of the development of electron accelerators.

Voprosy Filosofii, No. 12 (1959).

I. V. Kuznetsov, I. S. Panasyuk, pp. 120-127. On the effect of external conditions on radioactive decay.

Doklady Akad. Nauk SSSR 129, No. 3 (1959).

A. G. Kulikovskii, G. A. Lyubimov, pp. 525-528. The simplest problems containing a shock wave ionizing a gas in an electromagnetic field.

Izvest. Akad. Nauk SSSR, Ser. Fiz. 23, No. 12 (1959)

S. A. Baranov, et al., pp. 1402-1410. A large double-focusing alpha spectrometer.

P. S. Samoilov, pp. 1416-1430. New data on decay of Am^{241}.

A. G. Berkovskii, et al., pp. 1517-1519. Some characteristics of new photomultiplier tubes.

Izvest. Vyssh. Ucheb. Zaved. Fizika, No. 6 (1959).

Yu. M. Akimov, pp. 3-4. Contribution to the problem of extraction of electrons from a betatron chamber by a method of asymmetrical displacement.

V. A. Moskalev, pp. 5-9. Design and magnetic characteristics of the double-chamber 10 Mev stereobetatron.

N. G. Preobrazhenskii, pp. 31-41. On the deformation of the shape of the spectral line emitted in a high-temperature optically dense plasma.

I. I. Murav'ev, pp. 71-75. Contribution to the problem of measuring electron temperature and relative concentration of electrons by the probe method and the optical method.

A. E. Glauberman, L. A. Porfir'eva, pp. 76-84. On higher approximations in a new form of "plasma" breakdowns.

E. S. Kovalenko, pp. 85-89. Synchrotron with a generalized high-frequency field.

E. N. Gagin, et al, pp. 95-101. Some problems related to the electrostatic Van de Graaff electron accelerator.

P. A. Ryazin, A. B. Minervin, pp. 112-123. Contribution to the study of electron capture in the accelerative cycle in betatrons and synchrotrons.

Yu. N. Lobanov, N. I. Tulinova, pp. 124-130. On some features of electron trapping and acceleration in the betatron.

M. D. Avramenko, pp. 131-134. Some factors affecting the intensity of gamma radiation from a betatron.

S. P. Kruglov, et al., pp. 139-144. The relation between the "roentgen" and the energy of gamma radiation incident upon a square centimeter.

Izvestiya Tomsk. Politekhn. Inst. 96, No. 1 (1959).

V. G. Stepanov, V. A. Kukhtin, pp. 119-129. An ion frequency converter for the betatron power supplies.

Pribor. i Tekh. Éksp. No. 6 (1959).

L. Paty, pp. 3-10. Measurement of a hard vacuum. I.

A. M. Grivor'ev, pp. 10-13. Manometers for measurement of a hard vacuum.

Yu. M. Goryachev, et al., pp. 13-17. Measurement of distortions in a magnetic field in accelerators with strong focusing.

I. N. Usova, pp. 17-19. On the accuracy of absolute measurements of beam intensity of photons from a synchrotron target by use of ionization chambers.

A. V. Antonov, et al., pp. 20-24. Automatic adjustment of reactance parameters of a cyclotron resonant system.

I. I. Afanas'ev, et al., pp. 25-27. An ion slit source for a cyclotron.

N. D. Fedorov, Yu. A. Kholmovskii, pp. 27-29. Measurement of beam width of ions in the vicinity of a cyclotron ion source.

I. A. Grishaev, et al., pp. 30-32. Measurement of phase width of electron bunches accelerated in a linear accelerator.

G. D. Kuleshov, A. I. Pavlovskii, pp. 119-120. A cold cathode in the injector serving a betatron.

Sbornik Nauchnykh. Trud. Tomsk. Inzhen.-Stroit. Inst. 5 (1959).

A. N. Vyal'tsev, pp. 141-150. Perspectives of the development of nuclear physics.

Atomwirtschaft IV, No. 12 (1959).

R. Häfer, and G. Zinsmeister, pp. 528-532. A vacuum system for the ring vacuum chamber of the 25 Bev synchrotron at CERN.

Brit. J. Appl. Phys. 10, No. 12 (1959).

J. Sisefsky, pp. 526-529. Photographic method for identification of microscopic radioactive particles.

Canad. J. Phys. 37, No. 12 (1959).

M. Sodha, pp. 1380-1383. Spectral distribution of bremsstrahlung from an ionized gas.

A. Baerg, et al., pp. 1418-1437. Angular distribution of photofission fragments.

L. Katz, pp. 1455-1464. Calibration of fission in a betatron.

Indian J. Phys. 42, No. 9 (1959).

A Ghosh, pp. 395-400. $\bar{\Gamma}^0 n/D$ for a complex potential with a diffusion boundary.

J. Appl. Phys. 30, No. 11 (1959).

M. Sakuntala, et al., pp. 1669-1671. Electromotive forces in a highly ionized gas moving in a magnetic field.

H. Lewis, J. Reitz, pp. 1838-1839. Open-circuit voltages in the plasma thermocouple.

Kernenergie 2, No. 12 (1959).

G. Flach, K. Müller, pp. 1068-1071. On the dynamic correction used in computing the internal conversion coefficient of gamma rays.

Nucl. Energy 14, No. 140 (1960).

---- pp. 14-19. A new neutron physics laboratory at Harwell.

Nucl. Inst. and Methods 6, No. 1 (1959).

R. Livingston, F. Howard, pp. 1-25. The Oak Ridge isochronous relativistic cyclotron (ORIC).

H. Morinaga, T. Kuroyanagi, pp. 66-71. Internal betatron target.

Nucl. Phys. 14, No. 1 (1959).

J. Leblanc, et al., pp. 120-130. On the distribution of the maximum of the neutron force function near A = 55.

Nukleonik 1, No. 9 (1959).

W. Manner, T. Springer, pp. 337-341. Measurements of resonance neutron flux through activation of probes.

A. Özemre, pp. 347-351. Neutron flux as a function of time, in the light of multigroup diffusion theory.

Nuovo Cimento XIV, No. 5 (1959)

T. Goto, et al., pp. 1065-1075. On the mechanism of the pinch effect.

V. Emma, C. Milone, pp. 1149-1156. Photoneutrons from potassium and calcium.

Physica 25, No. 11 (1959).

H. Brinkman, pp. 1063-1066. Turbulence equations of magnetohydrodynamics.

II. NUCLEAR POWER ENGINEERING

Trudy Inst. Fiz. Khim. Akad. Nauk SSSR, No. 5(1959).

A. V. Byalobzheskii, V. D. Val'kov, pp. 119-132. Techniques for corrosion studies and electrochemical research on metals in a flow of liquid exposed to ionizing radiations.

A. V. Byalobzheskii, pp. 133-138. An instrument for studying atmospheric corrosion of metals exposed to ionizing radiations.

Trudy Nauchno-Tekhn. Obshchestva Sudostroi. Prom. 8, No. 5 (1959).

N. A. Agafonov, pp. 81-93. Design plans for electric-power propulsion of the icebreaker "Lenin."

Atomkernenergie 4, No. 11 (1959).

K. Thielheim, pp. 429-437. Multiplication of fast neutrons in fuel elements of great thickness.

M. Angelopoulos, pp. 437-442. Determination of thermal utilization factor in a lattice cell.

E. Schröder, pp. 442-445. Calculation of temperature and mechanical stresses in shielding facilities of reactors.

W. Kattwinkel, pp. 446-449. Determination of specific activity of a liquid as a function of dose rate measured at the surface of cylindrical vessels or tubes.

E. Fitzer, et al., pp. 449-455. Development of graphite reactors in West Germany.

W. Braunbek, pp. 455-458. Methods of measurement in nuclear physics. XII.

Atomkernenergie 4, No. 12 (1959).

W. Balz, R. Schwarzwälder, pp. 469-473. Calculation of circulating flow for a boiling-water reactor.

H. Benzler, et al., pp. 473-476. Creation of optimum heat-transfer conditions in gas-cooled reactors.

W. Kliefoth, pp. 493-500. Laboratory and training reactors.

W. Braunbek, pp. 501-503. Methods of measurement in nuclear physics. XIII.

Atomwirtschaft IV, No. 11 (1959).

E. Kintner, pp. 463-467. History of the building of the prototype for the submarine-borne nuclear reactor on the "Nautilus."

H. Daldrup, pp. 468-471. The first nuclear-powered merchant ship, the "Savannah."

G. Hildenbrand, pp. 479-487. The Argonaut-type nuclear reactor.

G. Hildenbrand, pp. 487-490. The location site for the Argonaut-type nuclear reactor.

Atomwirtschaft IV, No. 12 (1959).

---- pp. 505-520. An economic review of the development of the nuclear power industry as of 1959.

G. Kourim, pp. 533-536. Effect of temperature on reactor dynamics.

Energia Nucl., No. 12 (1959).

A. Ascari, et al., pp. 753-762. Preparations for start-up of the "Avogadro RSI" reactor.

V. Svelto, pp. 763-767. Analog computers for reator installations.

Industries Atomiques III, No. 9-10 (1959).

R. Darras, pp. 41-61. Corrosion occurring in gas-cooled reactors.

Jaderná Energie 6, No. 1 (1960).

J. Teplý, K. Seidl, pp. 3-8. Organic moderators and coolants.

Nucl. Energy. 14, No. 140 (1959).

---- pp. 11-13. Improvement of a water-reactor system.

A. Bowden, J. Drumm, pp. 22-25, 43. Planning of large gas canals.

Nucl. Engng. 5, No. 44 (1959).

J. Allen, pp. 5-9. Experiments in releasing a reactor-multiplier in Downry.

R. Vaughan, pp. 10-13. Control of reactor during quick burn-out.

H. Burgess, pp. 14-18. Conference on Ship Atomic Installations.

Nucl. Power 5, No. 45 (1960).

---- pp. 82-95. Review of national programs for the development of nuclear power.

R. Guard, pp. 96-98. Progress in reactor design.

D. Newmarch, pp. 98-99. New techniques in reactor physics.

C. Steiner, pp. 108-110. Perspectives for the development of nuclear-powered vessels.

G. Ford, pp. 111-116. Evaulation of four types of power reactors.

G. Hall, pp. 118-121. Problems of criticality in the design of chemical facilities.

Nucleonics 18, No. 1 (1960).

R. Mesler, Rapid assessment of neutron activation.

E. Hughes, J. Greenwood, pp. 76-80. Contamination and cleanup of the NRU reactor.

A. Mooradian, et al., pp. 81-85. Waterlogging damage to NRU fuel elements.

P. Fortescue, et al., 86-90. Principles of HTGR reactor design.

R. Dickinson, pp. 107, 109-111. Coolant damage blocks SRE fuel.

Nukleonik 1, No. 9 (1959).

H. Smets, pp. 351-357. Variation in reactor power as a function of change in linear reactivity.

R. Sizmann, pp. 357-368. Fundamentals of physical effects of radiation on solids.

Nukleonika IV, No. 5 (1959) (Poland)

W. Frankowski, pp. 491-504. Choice of reactor characteristics for a materials testing reactor.

M. Krejci, et al., pp. 505-521. Use of analog simulators in nuclear reactor design. The simulating machine used at the Czech Nuclear Physics Institute.

W. Dabek, pp. 523-546. An integrating ionization chamber used for control of nuclear reactors.

III. NUCLEAR FUEL AND MATERIALS

Doklady Akad. Nauk SSSR 129, No. 4 (1959).

D. A. Mineev, N. I. Stupnikova, pp. 916-918. On the nature of the radioactivity of orthites and the ratio of uranium, thorium, and rare earths in them.

I. E. Starik, et al., pp. 919-921. Concentration of thorium isotopes in the waters of the Black Sea.

Zhur. Neorg. Khim. 4, No. 11 (1959).

V. M. Vdovenko, et al., pp. 2502-2504. Distribution of Cs, Ca, Sr, and La between an aqueous solution and methyl butylketone, in the presence of uranium.

E. P. Maiorova, V. V. Fomin, pp. 2511-2514. Effect of sulfate ions on the distribution coefficient of macroscopic amounts of thorium, in extraction using trybutyl phosphate.

A. E. Klygin, et al., pp. 2623-2629. Investigation of the system $UO_2(NO_3)_2$ – EDTA – water, by the solubility method.

Izvest. Akad. Nauk Kirgiz. SSR, Seriya Estestv. i Tekh. Nauk 1, No. 3 (1959).

P. I. Chalov, Ya. A. Musin, pp. 113-118. Radiometric assay of the content of uranium-238 and thorium 234 in solutions in the presence of other radioelements of the uranium series.

Ya. A. Musin, P. I. Chalov, pp. 119-125. Contribution to the problem of the use of gamma emission from decay products of radium, as tracers in the quantitative determination of uranium content in ores.

Trudy po Khimii i Khim. Tekhnol. (Gor'kii) 1 (1959).

P. I. Levin, et al., pp. 3-7. Labeled-atoms applications in investigations of the reversibility of polymerization of methyl methacrylate.

Uspekhi Khim. Nauk 28, No. 12 (1959).

V. V. Kozlov, S. I. Vol'fkovich, pp. 1403-1449. The eighth Mendeleevian congress on general and applied chemistry.

Atomkernenergie 4, No. 12 (1959).

E. Fitzer, et al., pp. 476-480. Development of graphitic materials for reactors in West Germany (II).

Atompraxis, 5, No. 12 (1959).

N. Getoff, pp. 472-474. Radiometric determination of hafnium content in zirconium.

Atomwirtschaft IV, No. 12 (1959).

A. Hofmann, et al., pp. 525-527. Ventilation system in the radiochemical laboratory of a lacquer and paint factory.

Energia Nucl. 6, No. 12 (1959).

E. Cerrai, C. Testa, pp. 768-780. Extraction and separation of zirconium and hafnium by the method of liquid anion exchange resins in hydrochloric acid. II.

A. Ascoli, et al., pp. 781-783. A simple method of crystal growing.

B. Brigoli, S. Villand, pp. 784-792. Preliminary calculations in design of a deuterium separation facility.

L. Damiani, V. Fattore, pp. 793-798. The nitric acid– water– tributyl phosphate equilibrium system.

Industries Atomiques III, No. 9-10 (1959).

E. de Chanvalon, pp. 71-77. Laboratories for research on spent fuel.

Jaderná Energie 5, No. 12 (1959).

J. Vrtěl, pp. 397-404. Problems concerning materials for high-pressure tanks in nuclear reactor plants.

Jaderná Energie 6, No. 1 (1960).

J. Vrtěl, pp. 9-15. Materials for reactor control rods.

J. Appl. Phys. 30, No. 11 (1959).

D. Kline, A. Jacobs, pp. 1741-1747. Calculation of the rate of energy deposition in polyethylene by reactor radiation.

R. Hall, et al., pp. 1846-1847. Annealing study on a pile-irradiated crystal.

J. Inorg. and Nucl. Chem. 11, No. 3 (1959).

A. Kjelberg, A. Pappas, pp. 173-180. Rapid radiochemical isolation of arsenic from fragments, and independent yield of As^{78} in fission of U^{235} by thermal neutrons.

R. Harder, S. Chaberek, pp. 197-209. Interaction of ions of rare-earth elements with diethylenetriaminepentaacetic acid.

J. Elving, A. Krivis, pp. 234-241. Polarographic reduction of U(VI) in the presence and absence of complexing reagents. The nature of the sulfate complexes of U(V).

G. Herrmann, H. Scherff, pp. 247-248. Isolation of Zr^{95} freed from Nb^{95}, by extraction with thenoyltrifluoracetone.

H. Arnikar, pp. 248-251. Isotope effect in electromigration of lithium ions in an agar-agar gel.

R. Gatti, et al., pp. 251-253. Ion-exchange properties of mendeleevium.

J. Inorg. and Nucl. Chem. 11, No. 4 (1959).

C. Goodall, R. Moore, pp. 290-296. Coprecipitation of protoactinium with dioxides of manganese, lead, and tin.

T. Smith, pp. 314-319. Effect of fluorine ions on complexing of U(IV) with EDTA.

P. de Maine, E. Koubek, pp. 329-336. Inorganic salts dissolved in nonaqueous or mixed solvents. I.

Kernenergie 2, No. 12 (1959).

M. Ardenne, et al., pp. 1094-1104. Spectra of inorganic substances as the basis for a mass scale, for use in high-frequency mass spectrographs working with polyatomic molecules.

H. Steinkopff, F. Thumler, pp. 1105-1114. Alloys and compounds of uranium and silicon.

M. Fodor, pp. 1115-1118. Use of the separation method with complexing and participation of ion exchange resins, in quantitative uranium determinations.

A. Schneer, pp. 1119-1121. Use of a volumetric analytical technique for zirconium determinations.

D. Naumann, S. Riedel, pp. 1122-1125. Enrichment of Fe^{59} from ferrocene and acetyl ferrocene, by the Szilard-Chalmers method.

R. Munze, K. Jantsch, pp. 1126-1130. Formation of Ca^{45} as a result of the reaction $Sc^{45}(n,p)Ca^{45}$. I. Determination of yield of Ca^{45} under different conditions of irradiation.

Nucl. Engng. 5, No. 44 (1959).

N. Eaton, pp. 19-22. Electron-beam welding.

N. Scarlett, J. Cliffe, pp. 23-26. Irradiation-resistant lubricants.

---- pp. 31-32. Industrial production of beryllium.

Nucl. Power 5, No. 45 (1960).

G. Hall, pp. 101-103. Process chemistry.

J. Ball, pp. 103-105. Nuclear fuels and materials.

Nukleonika IV, No. 5 (1959) (Poland)

S. Minc, L. Stolarczyk, pp. 473-485. Problems in the radiation chemistry of aqueous solutions.

W. Szarpaty, W. Orechow, pp. 487-489. On the radiolytic reduction of nitrates in hydrogen-saturated aqueous solutions.

Research 12, No. 12 (1960).

W. Groth, pp. 467-474. Gas centrifuges.

Z. Metallkunde 50, No. 12 (1959).

H. Schleicher, pp. 687-690. Effect of palladium additives on the corrosion of zirconium immersed in hot water.

IV, NUCLEAR RADIATION SHIELDING

Izvest. Akad. Nauk SSSR, Ser. Fiz. 23, No. 11 (1959).

T. V. Timofeeva, T. P. Khormushko, pp. 1283-1285. New data on a slow-neutron detector.

Izvest. Akad. Nauk UzbekSSR, Ser. Fiz.-Matem. Nauk, No. 5 (1959).

U. A. Arifov, et al., pp. 12-18. Investigation of the gamma-ray method for preserving silkworm cocoons.

Izmerital'naya Tekh., No. 12 (1959).

Z. P. Balon, et al., pp. 47-51. Calibration of gamma dosimeters in diaphragmed beams of gamma rays.

R. S. Belova, I. I. Yankovskii, pp. 51-52. Measurement of fast-neutron flux using a personal dosimeter.

Med. Radiologiya IV, No. 12 (1959).

M. P. Domshlak, et al., pp. 3-11. Problems in experimental techniques regarding radiation effects, and some radiobiological data.

O. S. Andreeva, pp. 59-63. Health-physics evaluation of working conditions in handling of certain radioactive minerals and ore samples.

Okhrana Trudy a Sots. Strakhovanie, No. 11 (1959).

A. Belyaev, pp. 16-18. At the Voronezh nuclear power station. (work safety survey).

Uspekhi Khim. Nauk 28, No. 12 (1959).

F. Yu. Rachinskii, et al., pp. 1488-1522. Chemical means of prophylaxis for acute radition sickness.

AMA Arch. Industr. Health, 20, No. 5 (1959).

W. Harris, et al., pp. 365-382. Danger of radioactive injury associated with handling of radioactive ores.

Atomkernenergie 4, No. 12 (1959).

R. Wagner, pp. 481-490. Use of electrostatic filters in the study of radioactive aerosols.

R. Reiter, pp. 490-492. Use of radioactivity of air, precipitates and water during floods in northern Alpine regions.

Atompraxis 5, No. 12 (1959).

F. Scholz, pp. 475-481. Mutations induced by ionizing radiations, and raising of agricultural crops.

Atomwirtschaft IV, No. 11 (1959).

H. Muth, pp. 491-494. International radiological congress at Munich.

Jaderná Energie 5, No. 12 (1959).

J. Beneš, et al., pp. 409-412. Nuclear emulsions for neutron dosimetry.

A. Eckardt, U. Heinecke, pp. 1072-1079. Study of the operation of counters for radioactive radiations.

Kernenergie 2, No. 12 (1959).

M. Leistner, K. Renker, pp. 1080-1089. An automatic device for the absolute determination of radioactivity by the technique of β-γ-coincidences, using GM counters.

K. Renker, H. Erler, pp. 1090-1093. A pulsed device used for measurements with the aid of a spark counter.

Nucl. Engng. 5, No. 44 (1959).

---- p. 27. Removal of radioactive wastes. (Short report on the Monaco conference).

Nucleonics 18, No. 1, (1960).

W. Goldsworthy, pp. 92-99. Transistorized portable counting-rate meter.

F. Domer, F. Hayes, p. 100. Background vs. efficiency in liquid scintillators.

Nukleonik, 1, No. 9 (1959).

W. Verly, et al., pp. 325-329. Tritium dosimetry in a proportional counter.

P. Ciccarone, et al., pp. 329-332. Tritium dosimetry in a proportional counter. II. Preparation of specimens.

Nukleonika IV, No. 5 (1959).

A. Dancewicz, pp. 547-555. Radiobiological work of the health physics division of the Nuclear Research Institute (Poland).

W. Hermanowicz, pp. 557-566. Investigation of the radioactivity of the waters of the Vistula river within the bounds of Greater Warsaw.

Science 130, No. 3386 (1959).

P. Gustafson, pp. 1404-1405. Ratio of Cs^{137} activity to Sr^{90} activity in soils.

Sewage and Industr. Wastes 31, No. 11 (1959).

J. Smith pp. 1323-1326. Removal of liquid radioactive wastes from atomic ships.

V. RADIOACTIVE AND STABLE ISOTOPES; USES OF RADIOACTIVE RADIATIONS

Vestnik Sel'sko-Khoz. Nauki, No. 11 (1959).

V. A. Emel'yanov, A. I. Zaitsev, pp. 103-109. Balance sheet regarding applications of radioactive isotopes in land-amelioration studies.

Voprosy Ékonomiki, No. 12 (1959).

A. Sokolovskii, pp. 166-167. Study of the economic effectivness of the use of isotopes.

Zavodskaya Lab. 25, No. 11 (1959).

A. I. Nisnevich, pp. 1341-1342. On the amount of radiation used in studying wear on machine parts by means of radioisotopes.

Izmeritel'naya Tekh. No. 12 (1959).

V. S. Merkulov, A. V. Klimushev, pp. 52-54. Determination of the mass content of components of binary systems, by the method of attenuating beta and gamma radiations.

Mekhaniz. i Elektrifik. Sots. Sel'sko-Khoz., No. 6 (1959).

R. A. Srapenyants, pp. 14-19. Use of radioactive isotopes in study of tractor and farm-equipment engines.

Sbornik Trud. Vsesoyuz. Nauchno-Issled. Gorno-Metal. Inst. Tsvet. Metal., No. 5 (1959).

V. I. Plotnikov, pp. 7-12. Use of radioactive isotopes in the work of the VNIITsvetmet.

Soobshch. Giprokoksa, No. 22 (1959).

V. I. Zatyl'nikov, pp. 307-313. Use of radioactive means for automating the coke and chemical industry.

Industr. Chemist 35, No. 418 (1959).

G. Hall, pp. 577-579. Use of large radiation sources in industry.

Industries Atomiques III, No. 9-10 (1959).

C. Nordau, pp. 79-84. Isotope division at the Weizmann Institute.

Jaderná Energie 5, No. 12, (1959).

J. Bednář, and M. Křivánek, pp. 405-408. A 400 Curie activity Co^{60} gamma source.

Kernenergie 2, No. 12 (1959).

W. Dietzsch, pp. 1053-1067. Some special problems arising in using gamma rays to measure thickness.

Nucl. Energy 14, No. 140 (1960).

F. Paulsen, pp. 27-30. Production of isotopes in Holland.

Nucl. Instr. and Methods 6, No. 1 (1959).

D. Trageser, pp. 26-32. Techniques of electron-beam processing.

P. Delattre, pp. 83-93. Nuclear reactors as a reserach tool in physics.

H. Andrews, pp. 96-100. Accelerators for biology and medicine.

Nucl. Power 5, No. 45 (1960).

A. Maddock, pp. 105-106. Use of nuclear radiations.

Nucleonics 18, No. 1 (1960).

J. Coultry, H. Briggs, pp. 117-118, 120. The use of radioactive sources to monitor the axial position of a jet engine.

Nukleonik 1, No. 9 (1959).

D. Vincent, pp. 332-336. Absolute measurements of the intensity of radiation emitted by radioactive isotopes decaying by electron capture.

SOVIET

research in

ANALYTICAL CHEMISTRY

OF URANIUM

A collection of ten papers from the Consultants Bureau translations of the Soviet Journal of Analytical Chemistry and the famous "Doklady" of the Academy of Sciences (1949-58)... This collection will acquaint the analytical chemist working in this field with Soviet techniques for the determination of uranium in solutions, in ores and the products of their treatments, and in accessory minerals, plus methods for the determination of impurities in uranium.

heavy paper covers illustrated $10.00

CONTENTS

c/b CONSULTANTS BUREAU
227 WEST 17TH STREET, NEW YORK 11, N. Y.

Declassified and Approved For Release 2013/02/19 : CIA-RDP10-02196R000100050004-5

the latest Soviet techniques!

CONTEMPORARY EQUIPMENT for WORK with RADIOACTIVE ISOTOPES

A comprehensive review of the Soviet methods and technological procedures used in the production of isotopes and the preparation of labelled compounds from them. The shielding and manipulative devices are described as well as illustrated in detail. It is an excellent guide for all scientists and technologists concerned with radioactive isotopes.

CONTENTS

durable paper covers *67 pages* *illus.* *$15.00*

c/b CONSULTANTS BUREAU
227 W. 17th ST., NEW YORK 11, N. Y.